GEOMORPHIC MODELING OF HILLSLOPE SEDIMENT SIZE DISTRIBUTION INYO CREEK, EASTERN SIERRA NEVADA

A thesis submitted to the faculty of
San Francisco State University
In partial fulfillment of
The requirement for
The degree

Master of Science
In
Geosciences

by

Shirin Leclere

San Francisco, California

January 2017

CERTIFICATION OF APPROVAL

I certify that I have read *Geomorphic Modeling Of Hillslope Sediment Size Distribution Inyo Creek, Eastern Sierra Nevada* by Shirin Leclere, and that in my opinion this work meets the criteria for approving a thesis submitted in partial fulfillment of the requirements for the degree: Master of Science in Geosciences at San Francisco State University.

Leonard Sklar
Professor of Earth & Climate Sciences

John Caskey
Associate Professor of Earth & Climate Sciences

Jerry Davis
Professor of Geography & Environment

Leonhard Blesius
Associate Professor of Geography & Environment

GEOMORPHIC MODELING OF HILLSLOPE SEDIMENT SIZE DISTRIBUTION
INYO CREEK, EASTERN SIERRA NEVADA

Shirin Leclere
San Francisco, Ca
2017

Landscape evolution and climate are linked by river bed sediments, which regulate the efficiency of river incision into bedrock. The sediment delivered to a stream channel depends on the topography of the surrounding hillslopes, and climatic variables like temperature, precipitation, and vegetation. Yet there is little in the way of theory or data to predict how climate influences patterns in hillslope sediment size distributions at the watershed scale. To address this knowledge gap, we are investigating hillslope sediment production in the steep granitic catchment of Inyo Creek, in the eastern Sierra Nevada of California.We expect the geomorphic and climatic factors that influence temperature and water residence time, and thus the intensity of chemical versus mechanical weathering, will correlate with resulting hillslope sediment sizes.

The resulting map analysis predicts that 50% of the catchment will be dominated by boulder-size sediment, with smaller sediments dominating lower elevations. Our prediction accuracy is significant and we find a strong positive correlation with elevation. Including slope and aspect with elevation predicts areas where larger clasts dominate even at lower elevations. These results illustrate how climate-controlled hillslope sediment production can influence river sediment supply, and thus bedrock incision and landscape evolution.

I certify that the Abstract is a correct representation of the content of this thesis.

Chair, Thesis Committee

12/17/16
Date

ACKNOWLEDGMENTS

For assistance in field data collection I thank Nick Aiello, Omid Arabnia, Gionata Bianchi, Theresa Fritz-Endres, Gabriela Geyer, Jason Guldman, Andrea Key, Molly Mclaughlin, David Quicke, Sam Shaw, and Joey Verdian. For ideas, far-ranging discussions, and encouragement I thank my advisor, Leonard Sklar, my coauthors, Jennifer Genetti, Cliff Riebe and Claire Lukens, and my committee members, Jerry Davis, Leonhard Blesius, and John Caskey, as well as everyone in both the Earth & Climate Sciences Department and the Department of Geology & Environment at SFSU. Funding and equipment was provided by friends and family, NSFgrant, EAR 1324830, and the Doris and David Dawdy Fund for Hydrologic Science at SFSU. Field support as well as design advice, training, and assistance was donated by One Letter Studios and my most marvelous sweetheart, E. Gilliam. And most importantly I thank my friends and family, all of Gladyshouse near and far, for their love and support and throwing me a tremendous party when the first article published online on my birthday. And for never letting on when (if) they gave up on the final stages of writing and editing this master's piece.

TABLE OF CONTENTS

LIST OF FIGURES

LIST OF TABLES

1 Introduction & Background

Weathering breaks down rock and creates sediment on hillslopes. Erosion moves it to the stream channel. As the stream sweeps the sediment along, more sediment is continually being added by the downstream hillslopes. When we consider the effect of sediment on streams, we focus on the amount of sediment rather than the sizes of the individual sediment particles. The amount of sediment supplied to a channel is certainly important for assessing the effect on the stream channel, riparian habitats, and downstream depositional areas. But the size of the sediment particles also affects the stream channel morphology, the rate of incision into bedrock, habitats, and potential hazards of debris flows and floods. (Dietrich et al., 2003; Riebe et al., 2014; Turowski et al., 2015; Wagner et al., 2012) Unfortunately, we do not have established methods to predict sediment size distribution on the hillslopes.

While many studies address sediment once it reaches the stream channel, fewer focus on sediment while it's still on the hillslopes (Dietrich et al., 2003; Sklar et al. 2016). Some channel studies have shown how sediment size changes downstream: abrasion of particles wears down their edges producing fine particles as the original coarser particle moves downstream (Gasparini et al., 1999; Heller et al., 2001; Willett, 2006) or size selective deposition promotes downstream fining by dropping the larger sediments along the channel (Ferguson et al., 1996; Hoey and Ferguson, 1997; Paola et al., 1992). But regardless of what happens in the channel, in most steep valley streams more sediment is being delivered from the hillslopes at every downstream reach. So the standard trend of downstream fining of sediments means that not only are abrasion and size-selective deposition occurring but the particles delivered by local hillslopes to downstream reaches are no longer the coarse sizes delivered to upstream reaches. The hillslopes must be delivering finer particles in the downstream reaches of the watershed (Sklar et al., 2016; Sklar and Dietrich, 2006). If the hillslopes were delivering coarse particles downstream then the sediment size distribution in the channel would reflect this continual influx of larger particles and not show a consistent downstream fining.

There are studies of erosion patterns and rates on hillslopes (Fu et al., 2010; Larsen et al., 2009; Montgomery and Brandon, 2002; Schlunegger et al., 2009) but most use field and experimental data in the channel or at the bottom of the hillslope to determine transport paths, recurrence of erosion events, and erosion rates (Michaelides and Singer, 2014; Roering et al., 2001; Hales et al., 2012). These studies do not usually focus on the initial particle sizes before the erosion events but the particle sizes they do record are useful information for understanding the hillslope sediment patterns. Similarly, soil production studies focus on the production rate rather than the size distribution (Binnie et al., 2007; Heimsath et al., 1997; Ouimet et al., 2009). These studies examine the process of weathering bedrock in two transition zones: between soil-mantled hillslopes and exposed bedrock and between buried bedrock and the overlying soil and regolith. Weathering is the key process to consider in determining where in a watershed various sizes of sediment would be created. If we understood how weathering varies across watersheds, we could predict not only the amount and rate of sediment delivered to the stream but the spatial patterns of where the larger particles are delivered from - near the channel, on the ridge, at high elevations, or in low vegetated valleys. In this study, I address the question of what controls the size of sediment distributed within a watershed. To do this I consider landscape attributes that may control weathering, both topographic attributes like slope and aspect as well as climatic attributes like vegetation and the effects of precipitation and temperature. I combine remote data and field data to create a predictive model which functions at a scale of tens of meters - spatial patterns within hillslopes across a watershed.

2 Controls on Weathering and Sediment Production

Weathering by physical and chemical processes is a primary control on sediment size. Physical weathering is the breakage of rock by frost cracking, salt cracking, spallation, impact, extension of pre-existing joints, etc. and generally produces large rock fragments (Durgin, 1977). In contrast, chemical reactions dissolve individual mineral grains or cement, and tend to produce small particle sizes (Wright, 2007). The prominent processes of sediment production are shown in Figure 1. Some geomorphic processes combine both weathering styles. Disaggregation of granite involves chemical dissolution and physical cracking as altered clay minerals shrink and swell crumbling the rock into grus (Ruxton and Berry, 1957). Tree roots physically widen cracks in rock but also affect the chemistry of the soil and the chemical weathering of rock and regolith. And some processes are hard to distinguish; spheroidal weathering and exfoliation have similar effects on different scales – the first is a small scale rounding of boulders due to chemical weathering and the latter is a large scale process affecting large curved outcrops like Half Dome in Yosemite. But overall, the sediment size distribution should reflect the relative importance of each weathering style. Peltier (1950) illustrated the relationship between weathering style and gradients of precipitation and temperature: physical weathering predominates in cold temperatures (dependent on water availability - precipitation) while chemical weathering dominates at high amounts of precipitation and warmer temperatures. But landscape attributes such as slope, aspect, land cover, etc. affect how long water remains available to the weathering processes and therefore can also be considered controls on chemical and physical weathering (see Figure 1).

2.1 Attributes

One of the main controls on chemical weathering is water residence time (Burke et al., 2007; Dixon et al., 2009; Riebe et al., 2001; Schmidt, 2009). The longer water is in contact with rock, sediments, and soil, the greater the likelihood of chemical weathering and smaller sediment sizes (Phillips et al., 2008). Using precipitation as the source of water and temperature as a control on evaporation or freezing, these attributes become useful in mapping where longer water residence times would exist in a watershed. Elevation correlates with these factors and can serve as a proxy for precipitation and temperature (see Figure 1). Vegetation correlates with all three factors and is in a feedback loop with sediment; that is, vegetation increases where there is more sediment or soil but also increases the amount of sediment produced (due to root action - physical breakdown and acidification). Aspect has an effect on sediment production because it can be a control on temperature and therefore water residence time in arid environments or bedrock exposures. Lithology matters, as well as rock-strength, mineral composition, the likelihood and size of rock fractures and jointing, even the type and density of biota can be dependent on lithology. Slope affects both soil/sediment production and sediment and water residence time. In the next sections I consider specifically how sediment size might correlate with these topographic and climatic landscape attributes.

2.2 Topographic Attributes

2.2.1 Slope

Steeper hillslopes have thinner soils, erode more quickly, shed water more quickly, and if steep enough produce landslides (Heimsath et al., 2012). Slope, or rather the amount of runoff it promotes, is a control on water residence time. Gentle hillslopes retain water and promote chemical weathering and dissolution of rock over time while steeper hillslopes with greater runoff limit chemical weathering and promote physical weathering and larger sediment sizes. By measuring particle sizes and flux for both landslides and soil creep in the Feather River area of California, Attal et al. (2015) found a positive correlation between slope gradient and sediment size for both the chemical weathering process of soil production and the physical process of landslides, see Figure 2. Slope gradient is affected by the size of sediment as well. In most natural talus slopes the steepness of slope varies directly with the size of the rock fragments composing the hillslope (Burkalow, 1945) and the characteristic slope gradient is useful for determining if a landform was created by a rock avalanche (Jomelli and Francou, 2000), by small magnitude, scree-producing rockfall (Hales and Roering, 2005), or by landslides (Booth et al., 2013). Slope can be correlated with sediment size without necessarily being assumed to cause the sediment size distribution.

Gradient is not the only measurement of slope, other measurements include slope length – distance from channel to ridge, slope location – how far from the ridge or channel is the sediment located, and smoothness of slope – variations within the gradient such as hollows or cliffs. Sediment location along the slope correlates with sediment size (Hupp and Osterkamp, 1985; McGrath et al., 2013; Nakamura et al., 1997; Sklar et al., 2016). For example, in lowland streams where elevation above channel is connected with specific landforms like floodplains and terraces, sediment decreases in size with distance from the channel because the sediment is stream transported and the finer sediments travel furthest in a flood event (Nakamura et al., 1997). Sklar et al. (2106) found coarser sediments at ridge tops and finer sediments further from the ridges. McGrath et al. (2013) found distance to be more important than gradient: sediment size correlated more strongly with distance from the source, presumably ridges or cliff tops, than with slope gradient. Burke et al. (2007) found a correlation between chemical weathering rates and distance from the ridge, but that study was focused on soil production and only considered chemical weathering below the soil mantle. Soil production occurs even on steep slopes; hollows, also known as soil wedges, are concave areas in the bedrock where sediment accumulates and soil can develop (Dietrich and Dunne, 1978). Long water residence time in these wedges promotes chemical processes, leading to production of smaller sediment even on a predominantly steep slope. Wilkinson and Humphreys (2006) found that slope length (distance from channel to ridge regardless of sediment location) was a strong predictor of soil retention and forest density and that this correlation was slightly enhanced by aspect.

2.2.2 Aspect

Aspect, the direction a hillslope faces, and solar radiation, the amount of sunshine reaching a hillslope, have been studied for years (Bartlett, 1832), sometimes controversially (Blackwelder, 1933) by geomorphologists and material science engineers assessing its effect on brick (Ritchie, 1972), hillslopes (Hall, 2004), and individual rocks (Eppes et al., 2010; McFadden et al., 2005; McGreevy, 1985). Solar radiation is increased for south-facing (north of the tropics) hillslopes and can promote either chemical or physical weathering. In areas with available water, heat from the sun will increase the rates of chemical reactions. In arid climates or on steep bedrock slopes with little water retention, the solar radiation evaporates what little water there is and restricts chemical reactions, leading to a dominance of physical weathering. Across the variation of climates within the US, studies show that the steepest hillslope gradients can occur on either the sunny or shady hillslopes but in the arid southwest the steepest gradients tend to be on the south-facing slopes (Figure 3) (Burnett et al., 2008; Langston et al., 2015; Olyphant et al., 2016).

At arid sites in Arizona (Figure 3), soil was thinner and drier on sunnier (and steeper) slopes (Olyphant et al., 2016) while cliffs were more prominent and steeper on the south-facing, or equator-facing, slopes (Burnett et al., 2008). At arid sites near the California Nevada border, boulders were more prominent on the sunnier slopes (Sklar et al., 2016). In lab experiments and models, aspect and snowmelt events affected the depth and amount of soil moisture (Langston et al., 2015; Burnett et al., 2008). The sunny side experiences more evaporation due to insolation while the shady slope has more and deeper soil moisture (Burnett et al., 2008). Langston et al. (2015) suggest the soil moisture penetrates deeper on the north-facing, shady hillslopes because there are fewer snowmelt events allowing longer and larger accumulations of snowpack. Topographic attributes like slope and aspect combine with climatic attributes like temperature and precipitation to control the rates of chemical and physical weathering and therefore the size of sediment on the hillslopes.

2.3 Climatic Attributes

2.3.1 Temperature and Precipitation

Two fundamental climatic variables are mean annual temperature and precipitation and they both scale with elevation. Figure 4 compares plots of temperature, precipitation with sediment size from Marshal and Sklar (2012). In Hawaii the amount of rock fragments (percentage of particles larger than sand) increases with hotter temperatures (associated with increased evaporation) and decreases with precipitation. The amount of rock fragments also increases with the size of the fragments implying that size also increases with temperature and decreases with precipitation.

2.3.2 Elevation

Temperature and precipitation vary systematically with elevation; hence elevation can be used as a proxy for their effect on sediment size, assuming that lithology is consistent. (Hales and Roering, 2005). Steeper bedrock cliffs tend to be at higher elevation than soil-mantled gentle hillslopes, and tend to erode more rapidly (Montgomery and Brandon, 2002). Riebe et al., (2015) documented these relationships using age-dating techniques in the southern Sierra Nevada. They found that the higher elevations were steeper, colder, and drier than the lower elevations and, importantly, that sediment size increased with elevation.

2.3.3 Precipitation & Snowmelt

Whether precipitation falls as snow or rain will influence weathering on hillslopes. Snowpack is more likely to lead to longer water residence. The length of time between snowmelt events can be a control on depth of soil production and soil moisture. Less frequent melt events allow more snowpack to build resulting in more water infiltrating to a greater depth during snowmelt (Langston et al., 2015). Even slopes with little to no soil are affected by the seasonality of water availability. One would expect mobile water to infiltrate through talus quickly, leaving only thin films of water on the undersides of the boulders and cobbles. Surprisingly, water can reside for more than a year in talus slopes in alpine areas (Campbell et al., 2000). This promotes chemical weathering in the regolith below a talus slope as well as physical weathering in the talus itself.

2.3.4 Frost Cracking

Ice has long been associated with physical or mechanical weathering. Early work focused on ice crystal growth during periods of freezing and thawing (Potts, 1970); later investigators determined that rather than ice crystal breaking open rock, it is the effect of van der Waals forces and electrostatic forces that flakes rock in the tip of a crack and the availability of mobile water that fills that extension and furthers the growth of the crack (Hales and Roering, 2007; Hallet et al., 1991; Walder and Hallet, 1985). Frost cracking, or segregation ice growth occurs when the temperature is between -3°C and -8°C (at or below the surface of the rock). This temperature range is important for assessing the area in a watershed susceptible to frost cracking – if the temperature is too cold, below -8°C, there is not enough mobile water for the segregation ice wedges to increase in size; too warm and the ice itself is too mobile to create pressure or force against the rock. Hales and Roering (2005) suggest that frost cracking may be responsible for scree production at a specific elevation band in a limited-precipitation watershed; above that elevation they infer that frost cracking is limited by a lack of mobile water and temperatures below the frost cracking window. Riebe et al. (2015) used the average daily temperatures from PRISM Climate Group data to determine which spatial areas spend the most time in this frost cracking temperature window.

2.3.5 Vegetation

Just as elevation correlates with temperature and precipitation it correlates with vegetation or land cover because temperature and precipitation are controls on the type and density of vegetation. Vegetation and chemical weathering create a feedback loop where vegetation promotes chemical weathering over physical weathering by providing shade to retain water and roots to limit soil erosion. The action of chemical weathering then releases mineral nutrients as well as increasing soil production, both of which encourage more vegetation growth. The kind of vegetation is important when considering weathering styles. Grasses and scrub have shallow fine roots that hold the top layer of soil but rarely affect the regolith or buried bedrock. While they hold water in that top layer they do not provide much shade to prevent evaporation nor do they provide a canopy to increase the length of time precipitation takes to reach the ground and therefore increase the infiltration of water. Trees, on the other hand, have strong tap roots that not only affect rock physically but when the tree falls, soil and finer rock particles are moved downhill and more rock fragments are exposed to chemical weathering (Gabet and Mudd, 2010; Phillips and Marion, 2006; Roering et al., 2010). Evergreens in particular are noted for chemical weathering due to the acidification their roots encourage (Phillips et al., 2008).

2.4 Others

Many other landscape factors could be considered. It seems that many of these other factors could be correlated to elevation and therefore to sediment size distribution. Like vegetation, bioturbation and other effects of animal life can be correlated to elevation and therefore to sediment size. Rock spalling, fracturing due to wildfire or lightning, is limited by the lack of vegetation at higher elevations. Rockfall is clearly associated with exposed bedrock cliff faces and therefore is expected to be more prevalent at higher elevations. Other factors, which cannot be specifically correlated to elevation, include lithologic variations of rock strength, the percentage clay-altering minerals (biotite), and mineral grain size. At a larger scale lithologic variations include veining and fracture spacing and can be influenced by faulting as well as rock strength and composition. Once soil production has initiated, the rate of soil production is related to soil depth and chemical weathering dominates. Some processes, like disaggregation or grus, are a combination of chemical and physical weathering. Not all of these attributes will be addressed in this study as it is intended to produce a fast predictive map using easily obtainable data and GIS functions.

3 Study Overview

In a recent article, Sklar et al. (2016) discuss the potential sediment size spatial patterns within a watershed as if the patterns were determined by various single landscape attributes, i.e. for aspect they divide the watershed completely into the sunny, south-facing side and the shady, north-facing side while for elevation they use a simple linear gradient from outlet to peak. These patterns are excellent tools for an initial understanding but I intend to combine multiple landscape attributes to create a finer-scale map of the potential sediment size areas within a watershed. In this study, I will identify watershed-scale patterns in hillslope sediment size distributions by analyzing the processes of sediment production at locations throughout the watershed. Chemical and physical weathering will influence the process that dominates any given location. The topographic attributes that control the type of weathering can be identified using USGS Digital Elevation Model (DEM) data. Publicly available datasets provide the climatic attribute data - vegetation from the National Land Cover Database (NLCD) and temperature from the PRISM Climate Group. Combining the spatial patterns of topographic and climatic attributes should shed light on where chemical weathering would be promoted or restricted. This provides a way to predict the relative sediment size distribution in a watershed. Using aerial imagery, national database information, and GIS software should speed the process and reduce the time and money spent on field and lab work to assess a watershed.

3.1 Definitions

Multiple standards exist for describing various sizes of rocks or sediment and some terms have an implied size implication. For example, I use the terms fine scree and talus as separate terms based on their connotations of size. I use fine scree specifically to refer to small particles (> 5mm), because that was the smallest particle size the field team could reliably measure. This also emphasizes the field experience of skiing down fine scree, masses of tiny loose particles, as compared to climbing talus slopes, generally more stable slopes of angular rock fragments the size of large cobbles and small boulders. I will be using the term sediment to refer to any size loose particle, clast, or rock fragment from boulders to sand, soil, or fine scree. Also, I will be using the Wentworth naming strategy for particle sizes and the Krumbein phi scale conversion to millimeters with a slight modification (Krumbein and Tisdel, 1940).

$$Boulders > 256mm > Cobbles > 64mm > Gravel > 5mm > Fine\ Scree\ or\ Soil$$

3.2 Scale

The scale of analysis is important. As we scale down from regions to watersheds to hillslopes within a watershed, the spatial patterns are increasingly important. Knowing that one segment of a stream is downslope from a patch of fine sediment or that the upper reaches of a particular stream will receive large cobbles, gravel, and boulders but that lower reaches will only receive sand, gravel, and an occasional boulder would be very useful for predicting the evolution of the stream channel and the watershed itself. Predicting a spatial distribution of sediment sizes over a watershed requires assessing the factors or attributes that affect weathering processes.

3.3 Creating A Predictive Map

I will use the term Geomorphic Landscape Unit (GLU) to describe my method of identifying patterns in the landscape by overlaying some number of foundational attributes of the landscape: hillslope gradient, curvature of slope, drainage, aspect, vegetation or land cover, and lithology. In this section I discuss the concept and in the next section I address my application of the concept.

We tend to think about landscape in terms of bounded areas - a meadow, a valley, a waterfall, a cliff, rolling hills – even though we realize that the boundaries are not always clear and well–defined. Similarly we talk about arid or temperate areas, gentle foothills or steep mountainsides, and know that we mean these general areas that are clearly different and obvious even if we might not be able to draw exact boundary lines between them. Measurements of elevation, rainfall, and other variables are usually presented as relative numbers on a map with isometric lines for the areas with similar data but no clear boundaries between a steep area and a gentle one. Software tools make it possible to quickly outline some areas, i.e. watersheds, or to apply arbitrary categorization boundaries, i.e. steep slopes are those over 30° and to outline the resulting areas in polygonal units on a map.

Combining multiple categorizations overlaid on a map creates landscape units that can be spatially assessed (Adediran et al., 2004; Blaschke and Strobl, 2003; Minár and Evans, 2008). This concept, articulated as "land unit" in 1989 (Zonneveld, 1989) has been a critical tool for land-use planners long before the software tools shortened the process of analyzing the landscape (Booth et al., 2014; Chayka, 2011; Marchetti and Rivas, 2001; Zinck et al., 2015). The resulting patterns might be used to explain vegetation growth, topsoil loss, sediment production rates, soil production depths, erosion rates or in outlining weathering and erosional process regimes (Dietrich et al., 2003). Forestry management uses landscape units to identify areas where past forest fires and steep slopes increase the likelihood of massive sediment loss or potential landslides (Larsen et al., 2009). Soil scientists use geomorphic and pedologic units to assess topsoil loss, site suitability and sustainability issues (Zinck et al., 2015). Hydrologists use a similar concept referred to as Hydrologic Response Units (HRU) in watershed analysis (Booth et al., 2014; Chayka, 2011; Khan et al., 2013). These units have many names, such as Geomorphological Units, Terrain Mapping Units, or Terrain Units, and many make reference to the concepts without necessarily producing or requiring a spatial map of the various factors and resulting units (Iqbaluddin et al., 1999; Jiang et al., 2006; Meijerink, 1988).

A few studies have applied the concept as I do in this project. Chau et al., (2004) studied rockfall or talus locations by correlation with similar landscape attributes –

distance from road, from fault, curvature, slope, aspect, elevation. Shirzadi et al. (2012) addressed rockfall considering lithology, slope, aspect, and elevation alone. Booth et al. (2014) and Chayka (2011) have used this concept, described as Geomorphic Landscape Units (GLU) to specifically address sediment production, although they looked at production rates rather than spatial patterns. Figure 5 illustrates the process Booth et al. (2014) used to create their GLU analysis, qualitatively determining the effect of three different attributes – lithology, land use, and slope gradient - on sediment production rates. They divided each attribute into small/medium/large bins, indicating relative categories. The actual values and the relative proportions of small/medium/large vary between attributes, land cover cannot be categorized in the same way slope can, and between watersheds or study areas, forest and farmland studies would group land cover differently. Despite the fuzzy divisions, these categorizations generate useful information very quickly and the method is applicable to any watershed.

3.4 Method Overview

Figure 6 illustrates the approach I have taken in this GLU mapping project. The first step is to determine four attribute measurements that can be easily created as either a vector or raster dataset in a GIS program. Second, group each attribute dataset into three bins reflecting which values will encourage chemical weathering processes and which will encourage physical weathering processes, with a middle bin where neither weathering style dominates. This binning process involves many assumptions based on the particular watershed being mapped. Next, overlay two of these three-bin attribute maps to create a map of nine bin values. The two boxes in Figure 6 illustrate how two attribute dataset maps can be combined together using a 3x3 grid. The next step is to group, or reclassify, these nine values into three new bins reflecting the dominant weathering style expected from the combined attributes. The process is then repeated for the other two attribute datasets. The final step is to combine the two resulting maps and group the nine bins again into three. This final map predicts the areas in the watershed where chemical weathering will dominate, where the middle ground exists between the weathering styles, and where physical weathering will dominate. In effect, this map predicts areas of Small, Medium, and Large sediment size distribution.

3.5 What makes a good study site for this question?

As with any experiment, I wanted to limit the number of variable parameters, so a small watershed with similar lithology throughout and not much variety in vegetation would be ideal. This should let me focus on the topographic variables of slope, aspect, and elevation. But also I would want a site with a strong gradient in the variable values, for example, where the temperature or amount of precipitation varies dramatically from one part of the watershed to the other. I selected Inyo Creek, California, because it is an ideal site based on these requirements and has the added logistical advantage of current, on-going research where I could be part of a team of academic researchers.

4 Study site - Inyo Creek

Inyo Creek is a small (3.2 km^2), steep (2 km in relief) watershed southeast of Mt. Whitney near Lone Pine, California, (Figure 7) on the eastern face of the southern Sierra Nevada. The study site encompasses the watershed from the heights of Lone Pine Peak to the outlet point selected by previous studies (Riebe et al., 2015; Stock et al., 2006) (36.58886 °N, 118.20289 °W; WGS84), where the stream exits steep bedrock cliffs and flows through channeled alluvium onto the piedmont. Unlike the Mt. Whitney watershed just to the north, Inyo Creek did not experience glaciation in the Pleistocene (Stock et al., 2006).

4.1 Lithology

Inyo Creek is underlain entirely by granodiorite bedrock. There are three granodiorite plutons mapped in the watershed, the porphyritic Whitney, Kw, at higher elevations, the Lone Pine, Klp, at lower elevations, and the Paradise, Kp, in a thin band between the other two. Evidence for repeated emplacements, or nested intrusions, from 88 to 83Ma also suggest that each emplacement occurred while the prior was still cooling (Hirt, 2007). This suggests that the contact areas may exhibit a different pattern of rock fracture or strength. For this reason, the inset map in Figure 7 and most of the initial field maps have the lithology outlined. However, investigation of the Whitney formation at lower elevations in a nearby watershed indicates that the different formations do not differ in rock strength (Riebe et al., 2015). Even the slight differences in geochemistry and mineral grain sizes between the Whitney and Lone Pine formations do not correlate with the amount or size distribution of sediment produced from the Klp and the Kw granodiorites. (Riebe et al., 2015 [PNAS-Sup]). The stream channel profile shows no knickpoints or evidence of different bedrock incision rates that would indicate differing rock strengths across the watershed. Sediment transport downstream can sometimes be traced by looking for the large pink phenocrysts of potassium feldspar of the Whitney Formation. This may be helpful in determining source areas for downslope rocks.

4.2 Topographic Attributes

Inyo Creek is very steep. Very little of the watershed can be considered flat even near the channel. The channel itself is steep throughout the study area. The steepest areas of the watershed are exposed bedrock cliffs, especially a remarkable rock-climbers' ascent route on the south-facing side approximately half way up the watershed. The nearly straight, northeast-oriented channel of Inyo Creek divides the watershed into a sunny, southeast-facing side and a shady, northwest-facing side. Only at the highest elevations are there slopes that face northeast. The western summit, Lone Pine Peak, shades the high elevations around 3pm even in August. The sunny side is consistently steeper and less vegetated than the shady side.

4.3 Climatic Attributes

Inyo Creek watershed is in the rain shadow of the Sierra Nevada range. Average annual precipitation drops from 650 to 280 mm/yr as elevation drops from Lone Pine Peak (3947m) to the dry Owen's Valley piedmont at the outlet (approximately 2100m). Similarly mean annual temperature increases significantly from –0.7°C at the peak to 10.4°C on the piedmont (PRISM data, 2014).

Despite the dramatic variation in climate, the type of vegetation varies from sparse scrub and evergreen trees at the outlet to scattered conifers on bare rock at higher elevations. The upper third of the watershed is mostly bare bedrock with small patches of a variety of wildflowers and ground cover. The middle third has scattered evergreens across mostly steep talus slopes and a few small patches of lush, brushy vegetation near the channel. The lower third is mostly evergreens with mixed scrub and ground cover - berry bushes, coyote mint, and Mormon tea - on moderately steep scree slopes and in some meadow-like areas. In the channel riparian species, the bright green line of mostly alders and thicker brush in Figure 7, extend to higher elevations. Fire is not likely to contribute to the physical weathering potential as overall Inyo Creek is sparsely vegetated. There is too little fuel for the sustained fire needed to affect fire spalling and erosion rates (Hurst et al., 2013; Stock et al., 2006). Animal life has an effect on the production of sediment, as suggested by gopher mounds, and trail erosion, but the relative intensity of these effects should correlate with the land cover.

5 Methods – Maps

Much of the work for this study was done before visiting the field; I am dividing the methods section into two sections to emphasize the prediction process separately from the validation process. Figure 6 shows the path from 4 separate landscape attributes to a Geomorphic Landscape Units map predicting sediment size distribution for Inyo Creek. The sub-sections below detail the methods and software packages used to create these maps. All maps in this paper were created with ArcGIS from free and easily accessible data or images, and were and finished in Adobe Illustrator.

5.1 Topographic Attribute Maps: Slope & Aspect

Working from a United States Geological Survey (USGS) 10 m resolution, digital elevation model (DEM) I explored various individual topographic attributes using standard ArcGIS Spatial Analysis functions: *Slope*, *Curvature*, *Solar Radiation*, *Aspect*, and *Flow Direction*. Each exploratory map was originally displayed with a continuous stretched color bar and then the values were classified into three categories or bins. The classifications were not based on equal interval or natural breaks. Instead, I chose breaks that either accentuated a pattern, like the way the channel divides the watershed into sunny and shady sides, or that highlighted a logical break that we found during field work, for example dividing slope between the angles of repose for fine scree or sand-sized particles (~33°) (Hales and Roering, 2005) and for larger talus particles (~44°).

5.1.1 Slope

A simple raster map of slope values, top map in Figure 8, illustrates the lack of gentle slopes in the watershed. Slope was binned by angle of repose and accessibility; the field team was unable to traverse the steepest hillslopes. Figure 9 shows the resulting polygons. Areas with gradients less than the angle of repose of sand (33°) are shown in green and considered gentle. Yellow areas have gradients between 33° and 44° and hiking requires care and effort to navigate large talus slopes. The steepest regions, steeper than 44°, are fairly inaccessible bedrock and are shown in red. The gentle, medium, and steep hillslopes make up 19%, 48%, and 33%, respectively, of the watershed. Later analysis of bedrock boundaries supports the category boundary of 44°– the edges of polygons for that category align nicely with the bedrock boundaries.

5.1.2 Aspect

Figure 8 also shows simple maps of aspect, lower left, and solar radiation, lower right. Either of these could have served to clearly show the divide between the two sides of the Inyo Creek watershed. The solar radiation map, created using the ArcGIS *Points Solar Radiation* function summarizing both direct and diffuse radiation over half-hour daily intervals bi-weekly through an annual period, does not show the clear divide as strongly as the aspect map, perhaps because the higher elevations on both sides of the channel are shadowed by Lone Pine Peak in the early afternoon. Instead of using either aspect or solar radiation, I am using a map created with the *Flow Direction* function, which considers the direction water flows down hill. This map, in Figure 10, contains more contiguous polygons than aspect after the 10 compass directions are binned into 3 categories and illustrates the dramatic dichotomy of the watershed. It is binned logically into the shady side (SW, W, NW, N - 44% of the watershed), middle (NE – 21% in line with the channel), and sunny side (NE, E, SE – 35%).

5.2 Climatic Attribute Maps: Vegetation, Frost Cracking Days

5.2.1 Vegetation:

According to the National Land Cover Database (NLCD) there are four land cover classifications within Inyo Creek - bare rock (44% of the watershed), evergreen (18%), scrub/shrub (37%) and herbaceous (< 1%). While the vegetation does roughly diminish with elevation, there is a difference between the two sides of the watershed – evergreen dominant areas are prevalent at lower elevations on the shady, north-facing side of the watershed, see Figure 11.

5.2.2 Frost cracking:

To map the relative intensity of frost cracking at Inyo Creek, I estimate the fraction of time any given elevation spends in the frost cracking window (-3 °C to -8 °C) using the same methods as Riebe et al. (2015). These methods consider the amount of time spent within the temperature range rather than the number of times a temperature threshold is crossed. The frost cracking window can be calculated for depth below the surface of the rock (Hales and Roering, 2007) but that is outside the scope of this master's project. I estimate the mean annual temperature (MAT) for specific elevations from the annual temperature range (PRISM data) using the following equation.

$$\mathrm{MAT} = T_0 - z * L_r \qquad \text{(Equation 1)}$$

Where z is elevation in 50 m increments, L_r is the environmental lapse rate 0.0057 °C/m calculated from the prism data) and T_0 is 21.518 °C from the 800 m PRISM data for the ridge and the outlet of Inyo Creek (Riebe et al., 2015).

Next, I assume a sinusoidal daily average temperature (DAT) variation (Anderson, 1998; Hales and Roering, 2007; Riebe et al., 2015)

$$\mathrm{DAT} = MAT + \alpha\left(\sin\left(2\pi\frac{t}{P}\right)\right) \qquad \text{(Equation 2)}$$

where t is time in days, amplitude α = 12 °C and period P = 365 days. I then determined the number of days in a year where the daily average temperature is in the frost cracking window for each 50 m elevation interval, and divided the range of days (0 to 120) into three bins. The resulting graph in Figure 12 shows that from the outlet elevation of 2053 m up to 2350 m, less than 40 days per year are in the frost cracking window. On the main map in Figure 12, two bands are binned together; a middle section between 2350 m and 2700 m and the highest range, between 3225 m and the peak, experience between 40 and 80 days per year in the frost cracking window. The highest range is too cold for cracking some of the year; below -8 °C there is not enough mobile water for the segregation ice wedges to increase in size. The bin category of 80 to 120 days, or 2700 m to 3225 m, is a "sweet spot" for frost cracking where the rock is subjected to potential cracking longer than elevations above or below it. The next step is to decide how these bins translate into relative sediment size distribution by considering whether chemical or physical weathering will dominate.

5.3 Creating the GLU Maps – Reclassifying and Combining Attributes

As shown in Figure 6, the three bins of each attribute map indicate the dominant weathering style; one bin should identify areas that experience more chemical weathering relative to the others, one should identify physical weathering, and the middle bin where neither weathering style dominates. Overlaying two 3-bin attribute maps with the ArcGIS function *Combine* creates a new map with 9 bins, which is then classified with *Reclassify* according to weathering style and associated relative sediment size.

5.3.1 Topographic GLU Map – Slope & Aspect

Figure 13 shows the process I used for combining slope and aspect. Of the three bins (gentle, medium, steep) on the base map for slope, gentle indicates a low slope where chemical weathering dominates and steep indicates a slope with more rapid runoff and therefore less chemical weathering, where the physical weathering dominates. For the three aspect bins (wet, damp, dry), wet indicates the cool shady side and dry indicates the hotter sunny side where evaporation is intensified by the solar insolation and chemical weathering is restricted by the resulting lack of water.

Slope and aspect maps combine to produce a map of the nine possible combinations. This map has multiple small polygons with no discernable pattern. Those nine bins are reclassified into three sediment-size classifications using the strategy shown in the grid in Figure 6. The new bin category of Small (chemical weathering) includes the three bins wet/gentle, wet/medium, and damp/flat. Large (physical weathering) includes dry/steep, dry/medium, and damp/steep. Medium (neither style dominates) includes wet/steep, damp/medium and dry/flat. The combined grid for Slope and Aspect shows gentle NW-facing slopes as wet and flat, the prime chemical weathering bin and a steep, SE-facing slope as dry and steep, the prime physical weathering bin.

5.3.2 Climate GLU Map – Vegetation & Frost Cracking

The process of creating the climate GLU map is more complex. With vegetation there are two decisions – where to put the tiny (<1%) amount of herbaceous land cover and which land cover (shrub or evergreen) is most likely to encourage chemical weathering and therefore have smaller sediment sizes. Physical weathering dominates in the bare rock areas, which become the large sediment size bin. Trees, tree roots, and tree throw are associated with both chemical and physical weathering but since grasslands and scrub are not as likely to encourage chemical weathering as trees (especially evergreens) I classified Evergreen as chemical and therefore relatively smaller sediment sizes. The herbaceous areas are in the upper two thirds of the watershed in low slope, riparian areas next to the stream. I classified them with the Evergreens based on location and chemical weathering style.

The frost cracking classification may also vary based on study site. On one hand frost cracking as a physical process might imply that chemical processes are limited and that resulting sediment sizes would be large. On the other hand more time in the frost cracking window could imply that large sediment is cracking into smaller sediment and even in cold temperatures chemical weathering may be possible. I decided for this project that more time in the frost cracking window is likely to promote large particle sizes even if there are also some small particles produced. The 80-120 days bin therefore reflects the larger sediment size distribution.

Overlaying Frost Days and Vegetation creates a map with only 8 bins because there is no bare rock below 2350 m according to the NLCD. Based on the lower grid in Figure 6 these 8 bins are reclassified into 3 bins. This produces a climate map in Figure 14. Small (chemical weathering) includes the three bins with fewer frost days, and no bare rock. Large (physical weathering) includes bare rock and scrub with the most frost days. Medium (neither style dominates) includes only two bins, Evergreen with the most frost days and Scrub with 40-80 frost days; there are no points that fall into the 0-40 Frost Days with Bare Rock bin.

Interestingly, the break at 2700 m between 40-80 frost days and 80-120 frost days splits the tiny herbaceous spots into different bins in the climate GLU map - Small (40-80 Evergreen & Herbaceous) and Medium (80-120 Evergreen & Herbaceous), as small as these areas are it is not likely to make an impact but is it is surprising that both tiny areas are split by the boundary. A deeper understanding of how vegetation affects frost cracking might change the bin assignments for a specific watershed but for this project simple choices were made as an initial learning process. The Medium bin does show up in another interesting location on the climate map - at scattered areas near the highest ridges. The satellite images show lots of talus in those areas but there is also a large area of talus that is visible on the images yet is not reflected on the climate GLU map. Combining this climate GLU map with the topographic GLU map produces a sediment size predictive GLU map, Figure 14. As I mentioned with the vegetation map, the climate GLU map and the resulting sediment size GLU map are intentionally blocky and pixelated to reflect the coarse 30 m resolution of the NLCD information. The resolution of the DEM or gridded data can alter the calculated data values like slope and aspect (Zhang and Montgomery, 1994) and I would have preferred a finer resolution dataset for vegetation. In the next section I discuss an alternative to the NLCD based vegetation map.

5.4 Alternative Land Cover solution – Remote Sensing

The National Land Cover Database (NLCD) is a standard for showing vegetation in the United States. But after our field crew walked through the watershed of Inyo Creek the map created from the National Land Cover Database, Figure 11, seemed unsatisfactory. We found patches of exposed bare rock at lower elevations that were not shown in the NLCD 30 m resolution. More importantly, the classifications of Scrub/Shrub and Evergreen did not match the on-foot experience of the watershed. Scrub/Shrub is dominant on the alluvial fan below the watershed outlet, but not above the outlet. There, within the mapped watershed, vegetated areas are a consistent mix of Scrub/Shrub and Evergreen except along the channel where the dominant vegetation is riparian - alders and thick patches of low brush. This riparian vegetation shows as two patches in the NLCD map but in our experience it was a more consistent line along the channel. At the higher elevations bare rock is dominant, but there are areas that can only be described as scattered evergreens on bare rock. I addressed these issues by creating my own land cover map using remote sensing techniques, recent aerial imagery, and eCognition OBIA software.

5.4.1 OBIA overview

Object-Based Image Analysis (OBIA) attempts to model the way humans interpret aerial images (Machala & Zejdova, 2014). OBIA applies contextual information to the traditional pixel-based color analysis techniques. OBIA systems work in two phases: first a segmentation of the original raster into multiscale vector objects or polygons of similar pixels, based on color values and polygon shape in the panchromatic or multi-band imagery, followed by iterative classification and merging of these polygons with similar neighbors into larger polygons (Miliaresis and Argialas, 2000). In addition, fuzzy logic or iterative evaluation processes (similar to a supervised classification process), and hierarchical rule trees capture expert knowledge and create a quality control check on the resultant objects. These evaluations use texture, topological relationships (e.g., borders and connectivity), attribute table data, and class relationships to distinguish and refine each object (Benz, 2004).

Currently, eCognition, a software package created by Definiens and distributed by Trimble, is the leading commercial solution for OBIA (Meinel & Neubert, 2006; Zhang et al., 2010; Machala & Zejdova, 2014). It has been used to identify lithology, extent of gravel covering, even coatings on gravel from aerial imagery (Crouvi et al., 2006). This technique has determined relative age relationships between alluvial fan surfaces or lobes in the southern Israeli desert (Crouvi et al., 2006), in the Italian Apennines (Taramelli & Melelli, 2008), and in the KunLun Mountains on the north side of the Tibetan Plateau (Farr & Chadwick, 1996). In Death Valley, alluvial fans have been identified and outlined by using eCognition to combine color classification of aerial imagery with slope gradient information from a DEM. The fans' edges were determined by the change in gradient where the toe of the fan spreads out onto the playa (Argialas and Tzotsos, 2006). This Death Valley study inspired this project's alternative land cover map.

5.4.2 OBIA Method

Using the *Quick Map Mode* and *Nearest Neighbor Classification* in eCognition on a recent (2014), 1m resolution, National Agriculture Imaging Project (NAIP) aerial image, I ran multiple trials to determine which segmentation style and initial polygon size would most accurately capture Inyo Creek land cover. I chose multi-resolution segmentation over quadtree segmentation (Baatz and Schäpe, 2000) because the resulting polygons were a better match for the areas of bare rock and riparian vegetation that I could identify by eye on the image. For similar reasons I eventually chose a large initial polygon size despite my initial assumption that smaller polygons would be more accurate.

Vegetation is easy to identify in the false-color, three-band image and the distinction between riparian vegetation in the channel and the scattered scrub and trees of the rest of the watershed is very clear. Segmenting with small initial polygons consistently missed parts of the riparian channel areas, Figure 16, and led to classified polygons that consistently grouped large parts of the surrounding hillslopes with small sections of the channel. The small initial polygons also lead to arbitrary classification of the areas near bedrock boundaries; one trial would group an area with scrub and the next trial with the same initial size would group it with bare rock. Segmenting with large initial polygons produced overly large contiguous areas but the classification was consistent across multiple trials. It also created small polygons that merged well in the riparian areas. Despite the original impetus to overcome a coarse resolution, the larger initial polygons proved a more reliable choice.

5.5 Land Cover Map Comparisons

The most noticeable differences between the eCognition land cover map, Figure 18, and the NLCD map, Figure 11, are in the extent of bare rock and scrub. The percentage of area assigned to bare rock dropped from 44% to 22% and scrub increased from 37% to 52% while evergreen only varied from 18% to 24%. These comparisons are only approximate; the categories are not exact matches. The custom map does not have a category of Scrub/Shrub; the equivalent category is Scrub/Tree. Similarly, the rough equivalent for the NLCD Evergreen is Tree/Rock on the custom map, which designates scattered trees on bare rock and extends to higher elevations than on the NLCD map. Both maps show higher elevations as predominantly bare rock.

5.6 New Land Cover Discussion

Unfortunately, the higher elevations were not accessible by our field crew and I had to rely solely on aerial imagery to validate my map in those areas. Even lower elevation areas were inaccessible due to steep talus slopes and exposed bedrock cliffs. These lower elevation outcrops are obscured on the new map; the lower third of the watershed is classified completely as Scrub/Tree. The decision to select for larger initial polygons is responsible for the lack of variation in the lower elevations. Originally, I had assumed that I would want the smallest polygons to correct for the large, 30 m resolution of the NLCD map, but the arbitrary decisions merging polygons convinced me that the larger initial polygons were more appropriate. I did however make a land cover map with the smaller initial polygons, Figure 17, to compare with the larger initial polygon map. The eCognition maps were based on a 1 m resolution NAIP aerial image, which meant that in the small polygon map some polygons were less than 1 meter wide. Compared to this map, the original 10 m resolution aspect, slope, and frost cracking maps seem coarse, just as those 10 m maps had made the 30 m NLCD-based maps seem coarse. The issue of arbitrary choices in polygon boundaries manifested in the land cover maps as well. In the eCognition classification process I discovered that the small initial polygons created merged polygons that arbitrarily crossed visually obvious boundaries between exposed bedrock and vegetation. When I made climate maps from those small initial polygon maps, the climate classifications also appeared arbitrary and conflicting: two maps would often have similar polygons with opposing categorizations. In the end I chose to work with a large initial polygon segmentation scheme because it handled the small Riparian area and produced consistent polygon boundaries over multiple trials. It also accurately identified high elevation areas where talus and fine scree were known from differing roughness in aerial images and from rock climbers' photographs taken on various approaches to Lone Pine Peak.

Figure 19 illustrates the new climate GLU and sediment size GLU maps created by replacing the original NLCD-based land cover map with this alternative OBIA land cover map. Comparing the land cover maps shows that they are proportionally and spatially very similar as shown in Figure 20. There are two areas that may prove helpful in evaluating the accuracy of the map predictions. In the upper right the new map shows small sediment size expected where the original shows large and medium. In the lower left the new map expects medium where the old expected small. The higher location is inaccessible to field teams (although not rock climbers) but the lower is area is accessible to the field team and provides a logical place to test the predictions.

6 Methods – Field data collection and analysis

This section discusses the selection of the field sites and the methods used in the field to measure the sample sites. It also discusses the way the measured values are binned and compared to the predictive GLU map.

6.1 Site selection

Field sites were selected using the original, NLCD-based GLU map, left side of Figure 20. I selected 18 points spread roughly evenly along the longitudinal profile and divided in half by the channel. I randomized the selection by blindly placing a pencil eraser on a computer screen which displayed the original GLU map draped across the landscape in Google Earth, and having someone else mark the location of the pencil with a Google Earth place mark. If the points were well within the boundaries of a GLU polygon I retained them but some had to be reselected to avoid being too near an edge. Other spots were rejected and reselected because it was clear in Google Earth that they were inaccessible, such as along ridgelines. Still, once in the field we found that two sites were inaccessible and so two transects done the previous year were substituted for those points. We attempted to reach one point from two different directions and ended up with two separate points for a total of 19 points. The alternative land cover GLU map, right side of Figure 20, was created after the fieldwork and some of the points, which had been in the middle of polygons, were nearer to the edges of the polygons on the new GLU map.

6.2 Note on accuracy:

We used smartphones (charged nightly from solar panel battery packs) and handheld GPS units in the field. Both products required patience, up to 10 minutes to establish coordinates that varied in accuracy from 5 m to over 30 m at one site near towering cliffs. The smartphone apps, Google Maps and Trimble Outdoors, displayed both topographic maps and aerial images so when the accuracy was over 8 m we could compare our actual location with the given location on the app and make corrections while in the field. Each site was recorded on multiple devices. I was able to determine the appropriate location from the recorded locations, aerial imagery in Google Earth, and field notes and photographs. After the locations were determined I compared the sites, with a 10 m diameter buffer around each site, to the original GLU map and to Figure 21, the final GLU map with the alternative land cover assessment, to check that we were far enough inside the polygon edges for a reasonable assessment of the polygon.

6.3 Field Measurements

The predictive GLU map is based on 10m-resolution DEM for the 3.4 km^2 watershed with 34,043 points generated by the ArcGIS *Raster To Point* tool. Each of those points equates to a 10 m square in the field. So any field site we chose would need to measure a 10 by 10 square. In order to classify the sediment size distribution in that square we modified the standard Wolman pebble count method to facilitate 100 point counts in a 10 m by 10 m square on very steep, unstable ground. Instead of a grid we used lines forming an asterisk from the corners and the midpoints of the sides of the square, see inset in Figure 22. We measured the clasts every half-meter allowing for gaps at the center to avoid over-counting the clasts in the middle of the square. We measured the b-axis (the middle value of the height, width, and length of a clast) in the field using rulers, measured the accessible, aboveground portion of buried boulders or exposed bedrock, and recorded any particle smaller than a 5 mm cutoff as fine scree. Later in the lab Jennifer Genetti sieved bulk samples from the site areas and extended the finer sizes to the sub-millimeter scale.

6.4 Determining Sediment Size

To categorize the sediment size distribution I determined the D50, or median value (the size at which 50% of the clasts measured are equal or smaller in size) for each field site from a cumulative density function plot. This may not identify bimodal sites but it should accurately represent the relative size distribution between sites.

Because sizes in natural sediment follow a lognormal distribution I divided the range of D50 values into three equal intervals based on the Krumbein phi-scale (base 2 logarithmic scale). This established the Small, Medium and Large bins.

6.5 Assessing GLU Map Predictions

To assess the accuracy of the prediction I compared the predicted size bin to the measured size bin. If the predicted bin matched the measured I considered it a success. The probability of getting a specific number of successes purely by chance can be established from a standard binomial distribution. If the probability (P) is low enough I am able to reject the null hypothesis (that the number of successes is due to random chance). I created the binomial distribution curve for the number of sample sites by solving the standard binomial formula (using vassarstats.com) for each possible number of successes.

$$P = \frac{n!}{k!(n-k)!} p^k q^{(n-k)} \quad for\ k{=}0{,}n \qquad \text{(Equation 3)}$$

where

n=possible outcomes

k=successful outcomes

p=probability of success in any one comparison = ⅓

q=probability of incorrect prediction = ⅔

7 Results – Map Predictions

This first results section discusses the GLU map predictions and how those predictions compare to a simple prediction based on elevation alone. Since rocks may have fallen downslope into the field sample sites, which could skew the resulting predictions, this section also discusses potential upslope source areas of the GLU polygons and the boundaries of exposed bedrock locations.

7.1 GLU Map Prediction

Figure 23 explains the binning strategy to group the measured D50 values. The central graph shows the distribution of all measured particles at each of the 19 field sites. The 19 sites had D50 values that ranged from 1.06mm to 61.49mm. Using the millimeter equivalents of the Krumbein-Wentworth phi-scale, the range goes from 1 mm to 64 mm. Dividing that range into thirds, the D50 values were binned as Small < 4mm < Medium < 16mm < Large.

Figure 24 shows the locations of the 19 field sites and both the predicted and measured bins for each site. The site id values contain the elevation in meters and the sites labeled in red are the sites where the prediction did not match the measured bin. The predictions were very accurate: 13 successful predictions out of 19 sites. Using a binomial distribution and 1 in 3 probability of a correct prediction, the result of 13 correct predictions is significant with a p-value of 0.0015 – plotted in Figure 25. The null hypothesis is rejected with 99% confidence; the results cannot be explained by random chance. Figure 26, predicted bin size versus measured bin size, highlights the sites that were incorrectly predicted and whether the prediction was over or under the measured bin size.

7.2 Elevation Prediction

I also compared the D50 bins to a simple prediction based solely on elevation. Our accessible elevation range was 2100 m to 3000 m; assuming that size varies directly with elevation I created three bins predicting Small < 2400 < Medium < 2700 < Large which are shown in Figure 23. The results of this simple prediction are also statistically significant, with 12 successful predictions out of 19 comparisons for a p-value of 0.00555 (Figure 25). The middle grid in Figure 26 shows the plotted results of the elevation prediction versus the measured D50 values. Comparing the two plots identifies sites where either the GLU map predictions or pure elevation predictions over-predict or under-predict the sediment size distribution in the lower grid of Figure 26 and the details in Table 1. It is possible that the attributes of land cover, frost cracking, slope, aspect and their effect on chemical versus physical weathering may help explain why larger sediment sizes are found at higher elevation. It is also possible that certain of my attributes may increase the accuracy of a prediction beyond the simple direct correlation with elevation.

7.3 Potential Source Areas

Even if the GLU landscape attributes can explain whether small particles (chemical weathering) or large clasts (physical weathering) dominate an area in the watershed, they do not consider how rocks may change in both time and space. Specifically, the rocks we measured may have rolled down from somewhere upslope. I evaluated the potential source areas for each sample site using the ArcGIS spatial analysis function *Watershed* using the sample sites as pour points. I specifically did not use the ArcGIS function *Snap to Pour Point* to adjust the pour points in order to avoid overestimating the size of the source area because these tools are designed for waterflow not rockfall and water will travel further and through areas rocks cannot. Of the 19 sites, only two have large, wide subwatersheds, the rest are mostly straight-line falls of one or two pixels in width (Figure 24). Some of our sites showed very small source areas of just a pixel or two. This matched our experience in the field as those sites were usually on a large expanse of bedrock or at the bottom of a cliff where they were protected from rocks rolling down from uphill. The sample sites are reasonably representative of their source areas. The third column, Average GLU – Source, in Table 2 shows the calculated prediction for each source area - averaging the prediction bins (Small = 1, Medium = 2, Large = 3) for all the source area pixels and then rounding to 2 digits. All but three source areas matched either the measured or predicted bin value. The three unusual source areas are very small catchments, < 10 pixels. The largest source area, which has pixels in Large, Medium, and Small polygons, is very near our high camp location. It has a fairly gentle slope with deep gravelly sediment and scattered large boulders; it appears to be an old landslide surface. Elevation alone predicts it to be Medium, the GLU map predicts it to be Small, and the D50 value classifies it as Small. It would appear that even a large subwatershed involving source areas of larger size distributions does not introduce enough larger sediment to invalidate the GLU prediction.

7.4 Boundaries of Exposed Bedrock

The field team walked bedrock boundaries using GPS apps whenever we could reach the edges of the bedrock. The resulting lines were expanded by tracing visible bedrock boundaries on aerial images in multiple applications: ArcGIS, Trimble Outdoors, and Google Earth. Figure 27 shows the bedrock traces outlining the areas identified as steep slopes (< 44°) on the Slope map. This was not only a confirmation of the binning strategy for slopes but brings attention to an area roughly halfway up the watershed on the south-facing side. The bedrock traces show that bedrock is exposed at a lower elevation on the sunny side of the channel than on the shady side.

8 Regression Analysis

After evaluating the effectiveness of the GLU map predictions, I wanted to dig deeper into the correlation between landscape attributes and sediment size distribution. While I tend to picture the landscape in discrete areas similar to the bin concept, I don't want to artificially limit my analysis to these broad bins. I will use continuous data for each attribute and compare the attributes to the D50 values and to each other. I will use regression, standard least-squares analysis to establish whether elevation is the only significant correlation parameter and to determine what combination of attributes creates the best fit line for the 19 data points. I will compare solar radiation to aspect to determine if solar radiation would have been a more appropriate choice when creating the bins. Working with continuous data will also allow me to contribute to a weathering function described in Sklar et al. (2016) that combines climate, lithology, and erosion rate.

8.1 Normalizing Continuous Data

To eliminate scale and unit conversion conflicts, I normalized the GIS data (slope, elevation, and solar radiation) to a zero to one range, based on the minimum and maximum values of the 19 pebble count sites

$$Attribute_{Norm} = x_N = \frac{x - x_{min}}{x_{max} - x_{min}} \qquad \text{(Equation 4)}$$

where x is the slope in degrees, elevation in meters, or solar radiation in watt hours per square meter (WH/m2).

The effect of aspect does not vary linearly, so I normalized from azimuth degrees using the cosine function and a rotation of 110° to reflect the strongest solar insolation effect on the southeast-facing slopes.

$$Aspect_{norm} = \frac{\cos(x - 110) + 1}{2} \qquad \text{(Equation 5)}$$

where x is the aspect in azimuth degrees.

The number of days in the frost cracking window is normalized in a similar fashion but only after recreating the number of days with equations 1 & 2 using 5m elevation intervals instead of the 50 m intervals used for the GLU maps.

Data from either map (NLCD or the alternative OBIA land cover map) is already binned and does not easily convert to a normalized continuous range of data. Reusing the GLU map bins of Small, Medium, and Large not only connects the correlation analysis to the GLU map prediction but retains the expert knowledge that trees promote smaller sediment sizes than grasses and scrub. I normalized the bin values of 1-Small, 2-Medium, 3-Large into 0.333, 0.666 and 1.0 to avoid losing any potentially useful information from the GLU map when performing the regression analysis.

8.2 Excluding outliers

As part of the regression analysis, I used Cook's D analysis to systematically identify and exclude three outliers based on the distance the estimation moves without each of those points (Cook and Weisberg, 1982). These excluded points are the two largest D50 sizes, 61.9 mm and 40.7 mm, and the smallest D50, 1.06 mm. There was nothing particularly noteworthy about the site locations of the two largest outliers. The sites were at the highest sampled elevation near each other on a north-facing slope and across from two similar sites on northeast-facing slopes. The D50 values or the excluded sites were 4 and 6 times larger than two nearby northeast-facing sites. The smallest outlier, however, might be explained by its unusual site location; all the sites were intended to be on the hillslopes but this site was almost in the stream channel.

8.3 Initial Results of Multivariate Regression with Frost Cracking

For the multivariate analysis, I used ordinary least squares regression of empirical data where all uncertainty is assumed to be in the dependent variable, the D50 value. Success is determined by best fit (largest R-squared value) when all attributes are significant (p-values less than 0.05) and the residuals plot randomly. When comparing predictions with a different number of parameters, adjusted R-squared will be compared.

I explore these correlations in two ways - bivariate linear regression comparing single attributes with the experimental D50 values and multivariate regression to evaluate the correlation of combinations of potential attributes.

I tested many combinations of attributes and found that elevation alone and frost cracking alone both gave an R-squared value of 0.52 but adding slope and aspect to each of those attributes increased the R-squared value to 0.766 for slope, aspect, and elevation (SAE) and 0.787 for slope, aspect, and frost cracking (SAF). While adding land cover also increased the R-squared value, the resulting p-values for the attributes were not significant so I removed land cover from consideration. Interestingly, while solar radiation alone had a stronger correlation to sediment size than aspect alone, Figure 29, when those attributes were combined with other attributes, aspect increased the R-squared value and had significant p-values. Table 3 shows the various equations, R-squared values and p-values of various attribute combinations.

The best fitting equation correlates the log of the D50 with slope, aspect, and frost cracking (SAF), see Figure 31. The relationship can be linearly expressed as an equation from a log-linear plot as

$$Ln(D50) = intercept + a * slope + b * aspect + c * frost$$

(Equation 6)

or expressed as an exponential equation as

$$D50 = e^{intercept} * e^{a*slope + b*aspect + c*frost} \quad \text{(Equation 7)}$$

specifically,

$$D50 = 1.44 * e^{1.15*(Slope) + 0.52*(Aspect) + 1.38*(Frost)} \quad \text{(Equation 8)}$$

where *Slope*, *Aspect*, & *Frost* are the normalized values as described above and D50 is the median sediment size at a given location in the watershed. This equation has an R-squared value of 0.787 with an overall p-value of 0.0002 and individual p-values less than 0.05 for all three parameters. Specifically p equals 0.0024 for slope, 0.0295 for aspect, and 0.0002 for frost. The data is plotted on a log-linear plot; the log of the D50 values as the dependent variable and the normalized values for the attributes as the independent variable. Best fit lines for a log-linear plot indicate an exponential relationship between the dependent variable and the independent variables.

Based on the various combinations in Table 3, it seems clear that slope and aspect improve the correlation over either elevation or frost cracking alone. The algorithm for frost cracking includes elevation so it is not surprising that they are similar. The difference between elevation and frost cracking appears at the highest elevation where frost cracking is less effective because the winter temperatures are colder than the frost cracking window.

8.4 Considering the effects of Weathering on particle size

Of the four attributes I considered in the GLU analysis, frost cracking is unique in that it is a model of physical weathering effects as a function based on elevation and mean annual temperature. The other three attributes are plotted from data, whether the DEM for slope and aspect or NLCD for land cover. Because this model depends on a mean annual temperature interpolated across the range of elevation, frost cracking correlates precisely with elevation. It seems reasonable to consider whether frost cracking as a factor in sediment size could be replaced by elevation or perhaps by a more inclusive equation that would include precipitation, the effects of erosion rate, or the time sediment is exposed to the weathering processes.

Sklar et al. (2016) considers an equation describing the transformation of an initial sediment size distribution into the output of hillslope sediment size delivered to the channel. In this basic transformation, weathering (W) is considered an exponent in a power function on the sediment size distribution and is controlled by climatic, lithologic, and geomorphic factors.

$$D_{ch} = D_m{}^W D_0{}^{(1-W)} \quad \text{(Equation 9)}$$

where D_{ch} is the size distribution delivered to the channel, D_m is the minimum size particle possible (anything smaller would be considered part of the dissolved load), and where D_0 is the initial size distribution produced on the hillslope.

As part of the simplification of the model, Sklar et al. (2016) focuses solely on chemical weathering during sediment transport and relegate physical weathering effects to the initial sizes of sediment produced on a hillslope by cracking, jointing, and rockfalls. At first this seems hard to reconcile with my GLU analysis where I consider frost cracking as an indicator of physical weathering along with vegetation as an indicator of chemical weathering. However, it may prove a good fit for the field data since we were unable to access the high elevation regions where the frost cracking model suggested a reduction in sediment sizes. The model from Sklar et al. (2016) incorporates the climatic factors temperature and precipitation, which are controls on vegetation, as well as factors of lithology and time or erosion rate. In the following paragraphs I will address each of these factors and build the equation as I address them.

I first interpolated temperature and precipitation from the PRISM data at the peak and outlet, assuming a linear correlation with elevation where temperature varies inversely and precipitation varies directly. Inyo Creek is in the rainshadow of the Sierra Nevada range so there is less precipitation at the lower elevations. Then I plugged that information into an equation from Sklar et al. (2016) modeling chemical weathering potential (CWP) based on temperature and precipitation:

$$CWP = \left(\frac{P}{P_{max}}\right)^b e^{-\frac{E_a}{R}\left(\frac{1}{T+273} - \frac{1}{T_{max}}\right)} \quad \text{(Equation 10)}$$

For this CWP equation I use R = 8.3 J/Kmol for the universal ideal gas constant, b = ½ and activation energy Ea values of 60 kJ/mol for granitic rock in the Sierra (Riebe 2004; West et al., 2005) and the interpolated values for temperature (T) and precipitation (P) as elevation increases across the watershed. P_{max} = 1000 mm and T_{max} = 298 °K (25 °C) (Sklar et al., 2016) are reference values where the weathering potential is maximized, not the maximum temperature and precipitation expected in that area. The range of CWP values extends from 0.13739 to 0.00087 across an elevation range of 2053 m to 3948 m. When this chemical weathering potential is maximized (CWP = 1 when $P = P_{max}$ and $T = T_{max}$) Sklar et al. (2016) assume the possibility that all soluble minerals are dissolved leaving, at a minimum, only the insoluble minerals and crystals. The fraction of soluble minerals (F_{sm}) is therefore the maximum amount CWP could remove from the mineral mass of rock in an environment where sediment residence time is long and erosion rate is minimal.

This scenario can be called supply-limited (W_{sl}); the weathering process is limited only by the supply or amount of initial soluble material (F_{sm}) (Ferrier & Kirchner, 2008). In this environment W_{sl} ranges from 0 to F_{sm} as CWP ranges from 0 to 1.

$$W_{sl} = CWP * F_{sm} \qquad \text{(Equation 11)}$$

To factor in erosion however we must consider multiple scenarios: when chemical weathering is supply-limited and erosion is non-existent, when weathering is kinetically limited by erosion (i.e. weathering is limited as erosion removes sediment from hillslope), and when the rock is fresh and unweathered (where erosion removes sediment before weathering occurs). This can be envisioned with Figure 12 in Sklar et al. (2016).

$$W = F_{sm} * CWP\left(1 - \frac{E - E_{sk}}{E_{ku} - E_{sk}}\right)^{\frac{2}{3}} \qquad \text{(Equation 12)}$$

where E_{sk} is the threshold between supply limited weathering and kinetically limited weathering and E_{ku} is the threshold between kinetically-limited weathering and unweathered rock. I use values of 0.001 for E_{sk} and 2.001 for E_{ku} where Sklar et al. (2016) used 0.001 and 1. Increasing the value for E_{ku} to 2 ensures the range of values is non-negative. The exponent is set to 2/3 because sediment residence time has a non-linear dependence on erosion rate (Sklar et al., 2016); for relatively low erosion rates sediment (soil) residence time varies inversely, but in soil-mantled landscapes the erosion rate has been found to vary exponentially with soil depth (Heimsath et al., 1997; Larson et al., 2014). This is the final form of the equation but I still need to calculate the values for E, erosion rate, across the watershed.

To model erosion rates relative to elevation (z), Riebe et al. (2015) established a best-fit exponential equation from their Inyo Creek data. I use that equation as:

$$E = 0.22e^{2(\frac{z-2852}{1000})} \quad \text{(Equation 13)}$$

Combining these equations gives a function for the effects of weathering and erosion within Inyo Creek. This function was applied for each 10m by 10m pixel in the watershed and then used, similarly to frost cracking or elevation alone, as a potential correlating attribute to explain the sediment size field research values. As with frost cracking, a map of this weathering function follows elevation contours. Weathering, frost cracking, and elevation correlate individually with sediment size at the same R-squared value of 0.52; as both weathering and frost cracking functions include elevation as a parameter.

8.5 Regression results with Weathering

Revisiting Table 3 and including the weathering equation from Sklar et al. (2016) I find that the highest R-squared value of 0.79167, with a combined p value of 0.0002, comes from the equation which combines slope, aspect, and weathering (SAW). This is slightly higher than the SAF R-squared value of 0.787 with a combined p-value of 0.0002.

$$\text{Log10(D50)} = 1.84 + 1.13 * \text{Slope} + 0.47 * \text{Aspect} - 1.31 * \text{Weather} \quad \text{(Equation 14)}$$

or

$$D50 = 6.27 * e^{1.13*Slope + 0.47*Aspect - 1.31*Weather} \quad \text{(Equation 15)}$$

where *Slope*, *Aspect*, & *Weather* are the normalized values as described above and D50 is the median sediment size at a given location in the watershed. The bottom right graph in Figure 30, shows the equation on a log-linear plot, the log10 of the D50 values as the dependent variable and the normalized values for the attributes as the independent variable.

9 Discussion of GLU Map Predictions

For the discussion of results, I focus first on the GLU map predictions in this section and then the regression analysis in the following section. The GLU map discussion also serves as a baseline for the following discussion. Overall the accuracy of the GLU map prediction is impressive; 13 correct out of 19 sites gives a significant p-value of 0.0015. Whereas, a simple prediction of correlation with elevation returns 12 correct for a p-value of 0.0055. This suggests that generally sediment sizes do increase with elevation, but also suggests that the additional climatic and topographic attributes may explain why individual sites deviate from this general correlation.

9.1 Individual Site Predictions

Table 1 lists each of the 19 sites and the bin values for the attributes; the last column explains the sites where the D50 did not match the elevation prediction. This is probably due to specific local controls overpowering a general rule, as in Phillips' (2007) concept of the perfect landscape, wherein a location's geomorphology is explained by the perfect storm of local details above and beyond the global scientific laws. Slope is the strongest indicator of a site shifting up or down from the elevation prediction, although both aspect and vegetation can sometimes explain a shift that is not explained solely by slope.

9.2 Effects of Categorization Decisions

Some of these residuals can also be explained by examining the choices made in creating the GLU maps. Decisions made about attribute bins change the final prediction bins: whether to assign north-facing slopes to the shady bin or to the middle bin, whether to ascribe smaller sediment sizes to the actions of tree roots or to the water trapped by low ground cover scrub, even choosing which contour lines will bracket the elevation or frost cracking bins. Small changes can shift individual sites from success to failure, but usually a change also shifts some sites from failure to success. In particular, the bins chosen for aspect grouped the north-facing slopes with the shady, northwest-facing slopes. After analysis of the higher elevation sites, I would choose to bin the north-facing slopes with the mid-range northeast-facing slopes. Other decisions, for example predicting that the largest sediment sizes would be produced where frost cracking lasts the longest, appear to make a significant difference. Above 3225 m, frost cracking predicts a medium sediment size because fewer days are spent in the frost cracking window. Unfortunately the field teams were unable to reach this elevation range; therefore the field sites do not reflect the potential differences. Photo analysis of the higher elevations suggests that frost cracking may be more accurate in predicting sediment size than elevation alone.

9.3 Uncertainty in Categorizations

A detailed examination also highlights the inherent uncertainties of the GLU map – the edge of a polygon is an interpolation, so a site that appears to be near the boundary might actually be in the other classification; this is true whether the polygon is left as blocky pixels or smoothed for a more reasonable appearance. A site may change prediction based on purely whether it is shown on a smoothed polygon or the original DEM-based square pixelated polygon. Uncertainty can also be introduced by the resolution of the pixels. A few of the sites have different predictions, depending on which GLU map is used, purely because they rely on two different vegetation overlays with different resolutions; the National Land Cover Database (NLCD) has a 30 m resolution and my OBIA alternative map was created from a 1m resolution aerial image. The alternative land cover map introduced another source of uncertainty; the shadows thrown by boulders and talus at high elevations in the aerial image biases the eCognition classification towards the vegetation classes of evergreens and scrub over bare rock. These uncertainties, and the base uncertainty introduced by reliance on GPS devices, were analyzed by drawing a buffer of 10 m around each site and considering how the prediction would change if the site were shifted within the buffer zone. While some points did shift between the original and the alternative GLU maps, the binomial distribution of results was not affected significantly.

10 Discussion of Regression Analysis

There are three results to discuss from the multivariate regression: 1 – sediment size increases with elevation, 2 – slope and aspect improve the correlation with elevation, 3 – elevation-based weathering models may also improve our understanding of sediment size distribution. The first result confirms a previous finding of coarser sediment at higher elevation in Inyo Creek from detrital chronometry and cosmogenic nuclide dating (Riebe et al., 2015). This agrees with other studies that there is a correlation with elevation, although not all studies find the same correlation; Marshall & Sklar (2012) found the relationship between elevation and rock fragment size varied directly in Hawaii and inversely in California. Elevation may be correlated with, but it cannot be the cause of, sediment size patterns in a landscape.

The second result, that slope and aspect can improve the correlation, may shed light on the cause. Adding these attributes increases the R-squared values to around 0.78 from around 0.52 for elevation, frost cracking, or weathering as individual components. Aspect, while significant in the findings, contributes the least to the model. Wilkinson and Humphreys (2006) found a similar effect and surmised that there may be an effect of aspect that is not reflected in a standard sinusoidal representation of the annual temperature variation. Aspect seems to have a more significant effect than solar insolation, which may be due to Lone Pine Peak shading the higher elevations of Inyo Creek watershed – solar insolation is often correlated with elevation due to the increased radiation reaching higher elevations. Clearly aspect and slope are not dependent variables for elevation, and the regression analysis confirms that they are significant components to a final best fit equation. If slope and aspect control the water residence time by increasing runoff and evaporation, it would follow that they would affect both chemical and physical weathering, and therefore the size of sediment particle produced.

The third result, that climatic attributes are also important, is not as obvious; R-squared values only from 0.77 to 0.79 when comparing elevation, frost cracking, and weathering in combination with slope and aspect. The main differences between these three elevation-based models lies in the number of parameters considered: frost cracking includes elevation and temperature, while the weathering function from Sklar et al. (2016) also includes precipitation and erosion rates.

10.1 Comparing elevation-based models

When combined with slope and aspect, the difference in R-squared values is small but important between frost cracking, weathering, and elevation. I compare simple watershed maps and histograms of the frequency distributions of the D50 for the three combinations (SAF, SAE, SAW) and elevation alone (E). Figure 35 shows where the SAE and the E models predict the coarsest particles. The E model predicts the coarsest (>11 mm) particles will be at the highest elevation, interestingly it predicts the coarsest particles to be smaller than the other three models; the largest particle size is 15mm, rather than 23 in the other models. The SAE model shows the coarsest particle sizes at the highest elevations as well, but since the particle sizes are larger than predicted for E, SAE includes lower elevations than the E model. The SAW model in Figure 36 also shows the coarsest particle sizes at the highest elevations, covering more area than E but less than SAE. The histograms show that the coarsest particle sizes (>11mm) for SAW is a subset of the coarsest sizes for SAE. Figure 37 shows the coarsest particle sizes for the SAF model fall in a band below the highest elevations because the highest elevations spend less time in the frost cracking window. The lower half of Figure 37 shows the most common particle sizes predicted by the SAF model fall above and below the band of the coarsest particle sizes, just as they did in the original frost cracking field map. As with the SAE model, the patchiness indicates where slope and aspect affect the baseline frost cracking or weathering prediction. Figure 38 highlights the most common particle sizes for the SAE model. This model predicts a bimodal distribution of particle sizes, which between them encompass almost the entire watershed, except the area where the E model predicts the coarsest sizes, i.e. the highest elevations.

The probability density function graph of frequency of sediment sizes, Figure 39 shows that SAE shows a bimodal distribution while SAF and SAW have unimodal peaks, and all of them have long skewed tails to the right (larger D50 values). SAF has one broad peak at a lower frequency but at a higher particle size than E or SAE. SAW predicts a lower size value for the most frequent sediment size. Comparing cumulative distribution frequency of particle sizes – Figure 39 shows that elevation alone (E) has the narrowest range of sizes. The SAF model predicts the largest particle sizes, while the SAW model predicts the smallest sizes. SAF focuses on the physical weathering of frost cracking, while the SAW model incorporates chemical weathering and erosion rate and so emphasizes the smaller sediment sizes due to chemical weathering. Further field work at Inyo Creek could begin to explore these predictive models' accuracy.

10.2 Discussion of Outliers

With the regression analysis I excluded 3 points after running Cook's D analysis repeatedly. Including the three aberrant points lowers the R-squared value for elevation alone to 0.38 but for SAF it drops to 0.40 and only frost is significant. The lowest point is an obvious example of local conditions overriding a general expectation; it is practically in the channel while all other sites are on the hillslope. If we exclude just the lowest point (1.06mm); for elevation alone it is 0.56 while for SAF it is 0.70 but aspect is no longer a significant parameter. In either case if we substitute solar radiation for aspect the R-squared values are roughly equivalent but solar radiation is not a significant parameter. The two large outliers may also be explained by a local landscape attribute. Both are on a north-facing hillslope and as noted in the GLU map discussion, the north-facing slopes could have been grouped with the mid-range northeast-facing slopes rather than the shady northwest-facing slopes. Even without these outliers the original GLU predictions are able to explain more field site D50 values than the Elevation prediction.

11 Future Work

This study was done with limited resources in a single small bedrock watershed. The 19 field sites were chosen from the predictive GLU maps with the understanding that some areas were inaccessible and that vegetation and DEM were not available at the finest resolution. I would like to see further fieldwork at Inyo Creek supported by high resolution data, perhaps photo analysis using Structure from Motion or LiDAR datasets, to expand the accessible area in three specific areas: the highest elevations, the ridgelines at lower elevations and the south-facing slope in the middle elevations. Establishing ground control points for photo analysis within these areas safely and without disturbing the fine scree slopes will require significant effort but would provide data to validate the regression models. This could determine if the predictions of the SAF, SAE, or SAW models match the larger watershed, especially in terms of sediment size range and whether longer time in the frost cracking window correlates with larger sediment sizes. I would also like to see a study that includes information from cross sections perpendicular to the channel; I suspect that distance from ridge and curvature of slope may be useful information, similar to subwatersheds, to determine sources of sediment for each field site. Adding dominant wind direction to aspect or solar insolation could help determine the effect on evaporation and therefore water residence time. Adding solar radiation to elevation when interpolating temperature across the watershed from the PRISM data temperature range could also help identify local differences in water residence time. Finally, repeating this study in other watersheds would be useful for comparison between bedrock-incised stream channels and with non-bedrock channels.

12 Conclusions

The immediate objective of this project was to establish a fast, cheap, and safe GIS method to model spatial patterns of sediment size distribution at the watershed scale. That objective has been met. This project was a limited study in a single watershed but the data and methods have now been shown to be useful and should be applicable to other sites. The assumptions used to predict the effects of aspect and climate may vary in other sites (more humid sites may experience more intense weathering on sunny slopes than on shady ones due to increase in heat driving chemical weathering) but once those assumptions are codified, the strategy of combining variables into GLU polygons is applicable to any location. My successful prediction of sediment size distribution in a sparsely vegetated, semi-arid, strong bedrock watershed does not necessarily mean that my methods will work with the same accuracy in other watersheds, but it does bolster the value of using multiple climatic and topographic attributes to assess spatial patterns of geomorphic landscape units.

The second objective was to further our understanding of the connections between landscape attributes, climatic and topographic, and the spatial patterns of sediment size. That objective has also been met. There is a clear correlation where sediment size varies directly with elevation. But slope and aspect contribute to a more accurate prediction of sediment size distribution. My results indicate that slope is a significant contributor to the model, and that it can explain field sites that do not match the trend with elevation. Similarly, but with less significance, aspect can explain sites that deviate from the trend with both slope and elevation. Both these attributes should be considered with elevation when creating a model for watershed sediment size distribution.

Overall, my research is a contribution toward the long-term goal of reliable and automated mapping of hillslope sediment size distributions for use in sediment budgets and hazard delineation, and for understanding the feedbacks between climate, tectonic uplift, erosion and topography that drive sediment production and watershed evolution. This process could be useful in predicting the amount and size of sediment delivered to a stream on a regular basis as well as that available for entrainment in catastrophic debris flow events. As more people move to the foothills of major mountain ranges, this becomes an important consideration for suburban and exurban planning councils.

My research also contributes to our quantitative understanding of the feedbacks between climate, tectonic uplift, erosion, and topography that drive sediment production. The regression analysis implies that slope, aspect, and elevation are all important to quantifying the reduction in sediment size over time from an initial particle size distribution. Including these attributes in equations that model physical and chemical weathering, such as those developed and discussed in Sklar et al. (2016), would further our understanding of the distribution of sediment sizes ultimately delivered to the stream channel and to patterns of weathering and erosion in hillslope geomorphology.

FIGURES AND TABLES

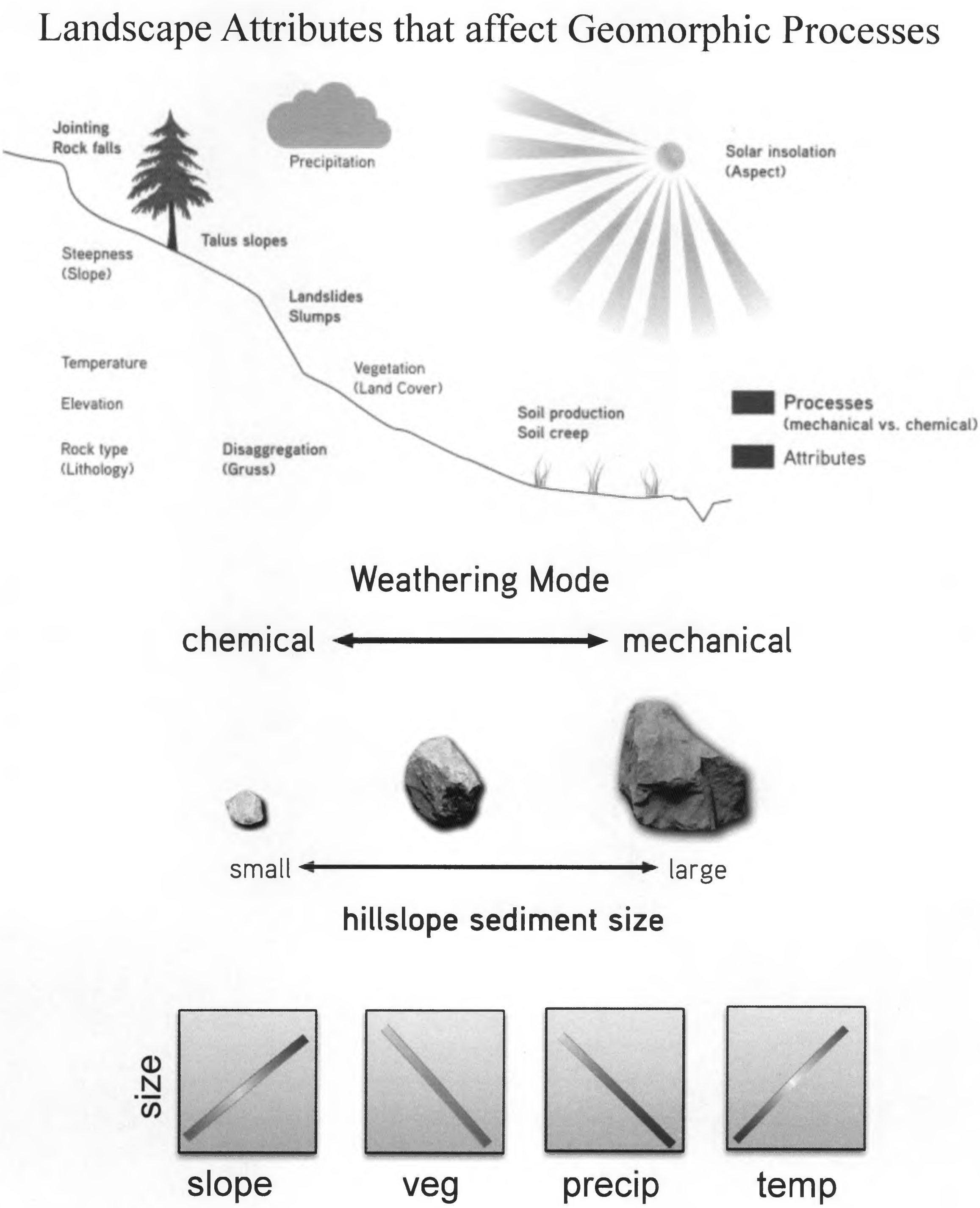

Figure 1. Landscape attributes like lithology, slope, temperature, precipitation, and aspect affect geomorphic processes, gruss, tree throw, landslides, etc. These attributes can be a control on chemical weathering and therefore could provide a means of predicting spatial patterns of relative sediment size. The four plots at the bottom of the image suggest correlations between attributes and sediment size.

Sediment Size Distribution Studies - Slope

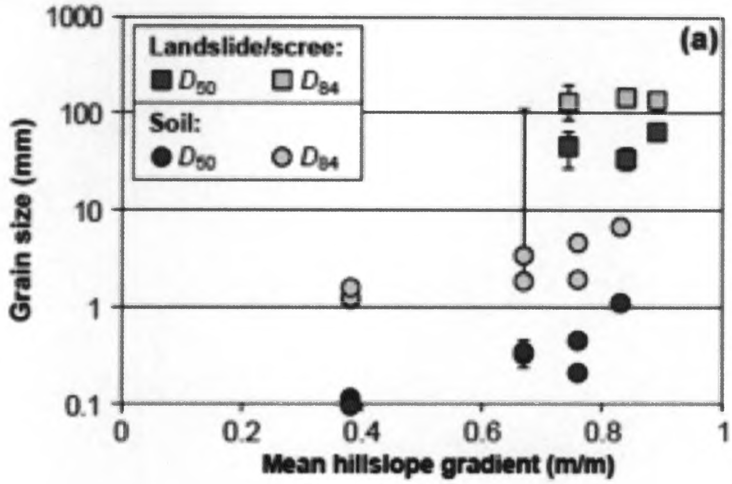

Figure 2. Grain size and size distribution vary directly with hillslope gradient on hillslopes next to the Feather River, California (Attal et al., 2015).

Sediment Size Distribution Studies - Aspect

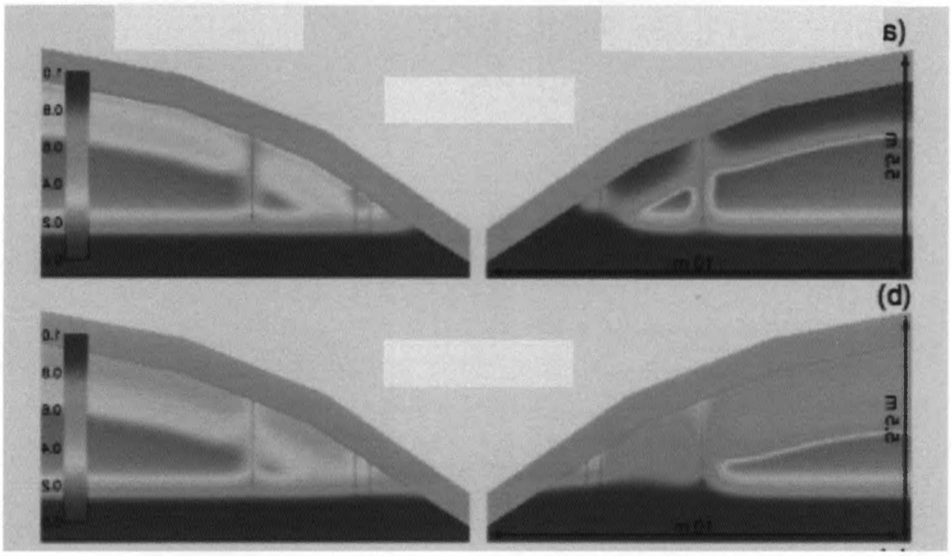

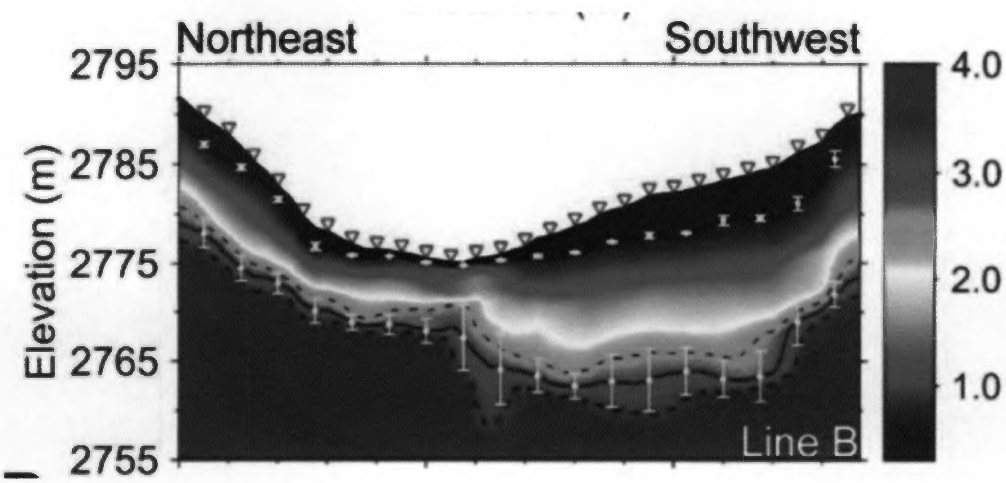

Figure 3. Results of Previous Studies of Landscape Attributes Affect on Sediment Size and Distribution. A) Models show north-facing slopes have more and deeper soil moisture (Langston et al., 2015). B) Field data from Arizona indicates gentler north-facing slopes with increased soil depth (Olyphant, 206).

Sediment Size Distribution Studies

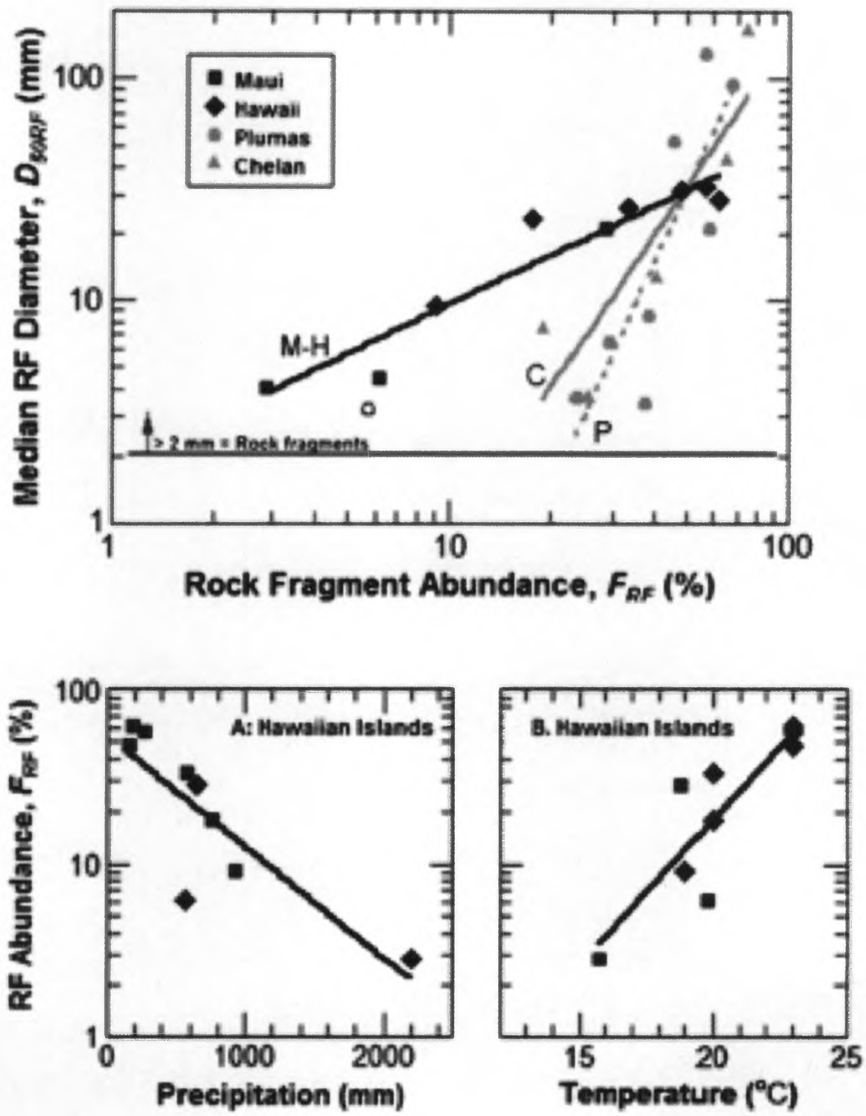

Figure 4. Results of Previous Studies of Landscape Attributes Affect on Sediment Size and Distribution. A) Rock fragment median size correlates with abundance in Hawaii, California, and Washington. Rock fragment abundance varies directly with temperature and inversely with precipitation in Hawaii (Marshall and Sklar, 2012).

Example of a Geomorphic Landscape Unit Map

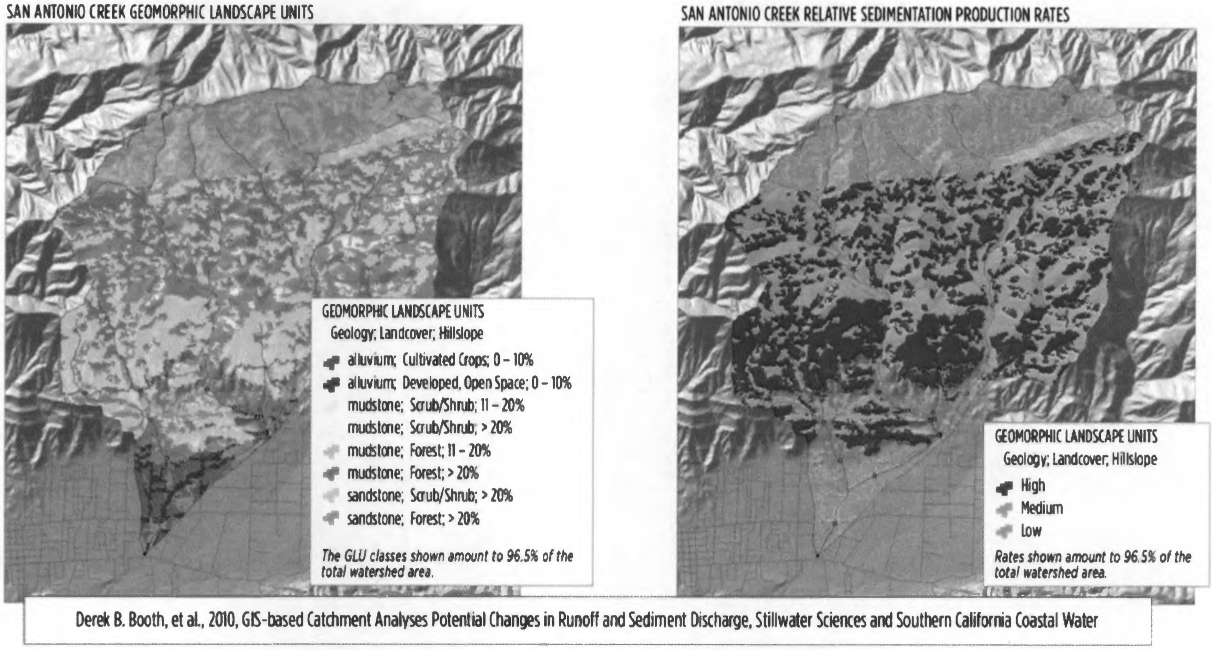

Figure 5. Geomorphic Landscape Unit (GLU) map using lithology, land cover, and slope to predict sediment production rates in southern California (Booth et al., 2010).

Constructing a Sediment Size Prediction Map

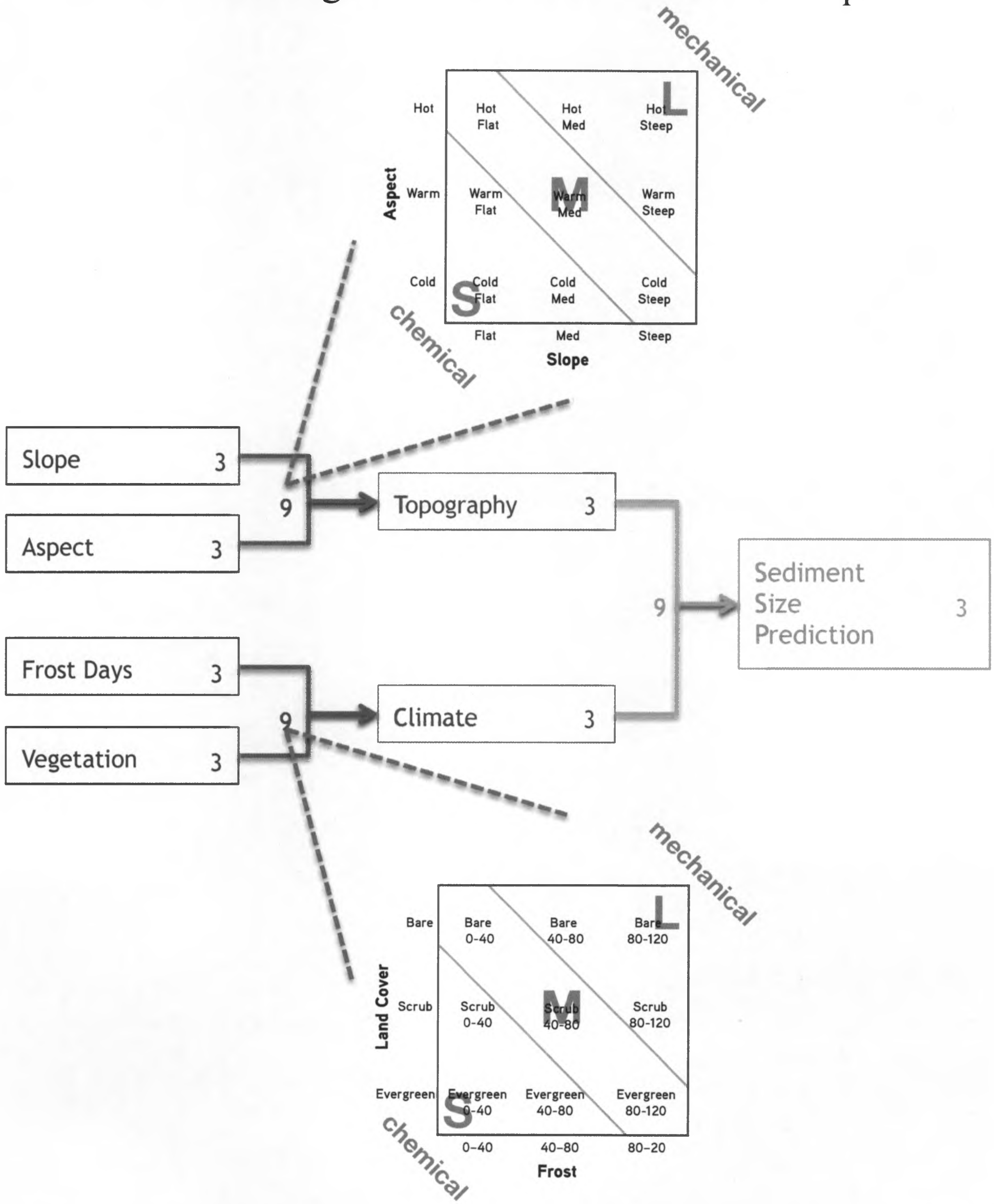

Figure 6. Order of operations to create GLU prediction map in this project. Values for slope and aspect are grouped into three bins and then combined according to the grid at the top. The nine resulting bins are simplified into Small Medium and Large based on the likely dominance of chemical or physical weathering resulting form the steepness of slope and intensity of solar insolation. Similar combinations are established for land cover and frost cracking.

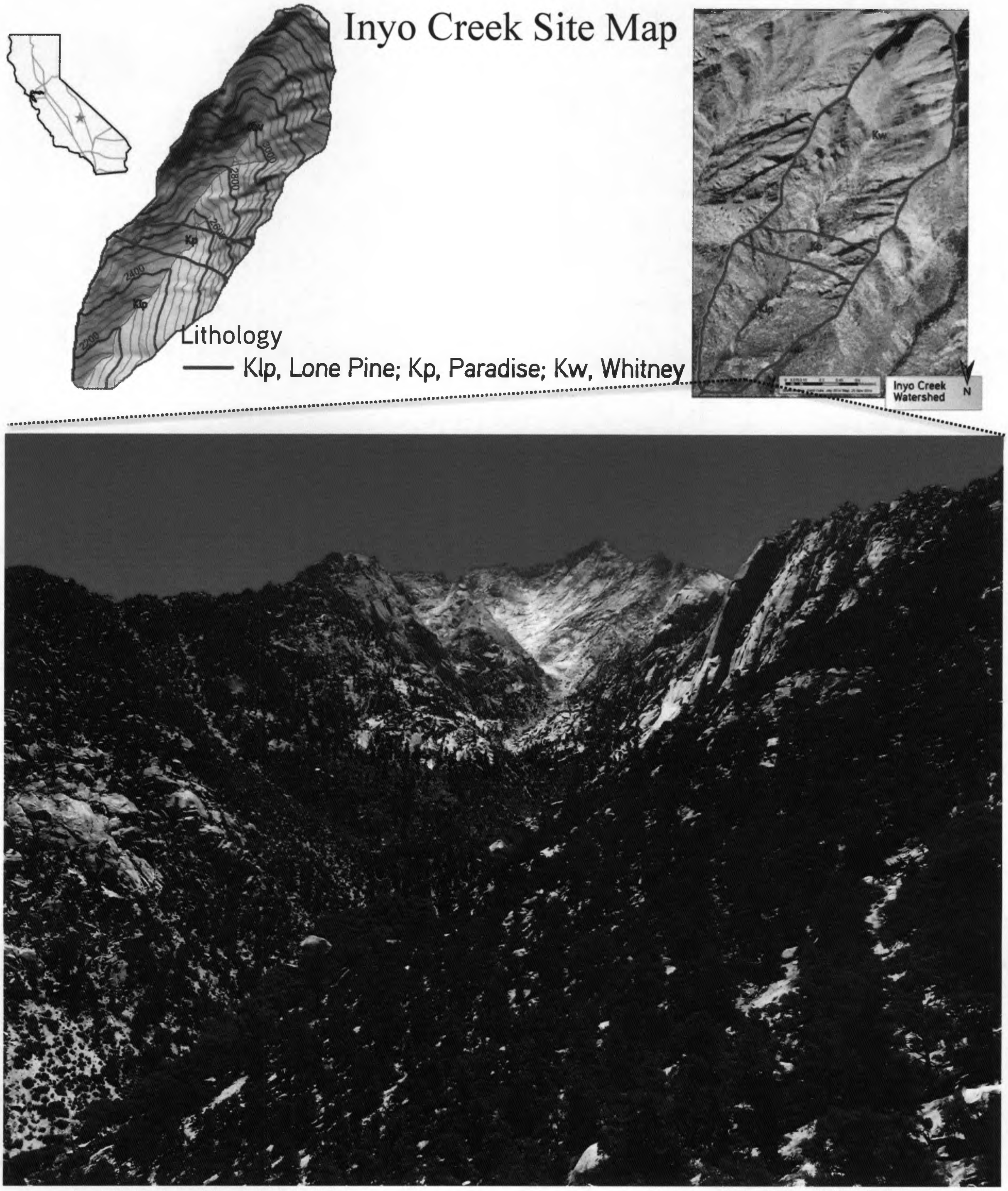

Figure 7. Inyo Creek is a sparsely vegetated watershed in the southeastern Sierra Nevada in California. It descends from Lone Pine Peak (3947 m) to the outlet at 2150m. This photograph was taken from the northern ridge line near the outlet (red star in aerial image – inset on the right) facing southwest towards the peak. Most of the vegetation is low scrub and scattered evergreen conifers with some riparian trees and brush along the channel. There are three Cretaceous granodiorite formations (shown in the aerial image inset) of similar rock strength. Inyo Creek flows northeast, all maps are presented south up.

Exploratory maps for Slope, Aspect, and Solar Insolation.

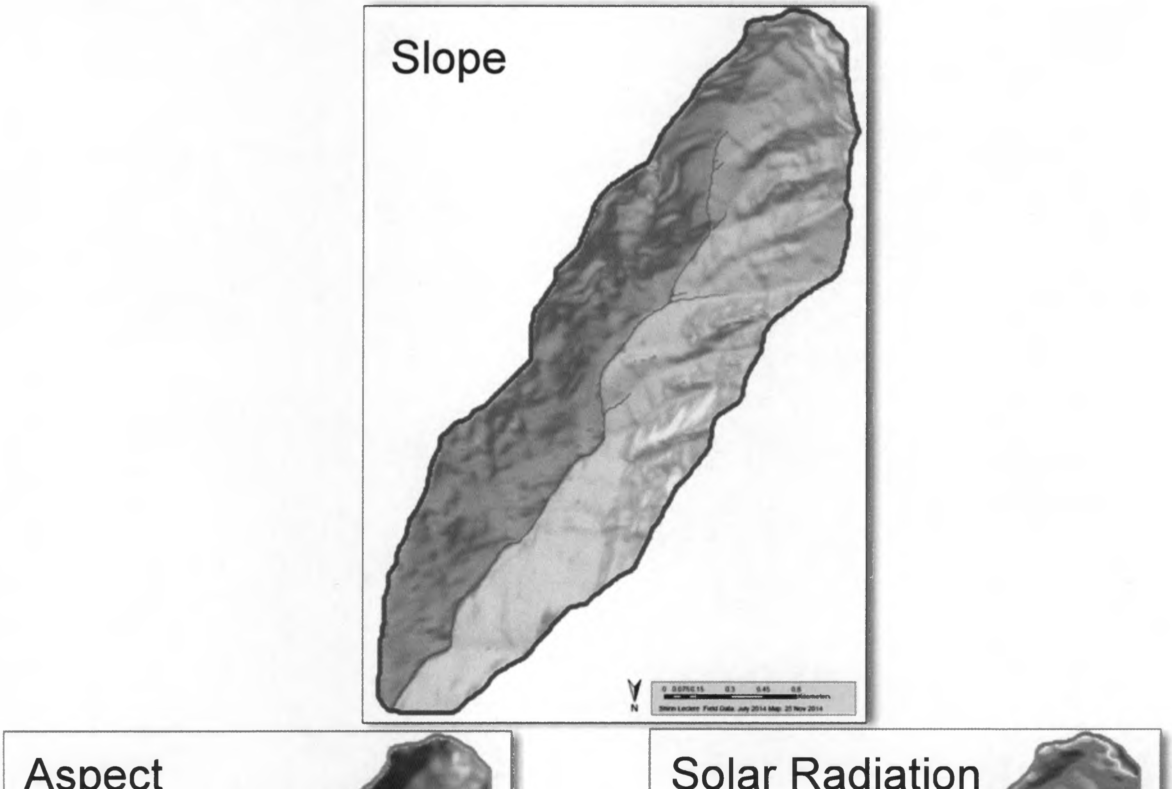

Figure 8 Exploratory maps for Slope Aspect and Solar Radiation. These stretched classification maps are the basis for the binned field maps Slope and Aspect. In order to emphasize the dramatic divide between the shady side of the watershed and the sunny side, aspect was selected over solar radiation.

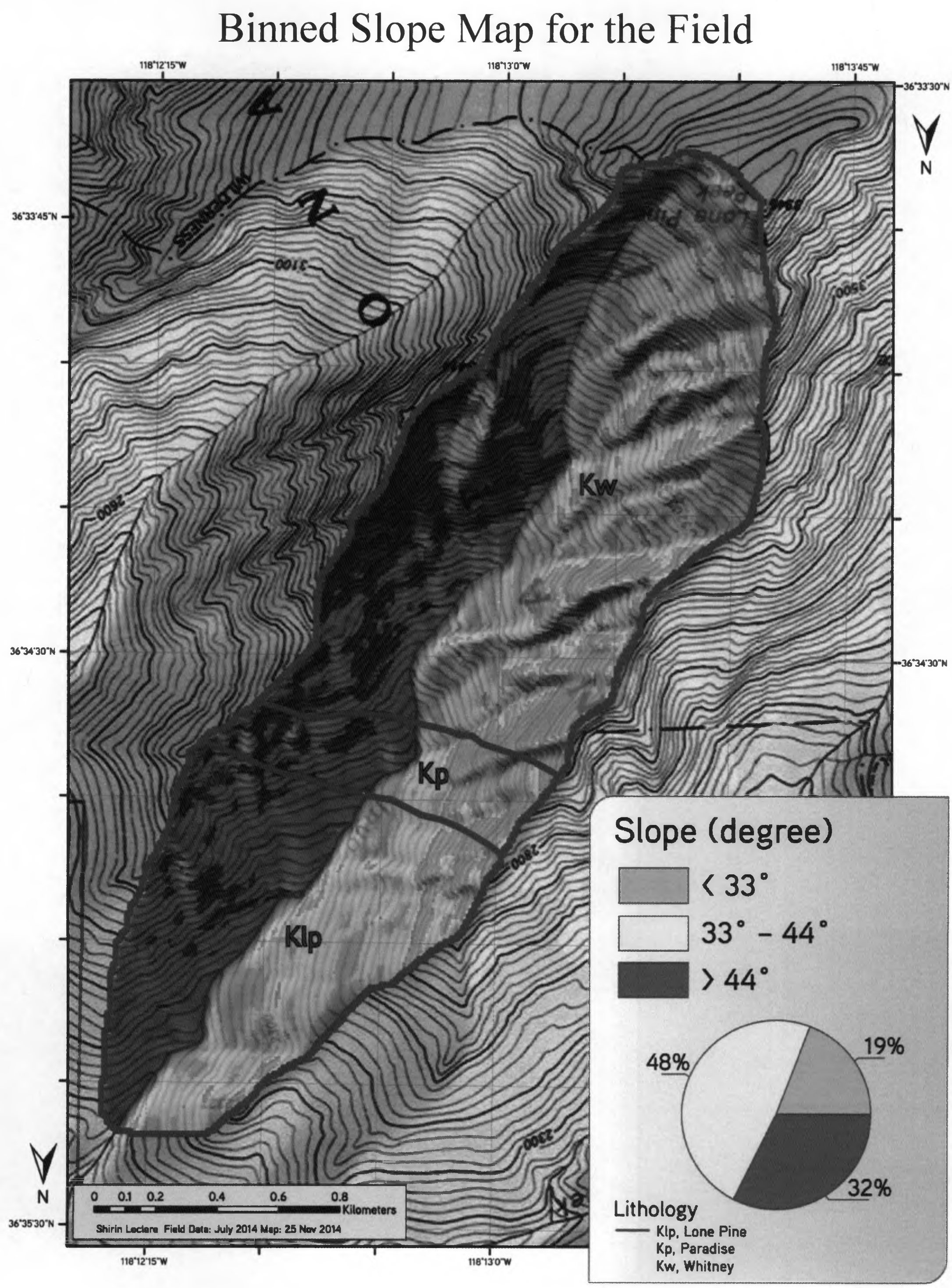

Figure 9. Field maps for slope with three classification bins on a topo map background . Inset, upper left, shows slope from a 10m USGS DEM in stretched classification to emphasize the lack of gentle slopes within the watershed..

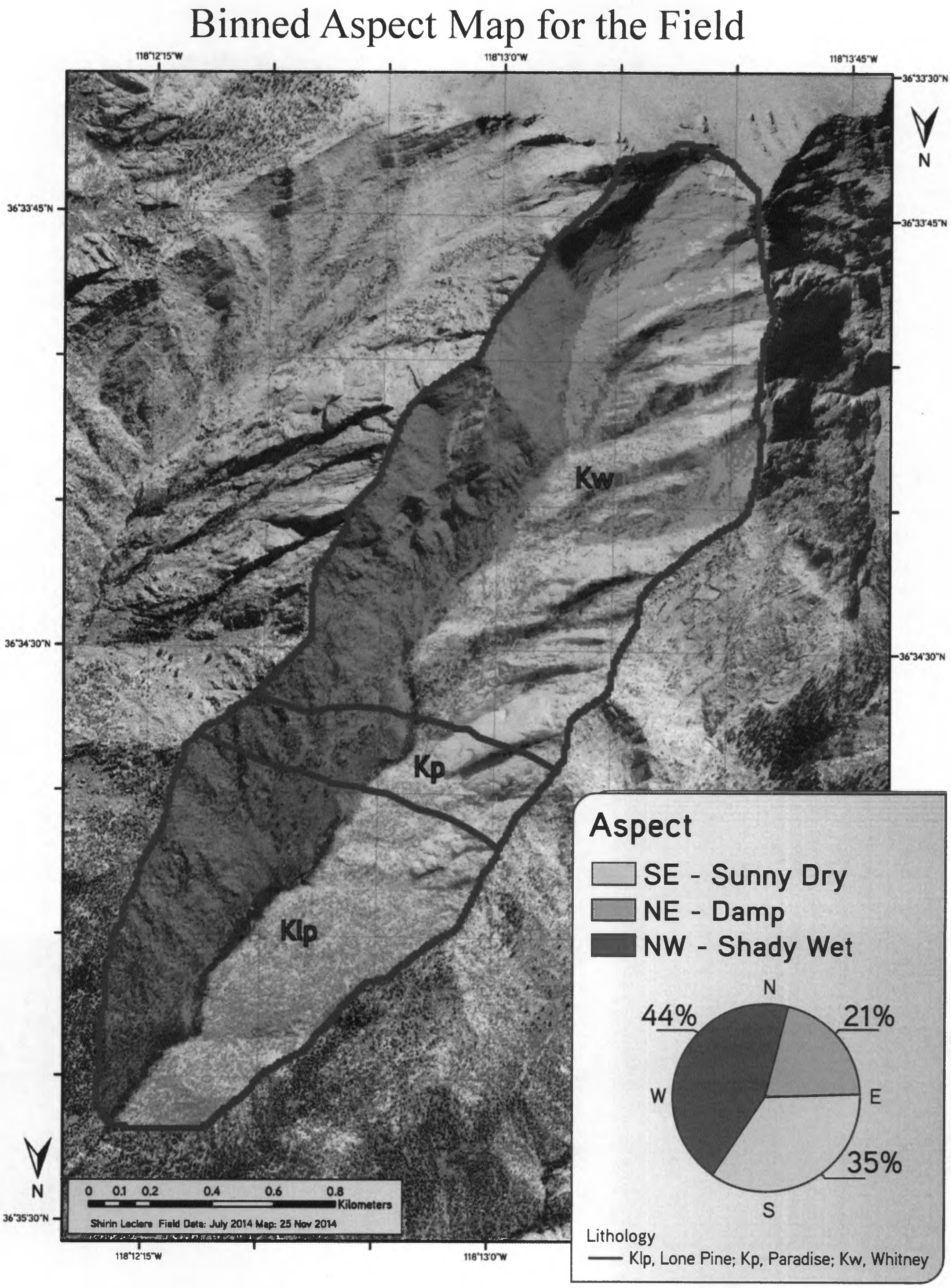

Figure 10. Field map of three bin classification of Aspect. This map is based on flow direction, used as a proxy because it created smoother more contiguous polygons, which illustrate the sharp divide between sunny and shady sides of this particular watershed.

Map from National Land Cover Database

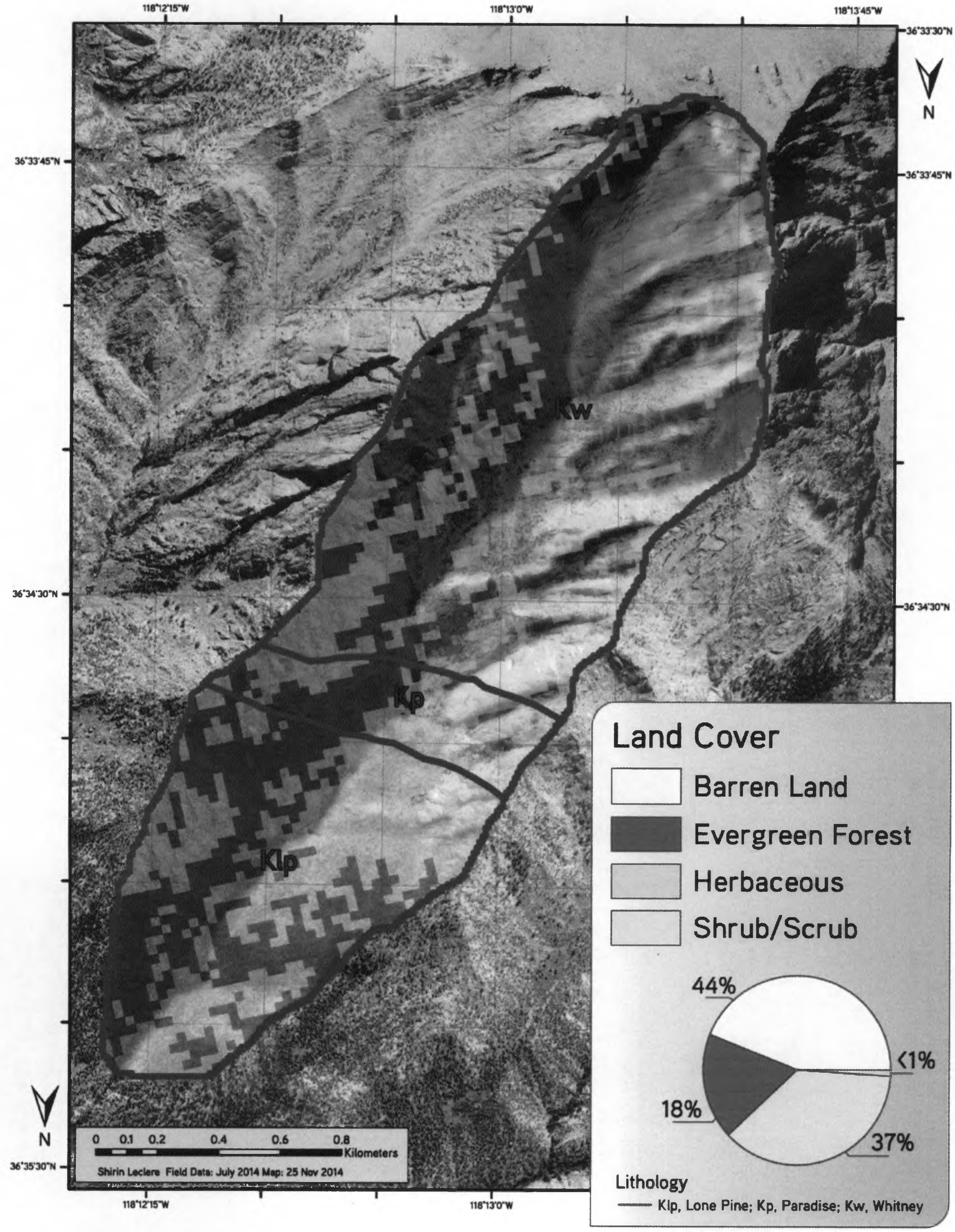

Figure 11. Original Land Cover Map. This map uses the publicly available, 30m resolution National Land Cover Database information and shows a division between Evergreen and Scrub/Shrub that did not match our field experience..

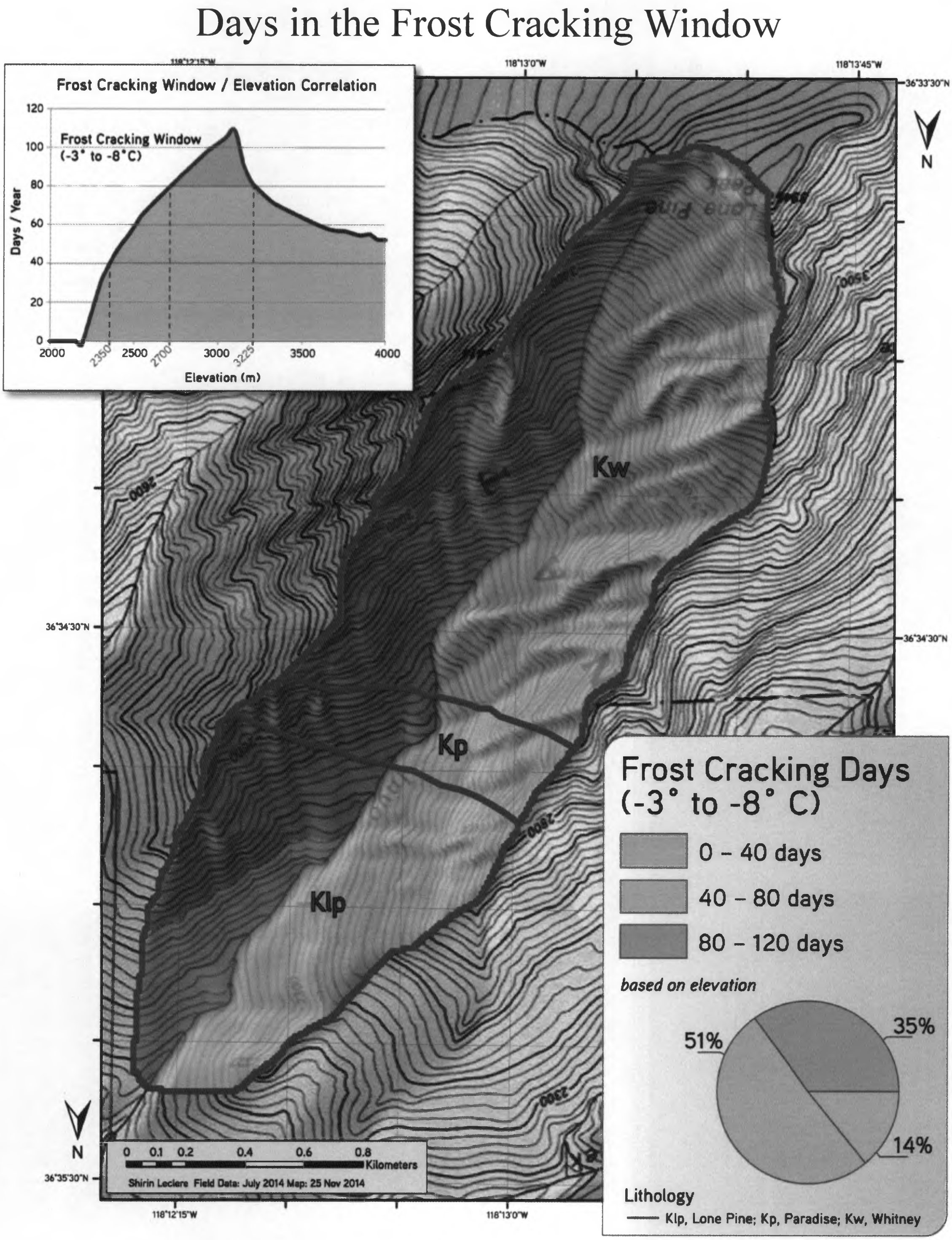

Figure 12. Map showing the number of days in the frost cracking window for various elevations of the Inyo Creek watershed. Note the "sweet spot" in blue, where the temperature is between -3°C and -8°C (ice crystals can grow because there is still mobile water available to add to the ice) more than 80 days a year.

Maps of Slope & Aspect Combine for Topographic Map

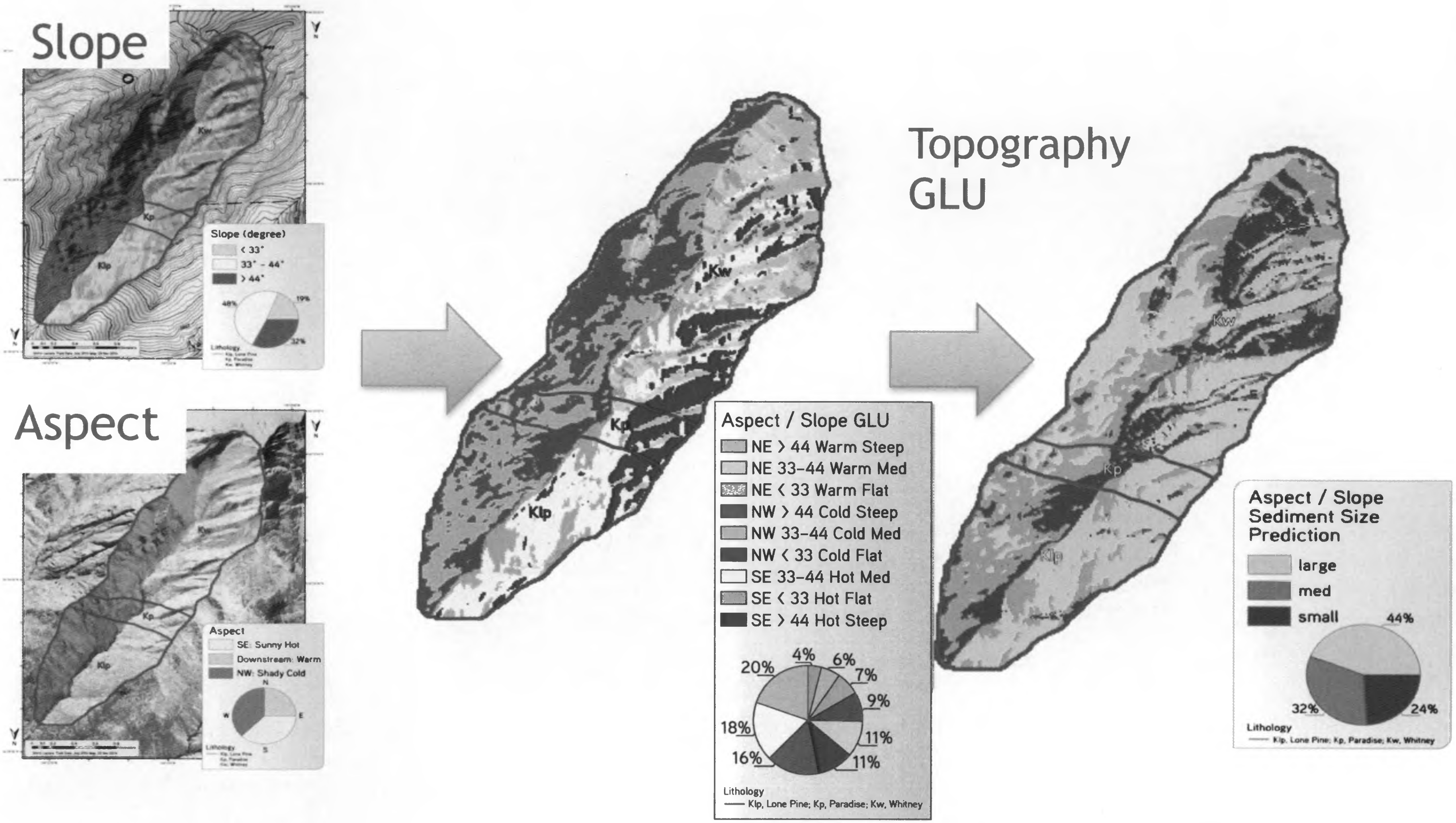

Figure 13. Slope & Aspect maps of 3 bins each, overlaid to create a 9 bin GLU map, which is then simplified to a 3 bin Topographic GLU map predicting small, medium, and large sediment size distributions across the watershed. Purple lines across watershed indicate 3 granodiorite formations of similar rock strength.

Maps of Frost Cracking Days & Vegetation Combine for Climatic Map

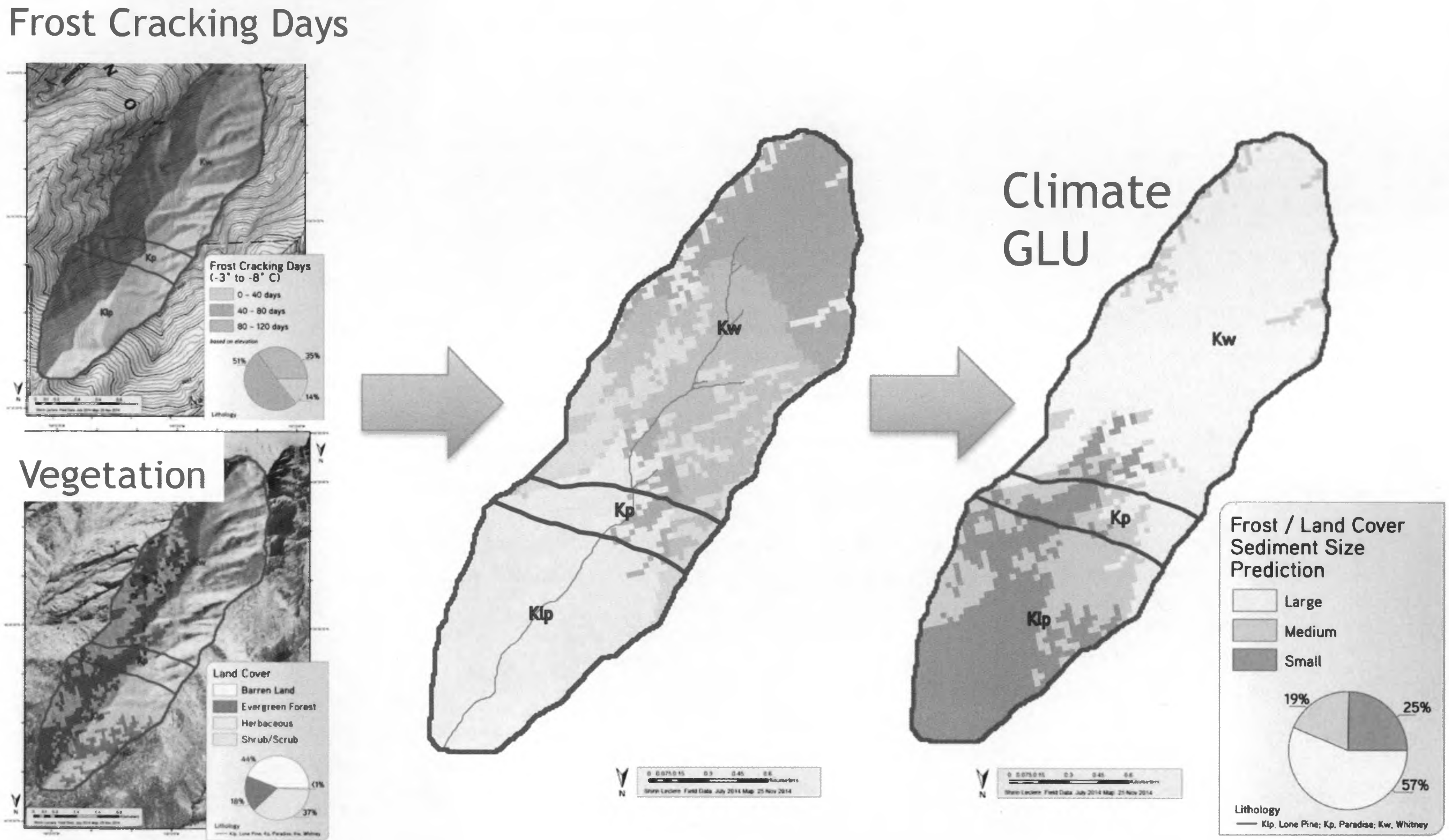

Figure 14. Similar to the Slope & Aspect maps, Frost Cracking Days and Vegetation maps of 3 bins each, overlaid to create a 9 bin GLU map, which is then simplified to a 3 bin Climatic GLU map predicting small, medium, and large sediment size distributions across the watershed. Purple lines across watershed indicate 3 granodiorite formations of similar rock strength.

Topographic & Climatic Maps Combine to Form a Sediment Size GLU Prediction Map

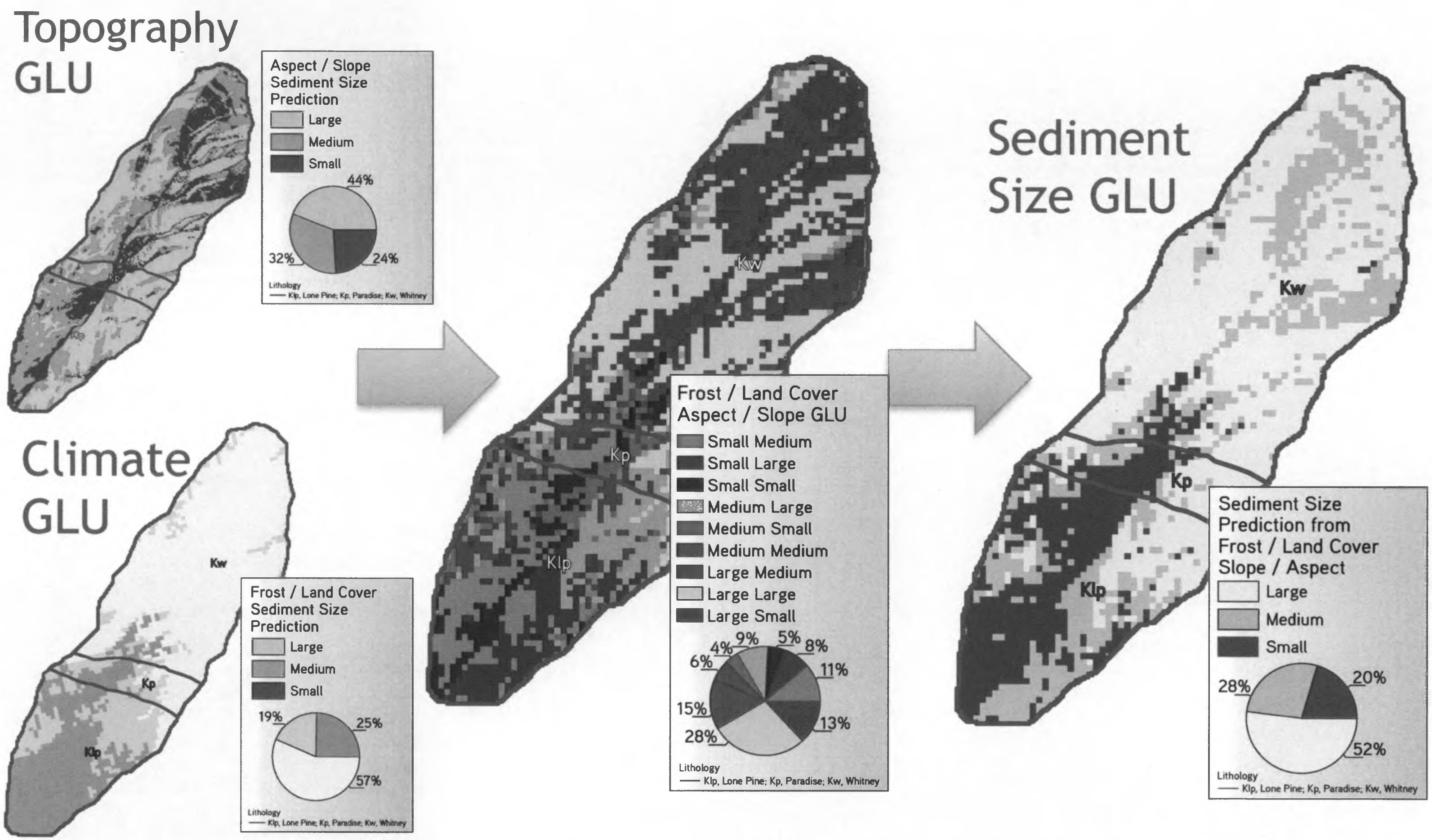

Figure 15. The resulting Topography and Climate maps of 3 bins each, are overlaid to create a 9 bin GLU map, which is then simplified to a 3 bin GLU map predicting small, medium, and large sediment size distributions across the watershed. Purple lines across watershed indicate 3 granodiorite formations of similar rock strength.

Creation of Alternative Land Cover Map

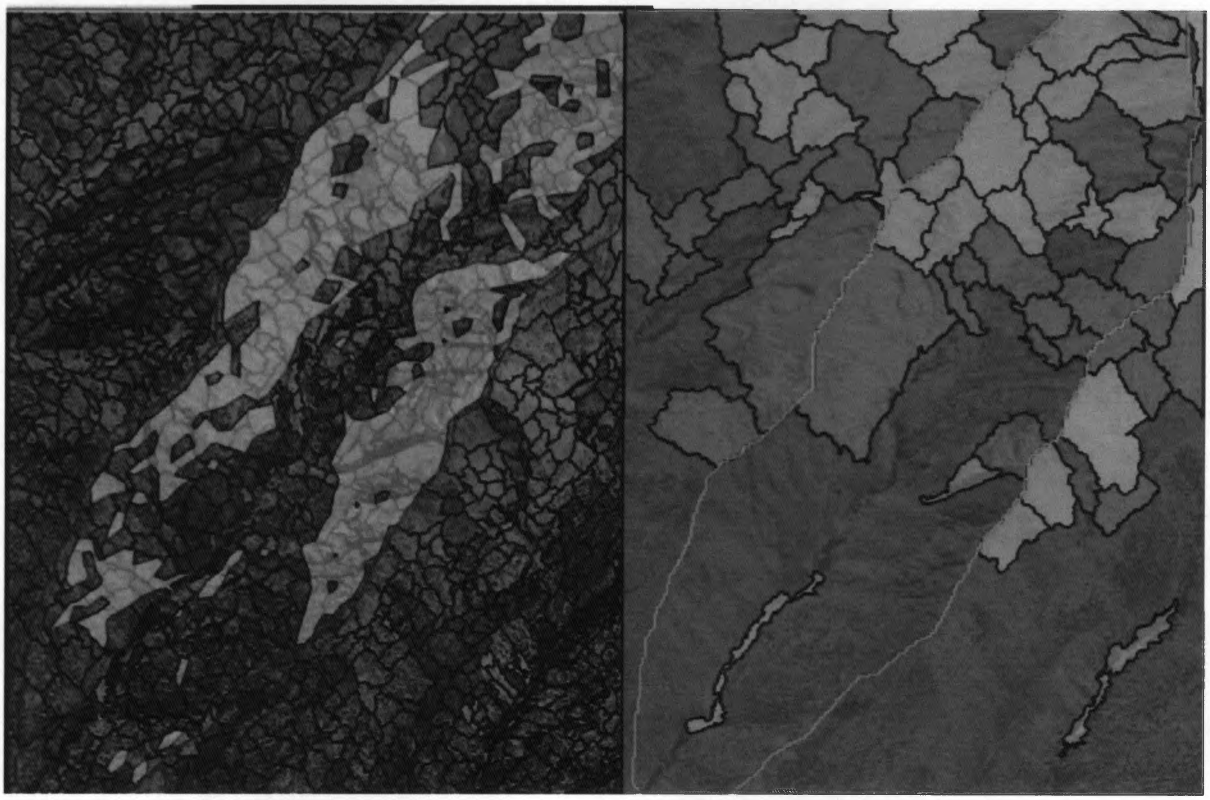

Figure 16. Detail of segmentation and classification in eCognition. A) Image on the left shows segmentation based on both color and texture and using small initial polygons. The dark red filled polygons in the lower left of the image have been classified as Riparian and merged. The small initial polygons were consistently patchy in this section. Pale overlay on the left shows a Thematic Layer created in ArcGIS to show the steepest slopes from 10m DEM. B) In progress detail of four land cover classifications (Riparian, Scrub/Tree, Tree/Rock, Bare Rock) from segmentation with larger initial polygons. In this image the Riparian section is the long thin grey polygon in the lower left of the image. The teal polygons are classified as Tree Rock and the grey as Bare Rock; these polygons are not yet merged. The olive areas are Scrub Tree polygons that have been classified and merged.

Comparison of Alternative Land Cover Maps

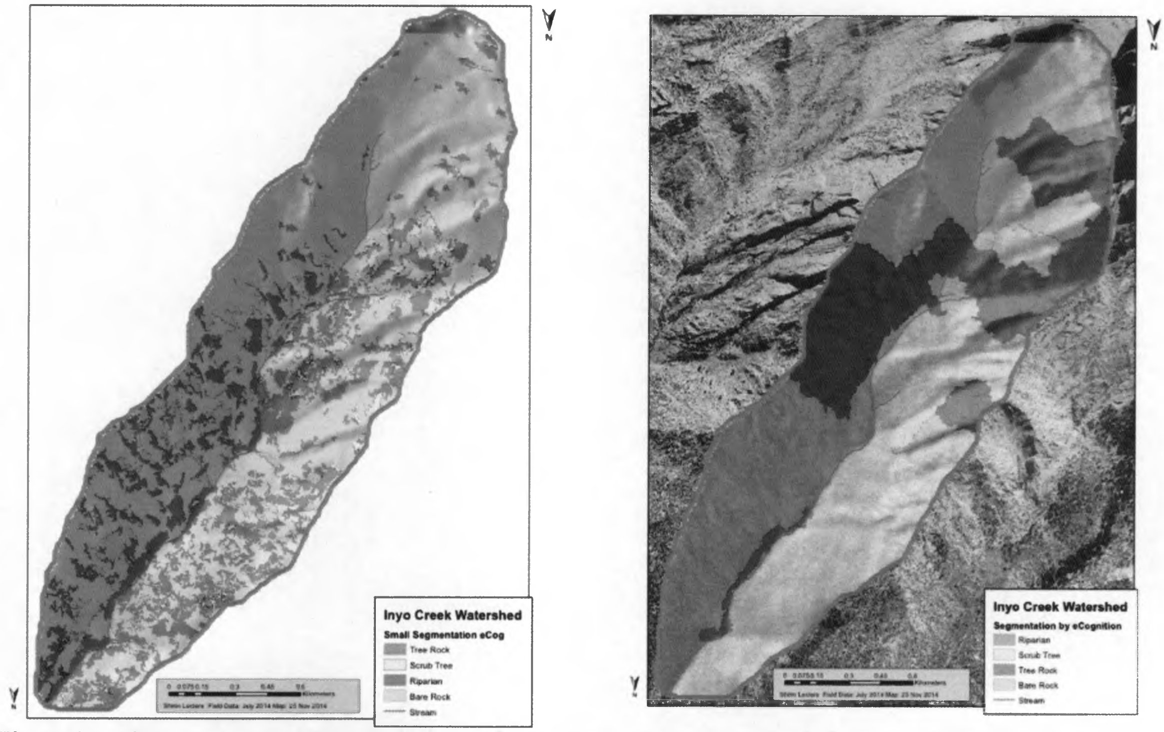

Figure 17. Alternate maps of the vegetation of Inyo Creek. The map on the left has small initial polygons. The map on the right has large initial polygons. Both are the result of eCognition Quick Map Mode techniques - Nearest Neighbor Classification and Segmentation using one Thematic Layer. Despite the apparent fine resolution of the small polygon map, it was inconsistent; the same polygon would be grouped with bare rock one time and scrub the next. the large polygon map proved to be more consistent in multiple classification trials in eCognition.

Alternative Land Cover Map

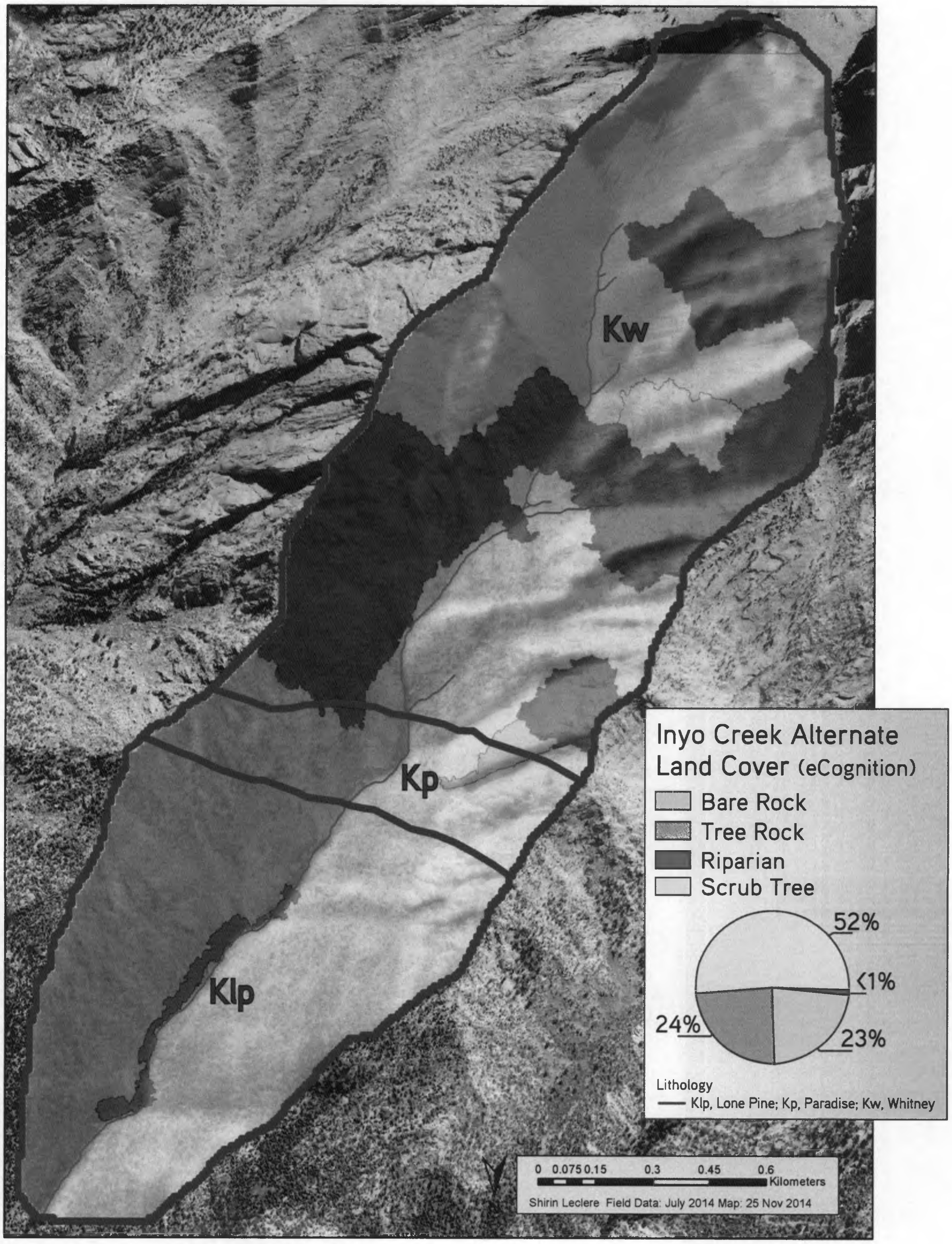

Figure 18. Alternative Land Cover Map created with eCognition software and NAIP Imagery. This map reflects the consistent mix of scrub and trees at lower elevations that the field team experienced rather than the patches of evergreen identified in the original NLCD map.

Alternative OBIA Land Cover, Climate, & GLU Maps

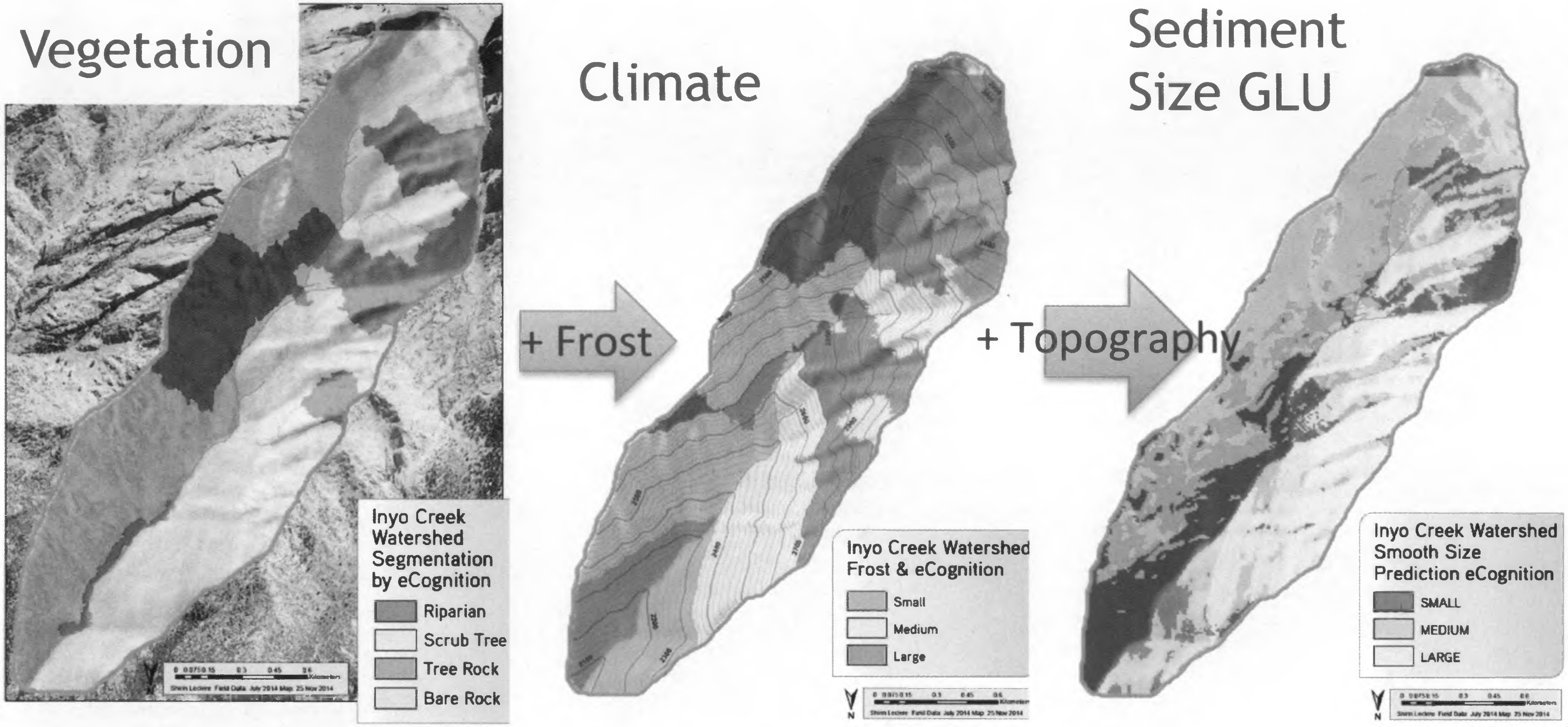

Figure 19. An alternative vegetation map would better represent the watershed because the NLCD distinction of Evergreen and Scrub/Shrub was not apparent when walking the watershed, instead the lower elevations were a consistent mix of trees and scrub while the higher elevations had patches of scattered evergreens. Replacing the NCLD map with an alternative vegetation map from a satellite NAIP image classified with eCognition produces the above maps for vegetation, climate and sediment size prediction GLU

Comparing Original and Alternative GLU Maps

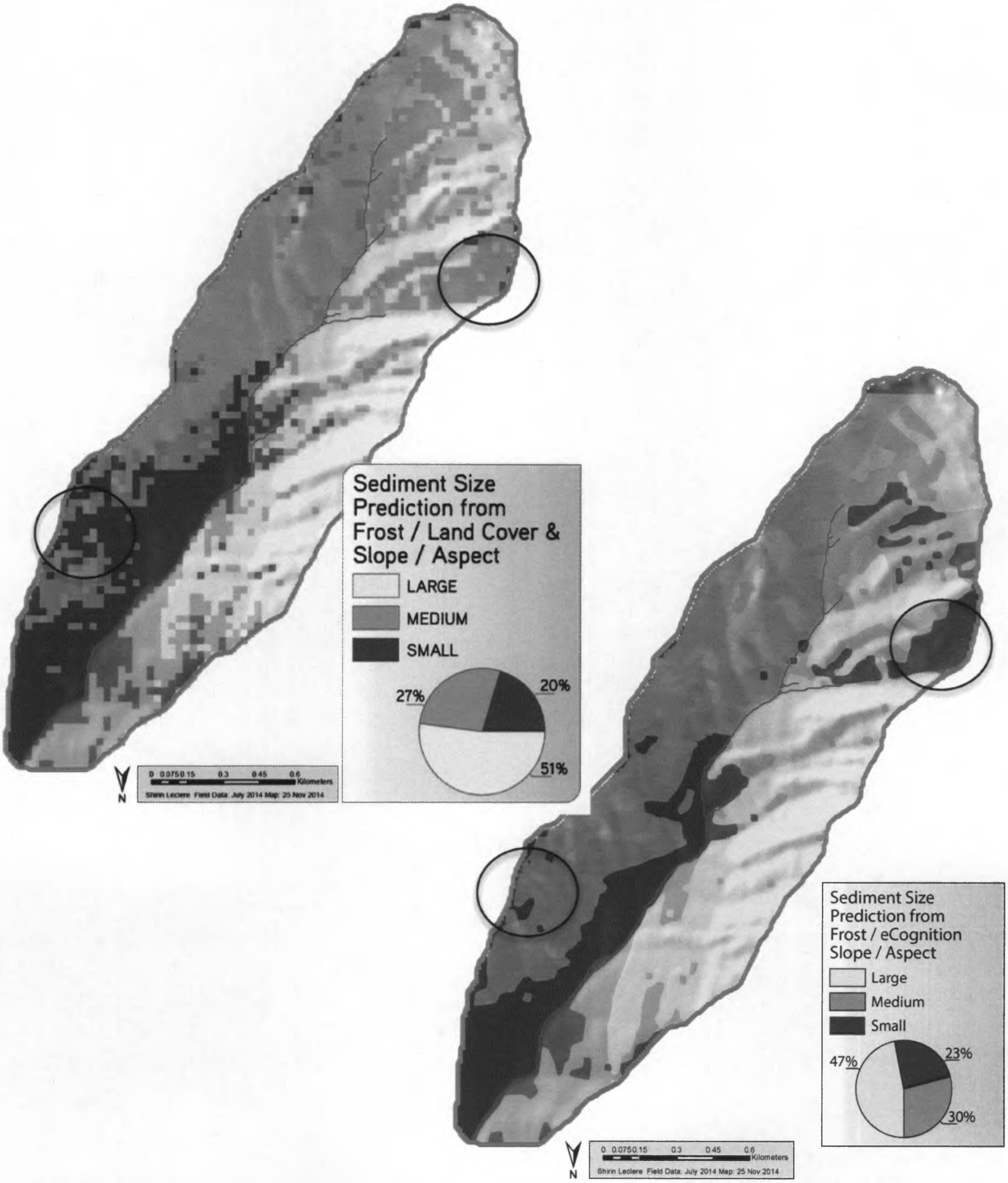

Figure 20. Comparing the GLU Maps. The upper left map is the original GLU map taken into the field . The lower right map is the new GLU map using the alternative OBIA land cover map from eCognition software and NAIP imagery rather than the NLCD data. Note that both maps have roughly the same percentages of sediment size distributions. The red circles highlight areas where the predictions differ.

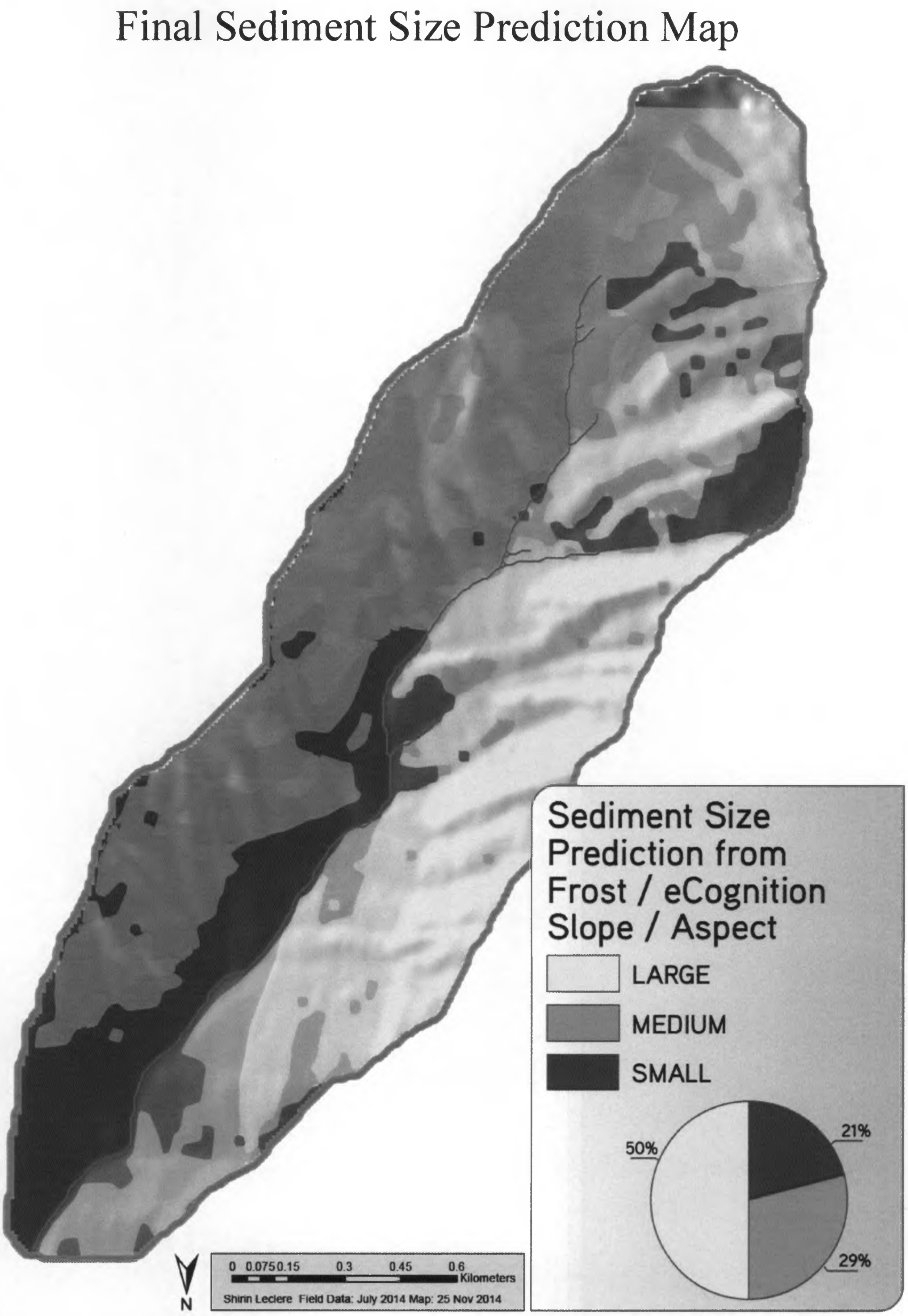

Figure 21. Final Sediment Size Distribution GLU Map. This map predicts the location of Small, Medium, and Large sediment size distributions throughout Inyo Creek watershed. Note that this map has been smoothed with the standard ArcGIS smoothing function.

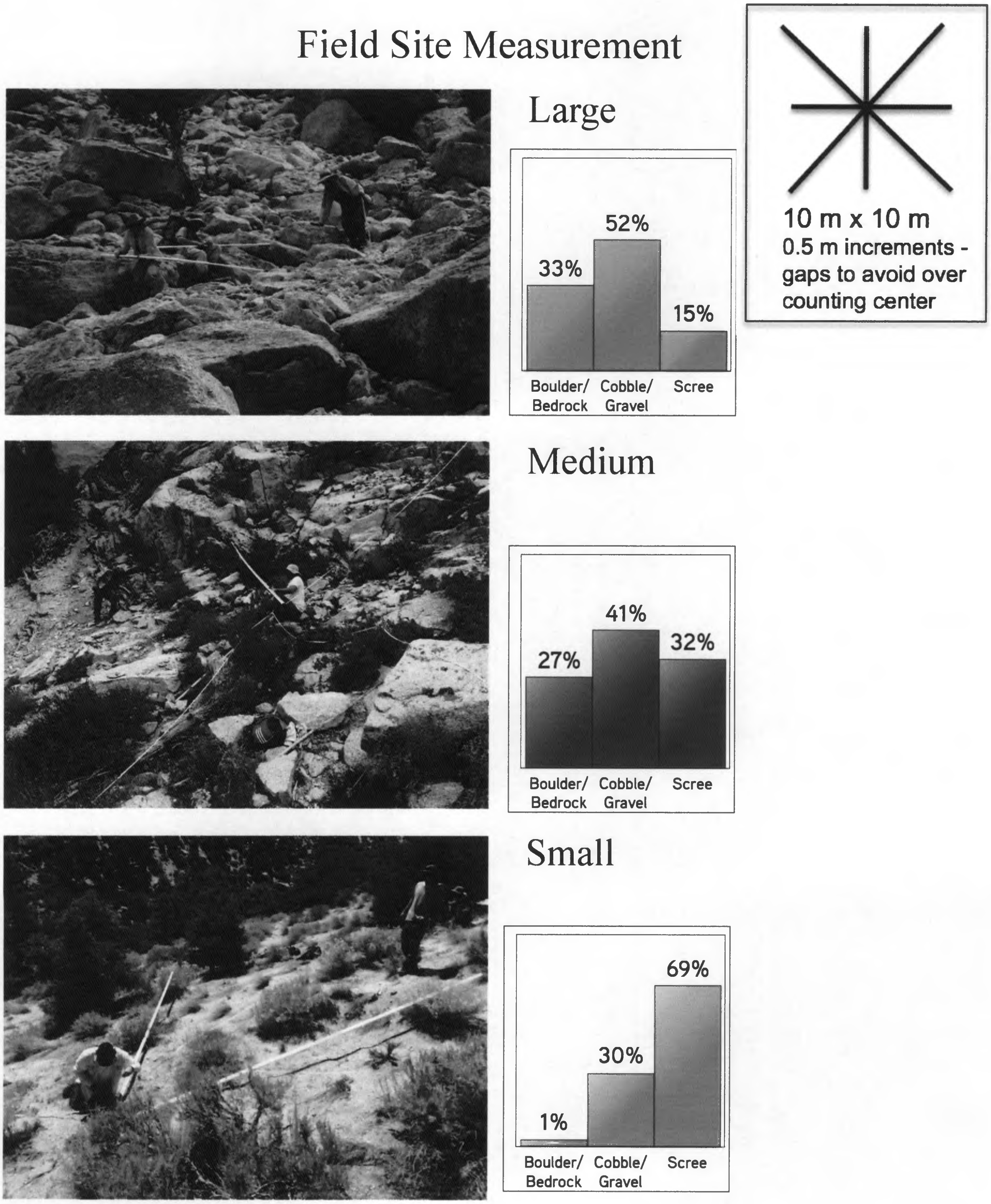

Figure 22. Examples of Small, Medium, & Large field sites with histograms showing percentages of boulders, cobbles & gravel, and scree-sized particles. Inset in upper right shows the pebble count variation – an asterisk was chosen instead of a grid pattern to minimize disruption of surface as we measured and to improve safety on steep talus slopes.

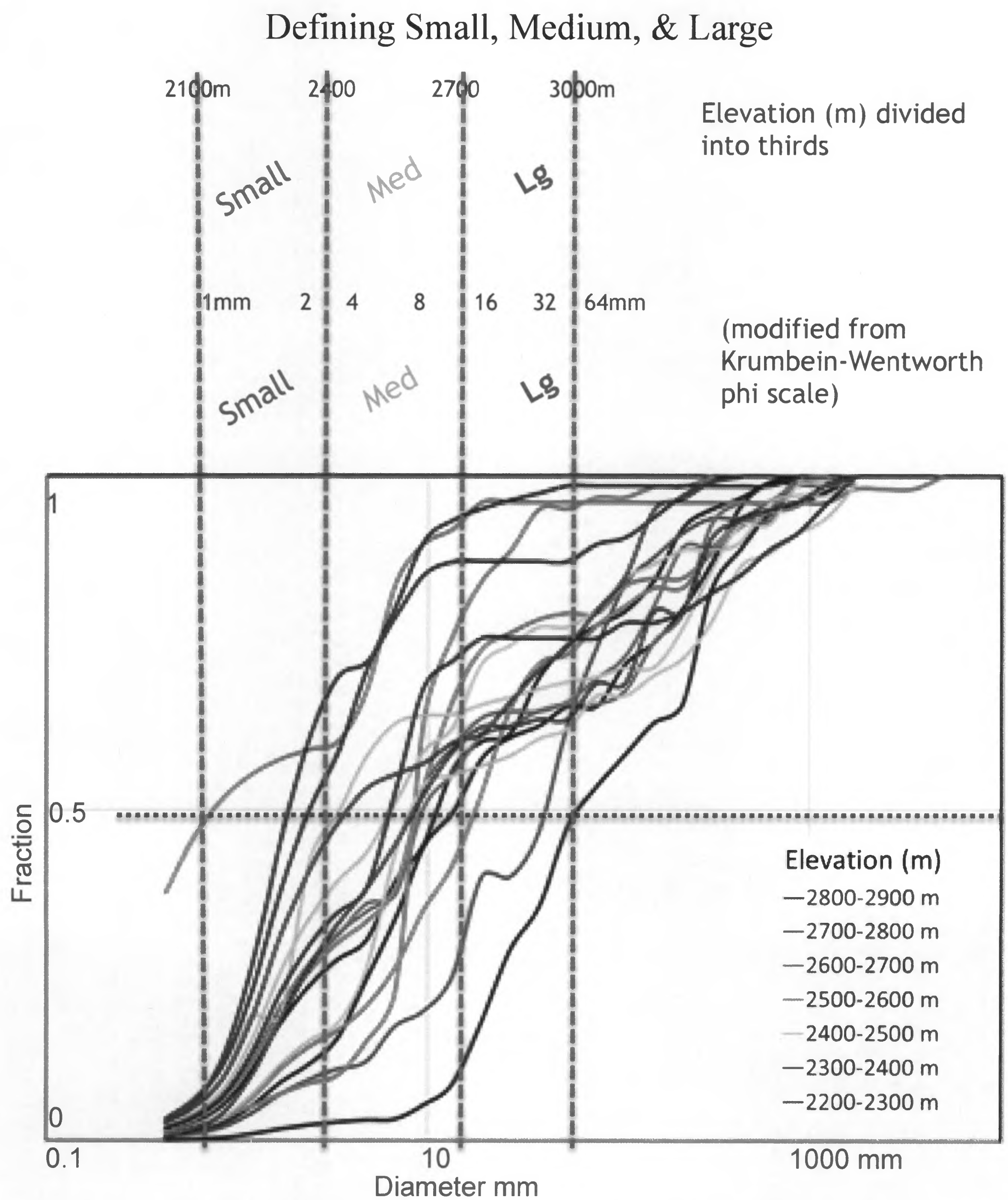

Figure 23. Defining Small, Medium, and Large. From the top, dividing the accessible elevation range into thirds to assign relative size predictions by elevation alone. Dividing the range of measured d50 (median particle size) values from the 19 field sites into thirds using the Wentworth-Krumbein Phi scale (to account for the higher frequency of small particle sizes found in standard pebble counts). Establishing the range of d50 values from the cumulative density function plot of field and sieve measurements. CDF plot byJennifer Genetti.

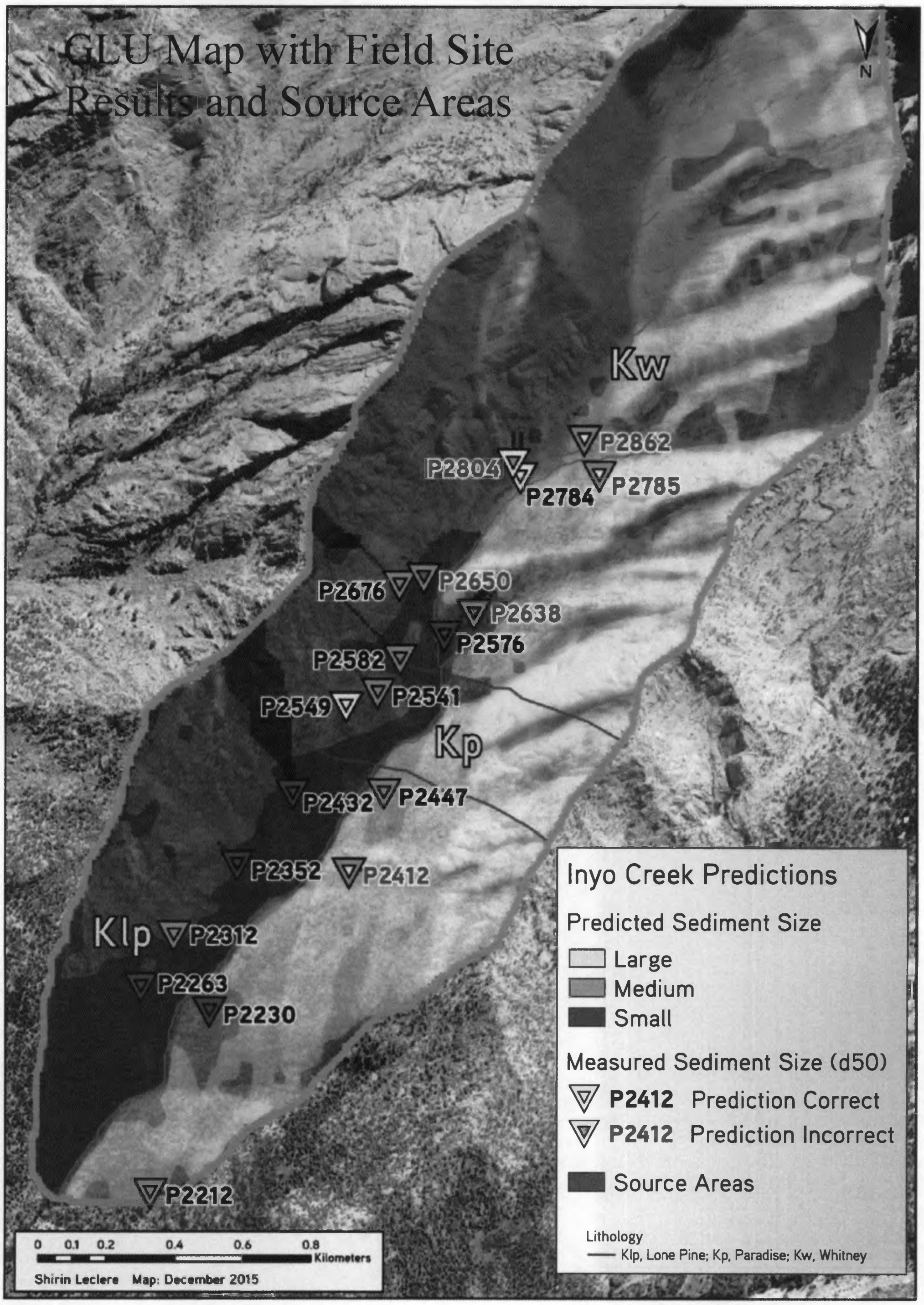

Figure 24. Locations of Field Sites. The site id values (P####) indicate the elevation in meters. The triangles show the measured d50 size (large triangle) and the predicted size (small triangle inside the larger triangle). The red site ids indicate that the prediction did not match the measured value. The brown polygons on the map show the potential source areas for rocks at each sample site using the ArcGIS function – *watershed.*

Data from Field Sites and Attribute Maps

Site_ID elevation (m)	Latitude	Longitude	Measured d50 mm	Measured d50 Bin	Predicted Elevation bin	Predicted GLU Bin	Lithology	Alternate LandCover	Alt LC Bin	NLCD	NLCD Bin	Frost Days	Slope (degree)	Slope Bin	Aspect	Aspect Bin	How Attributes Explain Prediction
P2212x	36.58878	-118.20583	6.27	2	1	2	Klp	Scrub	2	Scrub	2	0-40	36.3	2	E	3	SE-facing drier and med steep = increase in predicted size
P2230x	36.58463	-118.20742	2.37	1	1	1	Klp	Scrub	2	Scrub	2	0-40	25.8	1	E	3	SE-facing drier but flat = no increase in predicted size
P2263	36.58410	-118.20548	2.63	1	1	1	Klp	Scrub	2	Evergreen	1	0-40	39.2	2	NW	1	as predicted
P2312	36.58291	-118.20639	8.49	2	1	2	Klp	Scrub	2	Evergreen	1	0-40	45.4	3	NW	1	steep slope = increase in size
P2350	36.58130	-118.20817	3.81	1	1	1	Klp	Scrub	2	Scrub	2	40-80	32.9	1	NW	1	NW-facing and flat = as expected
P2412x	36.58145	-118.21127	8.34	2	2	3	Klp	Scrub	2	Scrub	2	40-80	36.9	2	E	3	drier and med steep should be an increase; note this site is near elevation/frost bin boundaries
P2432	36.57970	-118.20966	3.42	1	2	1	Klp	Scrub	2	Evergreen	1	40-80	23.8	1	N	1	very flat = decrease in predicted size
P2447x	36.57966	-118.21222	6.37	2	2	2	Klp	Scrub	2	Scrub	2	40-80	31.7	1	E	3	flat dry balances out
P2541	36.57741	-118.21201	8.45	2	2	2	Kp	Scrub	2	Evergreen	1	40-80	40.8	2	NW	1	med wet as expected
P2549	36.57771	-118.21113	17.5	3	2	3	Kp	Scrub	2	Evergreen	1	40-80	47.3	3	N	1	steep increases predicted size
P2576x*	36.57611	-118.21386	1.06	1	2	1	Kw	Scrub	2	Scrub	2	40-80	39.5	2	NE	2	site is in channel. Note: only site with moderate (NE) aspect
P2582	36.57665	-118.21262	8.74	2	2	2	Kw	Scrub	2	Evergreen	1	40-80	35.4	2	NW	1	med wet as expected
P2637x	36.57562	-118.21467	11.87	2	2	1	Kw	Scrub	2	Evergreen	1	40-80	29.2	1	N	1	flat and N-facing (grouped with wet NW-facing)
P2650	36.57482	-118.21325	9.37	2	2	1	Kw	Tree	1	Evergreen	1	40-80	40.0	2	NW	1	wet not as steep must have been a grid choice for med-med to go sm and for a sm-lg to go medium
P2676	36.57499	-118.21258	8.78	2	2	2	Kw	Tree	1	Evergreen	1	40-80	45.8	3	NW	1	NW-facing wet and tree should be a decrease; near elevation bin boundary
P2784*	36.57251	-118.21591	40.69	3	3	3	Kw	Tree	1	Bare	3	80-120	41.6	2	N	1	outlier
P2804*	36.57223	-118.21571	61.89	3	3	2	Kw	Tree	1	Bare	3	80-120	39.0	2	N	1	outlier; should be same prediction as above
P2862x	36.57169	-118.21769	11.48	2	3	3	Kw	Scrub	2	Scrub	2	80-120	28.6	1	E	3	flat; prediction should be medium
P2875x	36.57248	-118.21812	13.62	2	3	3	Kw	Scrub	2	Bare	3	80-120	35.7	2	E	3	hot and scrub; prediction wrong

Table 2. Individual Site Analysis. Data from field measurements (d50 in mm) and GLU map for 19 field sites. Site ID is based on elevation (m), x indicates north side of channel and * indicates the three outliers determined by Cook's D analysis. Bin categorizations are shown as 1 = Small, 2 = Medium, 3 = Larger relative sediment size expected.

Binomial Distribution Results

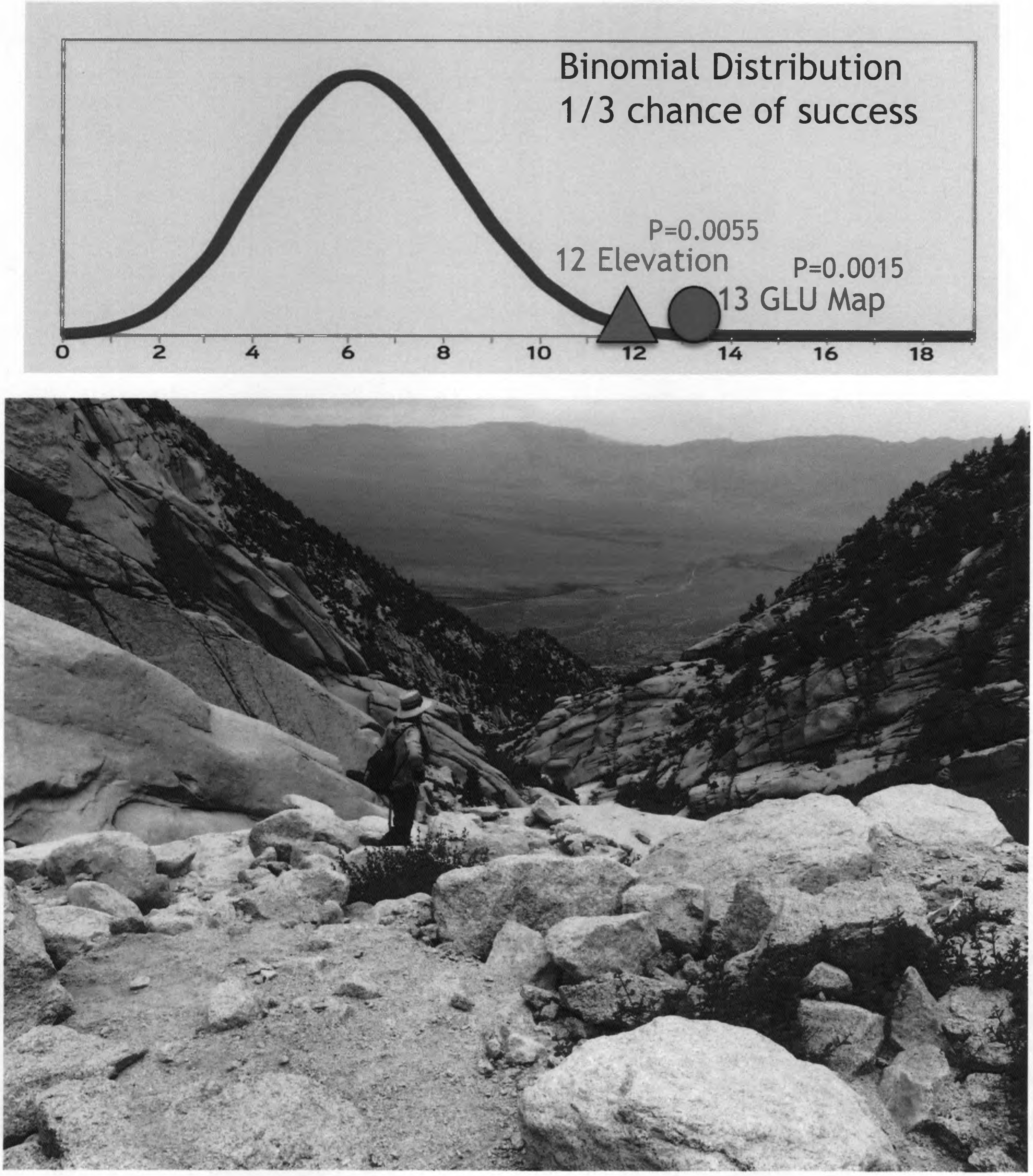

Figure 25. Binomial Distribution Analysis of GLU and Elevation predictions. The GLU map accurately predicted the relative sediment size at 13 sites (p = 0.0015). Elevation alone predicted 12 sites correctly (p = 0.0055).

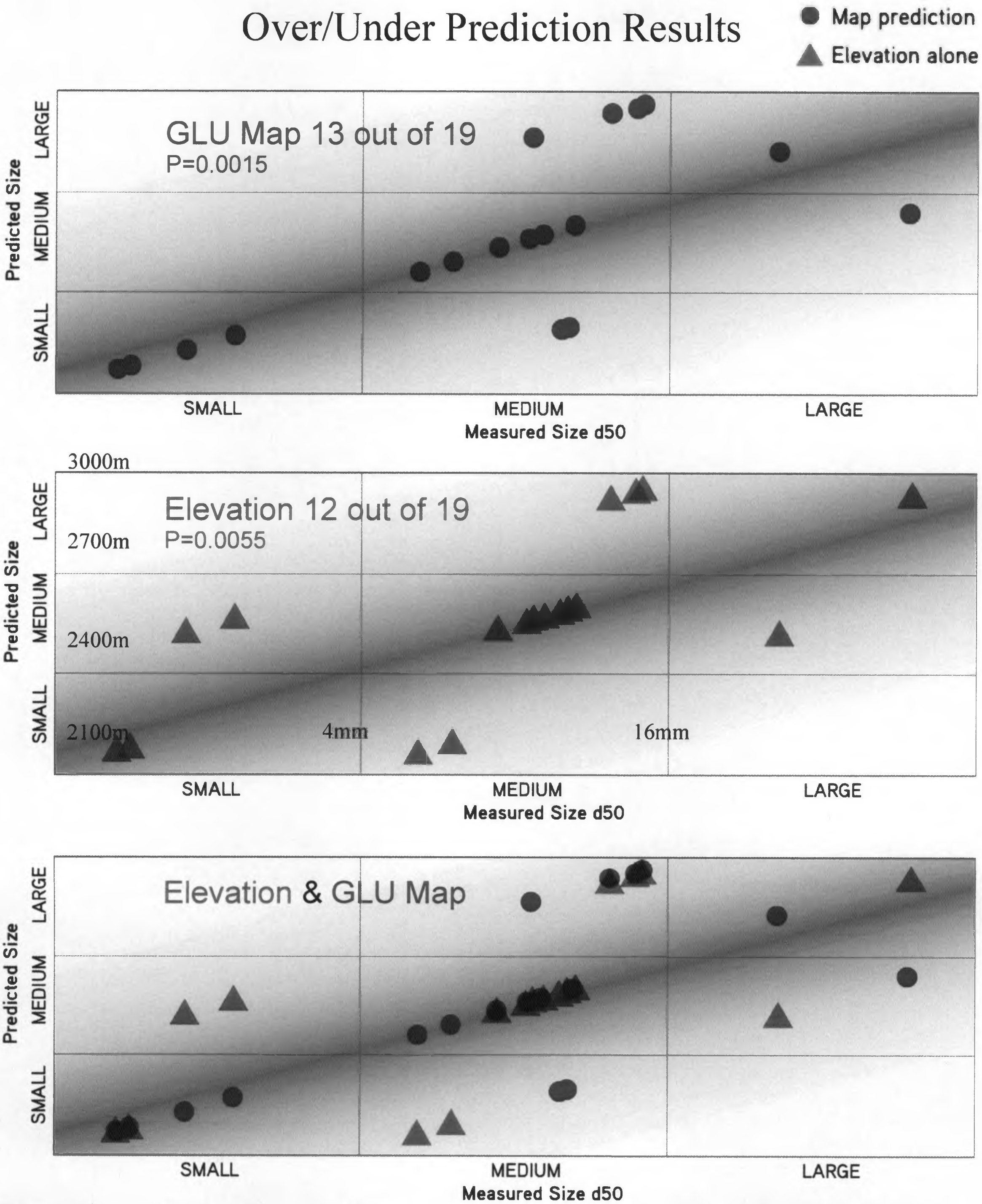

Figure 26. Individual Sites Plotted for Accuracy of Prediction to Measured d50 Values. Each plot shows the predicted size category correlated with the size category determined by the measure d50 values at each of 19 sites, within each grid cell the points are located relative to each other in proportion to their elevation. The diagonal line highlights the large number of accurate predictions. The bottom plot shows both the GLU prediction and the elevation prediction.

Potential Source Areas for Sediment Influx to Field Sites

Site Id - elevation (m)	Source area (pixels)	Avg GLU Source	Matches? GLU/d50	GLU at Site	Measured d50 bin	Source improves prediction?
P2212x	13	1.38	N/N	2	2	no
P2230x	2	1.00	Y/Y	1	1	
P2263	2	1.00	Y/Y	1	1	
P2312	4	1.75	Y/Y	2	2	
P2350	6	2.00	N/N	1	1	no
P2412x	9	2.56	Y/N	3	2	not enough
P2432	423	2.42	N/N	1	1	no
P2447x	2	2.00	Y/Y	2	2	
P2541	11	2.18	Y/Y	2	2	
P2549	4	3.00	Y/Y	3	3	
P2576x*	36	1.31	Y/Y	1	1	
P2582	16	1.69	Y/Y	2	2	
P2637x	11	1.36	Y/N	1	2	not enough
P2650	7	2.00	N/Y	1	2	yes
P2676	94	1.99	Y/Y	2	2	
P2784*	12	2.17	N/N	3	3	no
P2804*	9	2.11	Y/N	2	3	not enough
P2862x	4	2.50	Y/N	3	2	not enough
P2875x	1	3.00	Y/N	3	2	no

Table 2. Measurements of potential source areas (subwatersheds) for each field site and the possible changes to the accuracy of GLU prediction if source areas were included in prediction. In general, while some predictions would have improved only one would have improved enough to actually change the value of the predicted bin (1-Small, 2-Medium, 3-Large)

Bedrock Boundaries Against Binned Slope Field Map

Figure 27. Bedrock boundaries on original Slope field map. The different colored lines represent different methods for determining bedrock boundaries from walking along the edges in the field to analyzing satellite imagery in Google Earth and Arc GIS.

Multivariate Correlations

	lnd50	Frost5m_norm	weather	Elev_Norm	Slope_Norm	ASp110	Solar_Norm
lnd50	1.0000	0.7220	-0.7367	0.7219	0.4530	0.0278	-0.2717
Frost5m_norm	0.7220	1.0000	-0.9933	0.9790	0.0787	-0.0762	-0.2585
weather	-0.7367	-0.9933	1.0000	-0.9944	-0.0672	0.0248	0.2122
Elev_Norm	0.7219	0.9790	-0.9944	1.0000	0.0425	0.0306	-0.1560
Slope_Norm	0.4530	0.0787	-0.0672	0.0425	1.0000	-0.5080	-0.6541
ASp110	0.0278	-0.0762	0.0248	0.0306	-0.5080	1.0000	0.9319
Solar_Norm	-0.2717	-0.2585	0.2122	-0.1560	-0.6541	0.9319	1.0000

Scatterplot Matrix

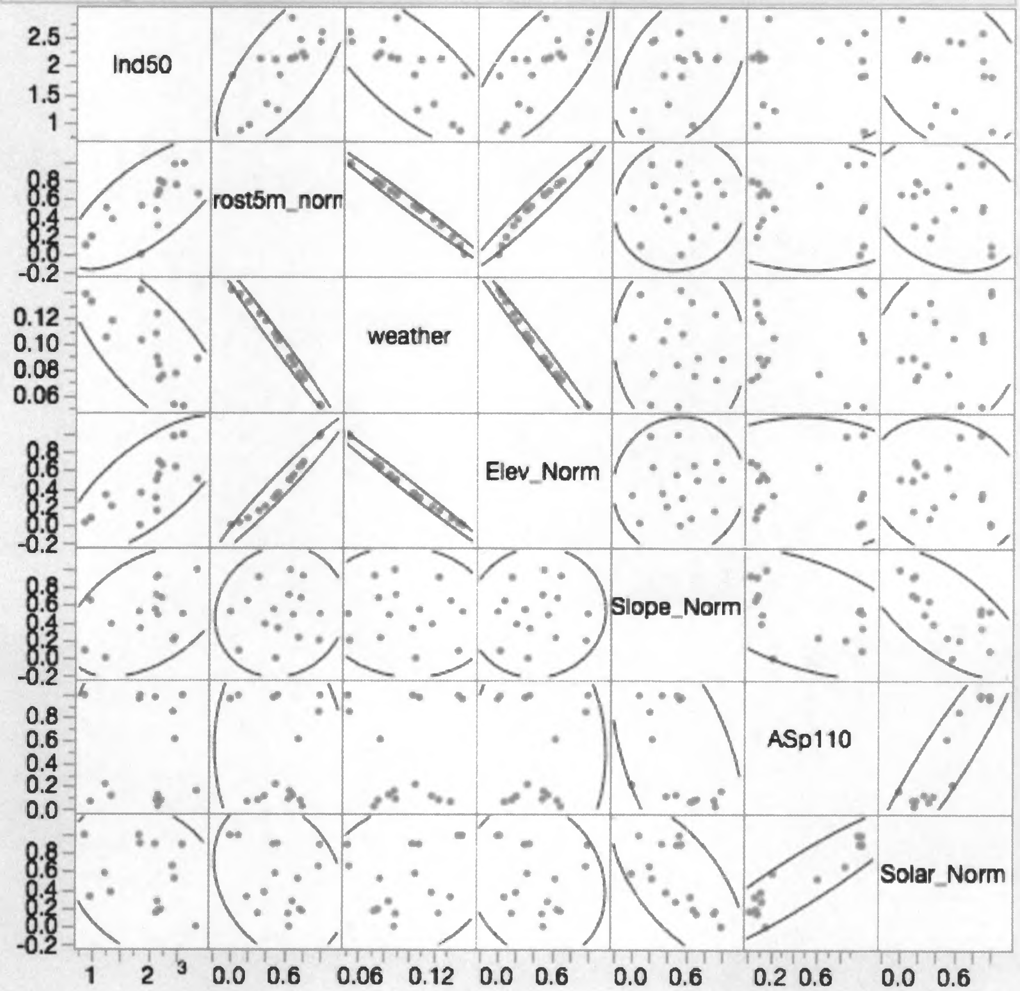

Figure 28. Multivariate Correlation Analysis of Landscape Attributes and the Measured d50 Values. Sediment size is represented logarithmically by LnD50. All the attribute values have been normalized. Azimuth values for aspect were normalized using a cosine function offset by 135° to reflect the highest solar insolation on the southeast face.

Individual Attributes Correlated with Sediment Size

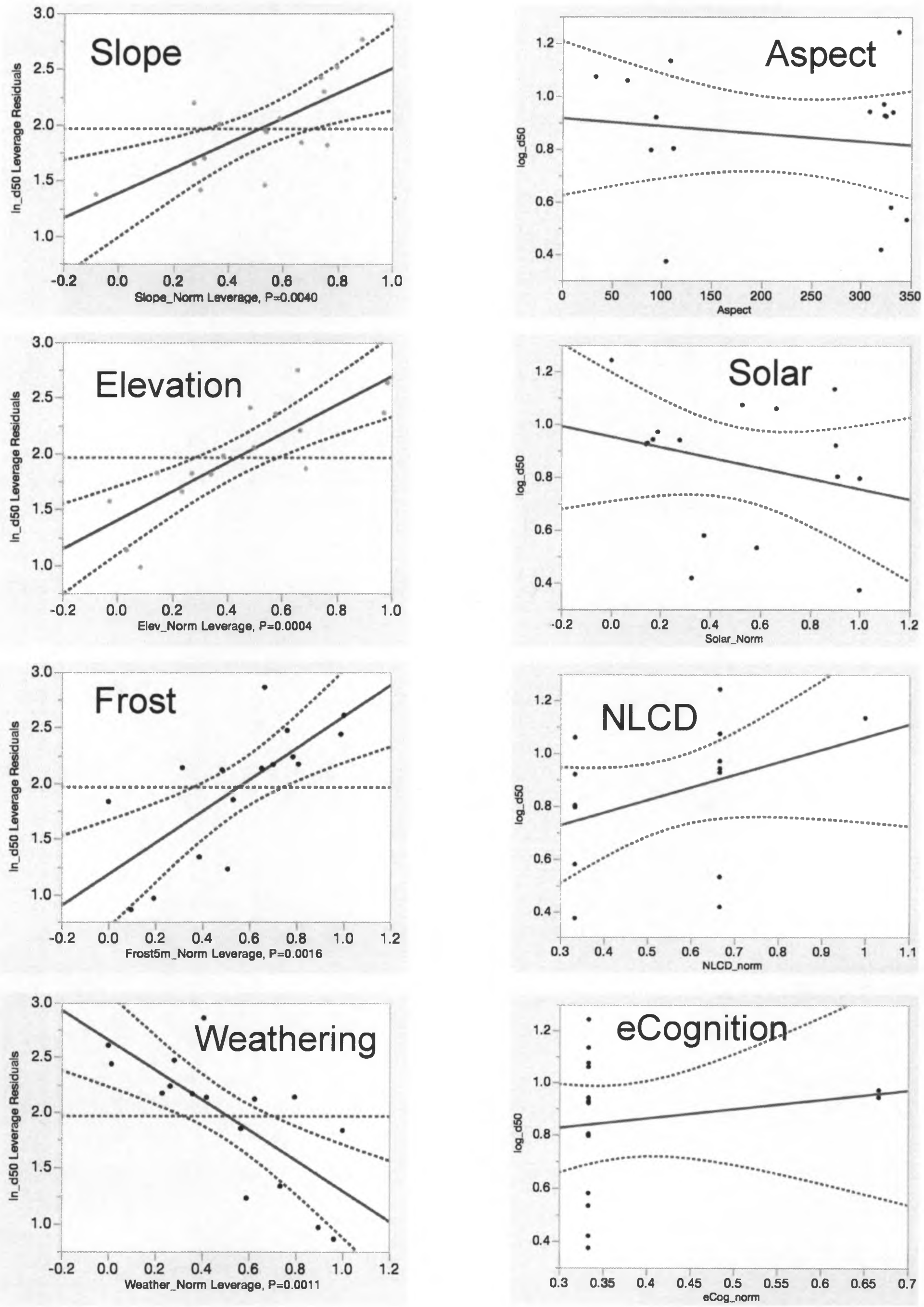

Figure 29. Correlations of various attributes with sediment sizes recorded at Inyo Creek. Note that Frost and Weathering are models based on Elevation and other climate variables. NLCD and eCognition are the two land cover mapping values from the National Land Cover Database and from a satellite image classified using the eCognition software.

Correlations with Sediment Size

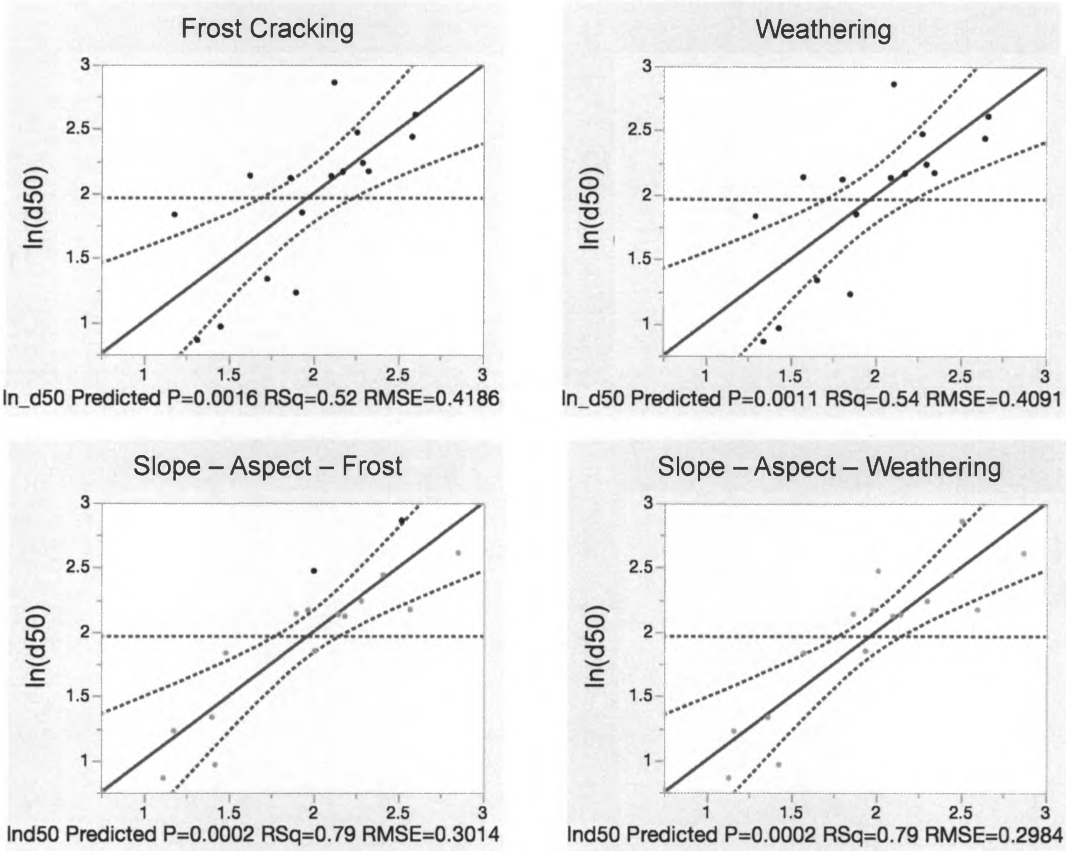

RSquare	RMSE	Prob> F
0.79	0.3014	0.0002

Term	Coefficient	Prob>|t|
Intercept	0.3618416	0.2116
Slope_Norm	1.1547339	0.0024*
Aspect110	0.5246428	0.0295*
Frost5m_Norm	1.3832952	0.0002*

RSquare	RMSE	Prob> F
0.79	0.2984	0.0002

Term	Coefficient	Prob>|t|
Intercept	2.5806434	<.0001*
Slope_Norm	1.1275677	0.0027*
Aspect110	0.4653275	0.0469*
Weather_Norm	-1.309772	0.0002*

Figure 30. Best Fit Models of landscape attributes correlated with the natural log of the d50 values for 16 field sites. **A)** Correlation of Frost Cracking Days with ln(d50) R-squared = 0.52 **B)** Correlation of Weathering function with ln(d50) R-squared = 0.54 **C)** Slope, Aspect, & Frost Cracking Days function, R-squared = 0.79 **D)** Slope, Aspect, & Weathering function R-squared = 0.79. Adjusted R-squared values are slightly lower for all correlations. Note that both Frost and Weathering functions include elevation in their formulation, elevation alone correlated with an R-squared = 0.52.

Multivariate Fit Model Analyses

derived from 16 of the 19 points, outliers removed after Cook's D analysis

Name	RSquare	RSquare Adj	Prob>F	Term	Estimate	Prob>|t|	Equation
Aspect	0.000775	-0.0706	0.9185	Intercept	1.947642	<.0001	Ln(D50)=1.95 + 0.04*Aspect
				Aspect110	0.038227	0.9185	D50=7.01 * e^(0.04*Aspect)
Solar	0.073821	0.007665	0.3087	Intercept	2.195500	<.0001	Ln(D50)=2.20 -0.45*Solar
				Solar_Norm	-0.454683	0.3087	D50=8.99 * e^(-0.45*Solar)
Slope	0.205222	0.148452	0.078	Intercept	1.509372	<.0001	Ln(D50)=1.51 + 0.88*Slope
				Slope_Norm	0.884202	0.078	D50=4.52 * e^(0.88*Slope)
Frost	0.521257	0.487061	0.0016	Intercept	1.180709	0.0001	Ln(D50)=1.18 + 1.42*Frost
				Frost5m_norm	1.417612	0.0016	D50=3.26 * e^(1.42*Frost)
Elev	0.521158	0.486955	0.0016	Intercept	1.371504	<.0001	Ln(D50)=1.37 + 1.36*Elev
				Elev_Norm	1.356677	0.0016	D50=3.94 * e^(1.36*Elev)
ESlope	0.699832	0.653652	0.0004	Intercept	0.960495	0.0006	Ln(D50)=0.965 + 0.83*Slope + 1.32*Elev
				Slope_Norm	0.825777	0.0156	D50=2.616 * e^(0.83*Slope + 1.32*Elev)
				Elev_Norm	1.322867	0.0005	
ESSe	0.776968	0.695865	0.0014	Intercept	1.037183	0.0394	Ln(D50)=1.04 + 1.23*Slope + 1.51*Elev -1.36*eCog + 0.28*Solar
				Slope_Norm	1.233438	0.0077	D50=2.82 * e^(1.23*Slope + 1.51*Elev -1.36*eCog + 0.28*Solar)
				Elev_Norm	1.507698	0.0003	
				eCog_norm	-1.363119	0.1329	
				Solar_Norm	0.283195	0.398	
ESAe	0.801334	0.729092	0.0007	Intercept	0.985330	0.0193	Ln(D50)=0.99 + 1.23*Slope + 0.33*Aspect + 1.42*Elev -1.14*eCog
				Slope_Norm	1.227268	0.0024	D50=2.68 * e^(1.23*Slope + 0.33*Aspect + 1.42*Elev -1.14*eCog)
				Asp110	0.330855	0.1646	
				Elev_Norm	1.419496	0.0003	
				eCog_norm	-1.138768	0.1897	
ESAN	0.767663	0.683177	0.0017	Intercept	0.698939	0.0871	Ln(D50)=0.70 + 1.14*Slope + 0.39*Aspect -0.15*NLCD + 1.34*Elev
				Slope_Norm	1.141191	0.006	D50=2.01 * e^(1.14*Slope + 0.39*Aspect -0.15*NLCD + 1.34*Elev)
				Asp110	0.385627	0.1507	
				NLCD_norm	-0.154762	0.7873	
				Elev_Norm	1.340635	0.0016	
SAE	0.766048	0.707559	0.0004	Intercept	0.629752	0.0348	Ln(D50)=0.63 + 1.12*Slope + 0.41*Aspect + 1.29*Elev
				Slope_Norm	1.123823	0.004	D50=1.88 * e^(1.12*Slope + 0.41*Aspect + 1.29*Elev)
				Aspect110	0.411014	0.0902	
				Elev_Norm	1.293474	0.0004	
FSlope	0.67919	0.629835	0.0006	Intercept	0.813601	0.005	Ln(D50)=0.81 + 0.78*Slope + 1.36*Frost
				Slope_Norm	0.778084	0.0251	D50=2.26 + e^(0.78*Slope + 1.36*Frost)
				Frost5m_norm	1.355989	0.0007	
FSAe	0.817245	0.750789	0.0005	Intercept	0.669026	0.0827	Ln(D50)=0.67 + 1.25*Slope + 0.46*Aspect + 1.49*Frost -1.04*eCog
				Slope_Norm	1.252572	0.0016	D50=1.95 * e^(1.25*Slope + 0.46*Aspect + 1.49*Frost -1.04*eCog)
				Asp110	0.461157	0.0514	
				Frost5m_norm	1.494701	0.0002	
				eCog_norm	-1.039887	0.2064	
FSAN	0.787699	0.710498	0.0011	Intercept	0.392343	0.2914	Ln(D50)=0.39 + 1.16*Slope + 0.51*Aspect + 1.41*Frost -0.08*NLCD
				Slope_Norm	1.163980	0.004	D50=1.48 * e^(1.16*Slope + 0.51*Aspect + 1.41*Frost -0.08*NLCD)
				Asp110	0.514082	0.0496	
				Frost5m_norm	1.406042	0.001	
				NLCD_norm	-0.076406	0.8863	
FSS	0.732279	0.665348	0.0009	Intercept	0.270162	0.5324	Ln(D50)=0.27 + 1.17*Slope + 1.49*Frost + 0.53*Solar
				Slope_Norm	1.172416	0.0107	D50=1.31 * e^(1.17*Slope + 1.49*Frost + 0.53*Solar)
				Frost5m_norm	1.485542	0.0004	
				Solar_Norm	0.530147	0.1489	
SAF	0.787285	0.734107	0.0002	Intercept	0.361842	0.2116	Ln(D50)=0.36 + 1.15*Slope + 0.52*Aspect + 1.38*Frost
				Slope_Norm	1.154734	0.0024	D50=1.44 + e^(1.15*Slope + 0.52*Aspect + 1.38*Frost)
				Asp110	0.524643	0.0295	
				Frost5m_norm	1.383295	0.0002	
Weathering	0.542743	0.510082	0.0011	Intercept	2.660769	<.0001	Ln(D50)=2.66 -1.37*Weather
				Weather_Norm	-1.366121	0.0011	D50=14.31 + e^(-1.37*Weather)
WA	0.544873	0.474853	0.006	Intercept	2.632559	<.0001	Ln(D50)=2.63 -1.37*Weather + 0.06*Aspect
				Weather_Norm	-1.368247	0.0017	D50=13.91 * e^(-1.37*Weather + 0.06*Aspect)
				Asp110	0.063390	0.8091	
WSol	0.556676	0.488472	0.0051	Intercept	2.738905	<.0001	Ln(D50)=2.74 -1.32*Weather -0.20*Solar
				Weather_Norm	-1.318585	0.0024	D50=15.47 * e^(-1.32*Weather -0.20*Solar)
				Solar_Norm	-0.202136	0.5338	
WSS	0.744482	0.680602	0.0007	Intercept	1.873502	0.0002	Ln(D50)=1.87 + 1.12*Slope -1.40*Weather + 0.44*Solar
				Slope_Norm	1.123593	0.0117	D50=6.51 * e^(1.12*Slope -1.40*Weather + 0.44*Solar)
				Weather_Norm	-1.398691	0.0003	
				Solar_Norm	0.443382	0.2055	
WSlope	0.70632	0.661138	0.0003	Intercept	2.227093	<.0001	Ln(D50)=2.23 + 0.79*Slope -1.32*Weather
				Slope_Norm	0.791191	0.0185	D50=9.27 * e^(0.79*Slope -1.32*Weather)
				Weather_Norm	-1.315634	0.0004	
SAW	0.791495	0.739369	0.0002	Intercept	1.835638	<.0001	Ln(D50)=1.84 + 1.13*Slope -1.31*Weather + 0.47*Aspect
				Slope_Norm	1.127568	0.0027	D50=6.27 * e^(1.13*Slope -1.31*Weather + 0.47*Aspect)
				Weather_Norm	-1.309772	0.0002	
				Asp110	0.465328	0.0469	

Table 3. Linear regression analyses of various combinations of attributes correlated with sediment size.

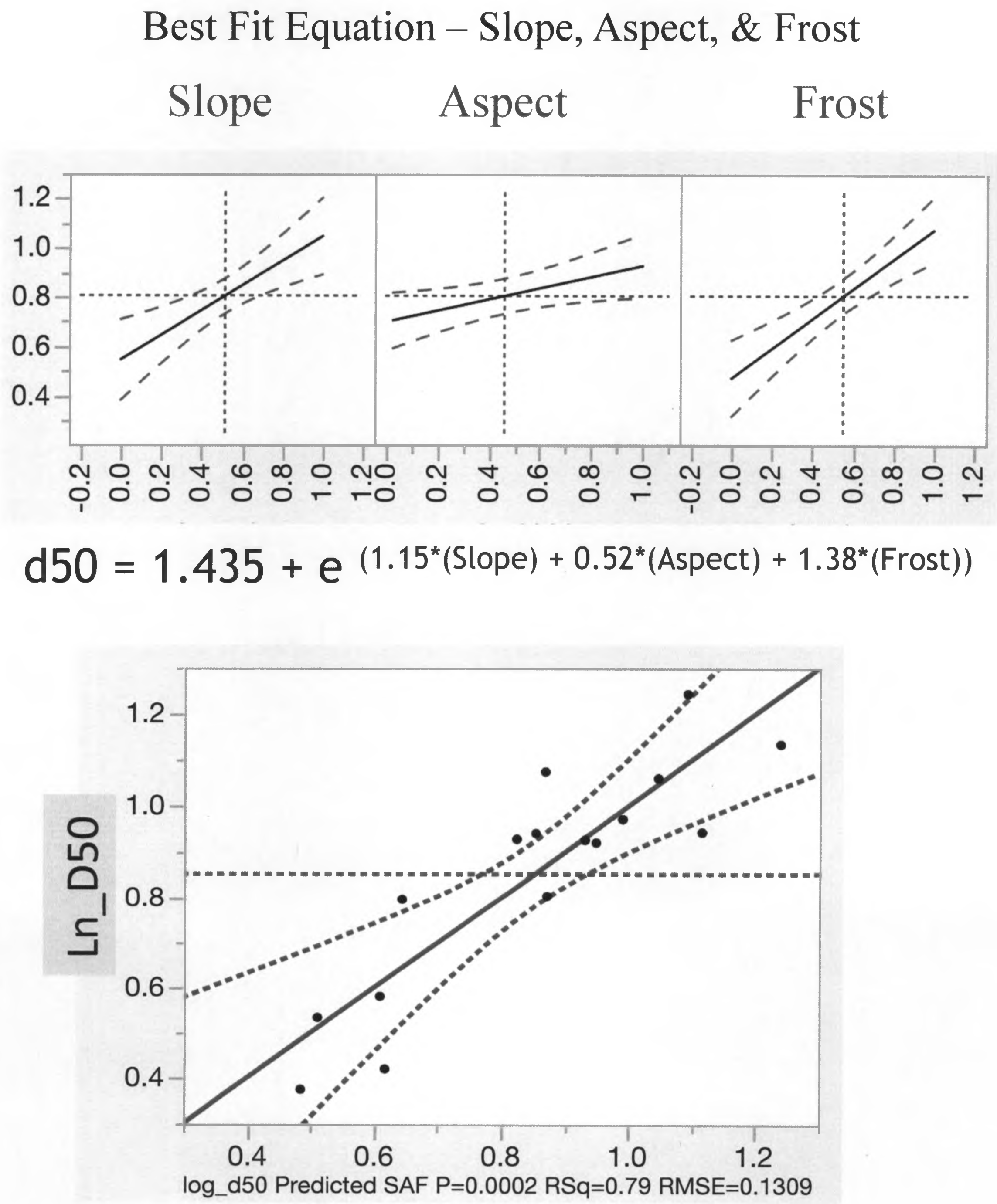

Figure 31. SAF Plot Correlating Slope, Aspect, and Frost Cracking Days with the Sediment Size found in Inyo Creek.

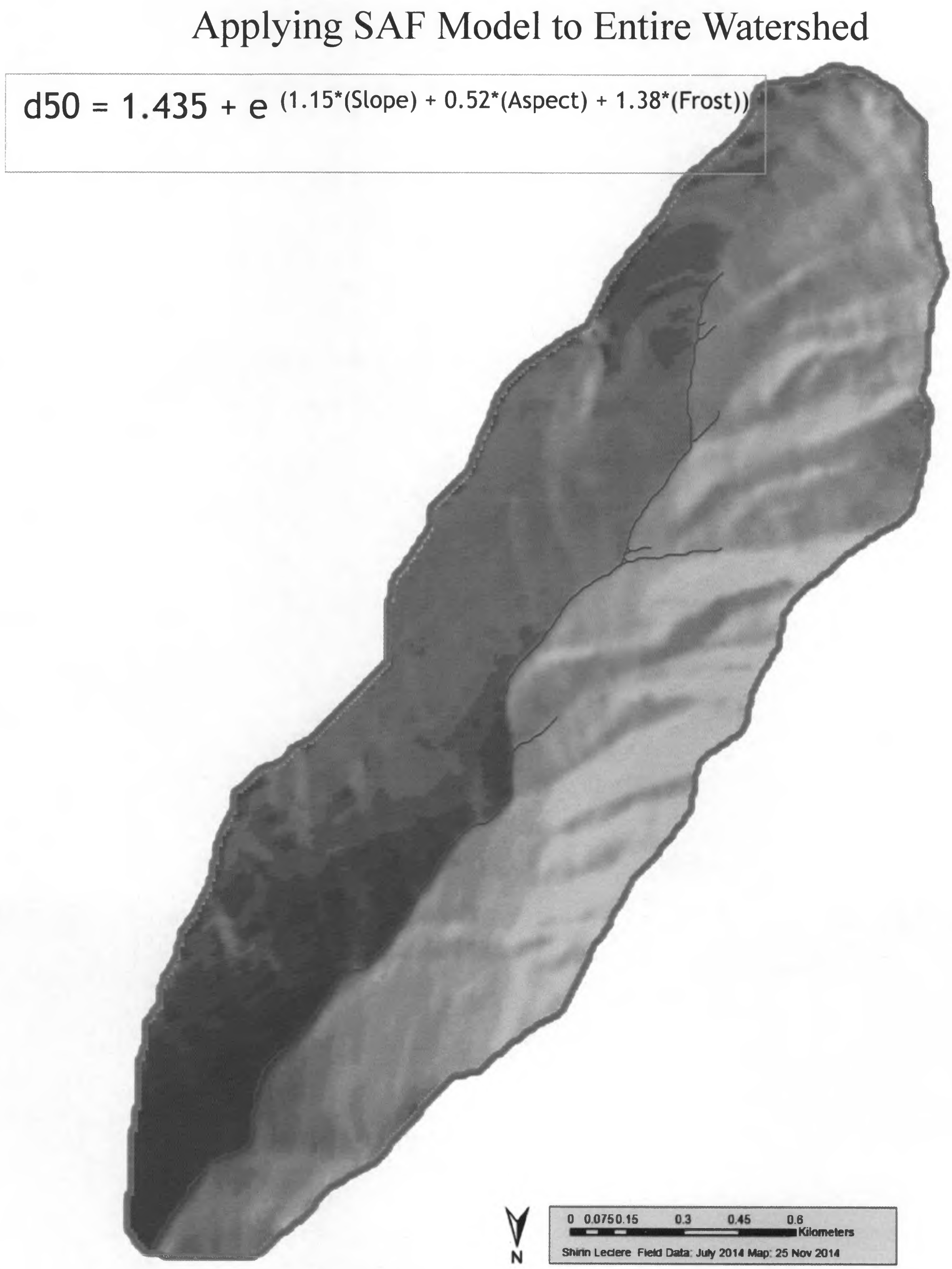

Figure 32. Applying the best-fit equation derived from 16 field site d50 values to the whole watershed.

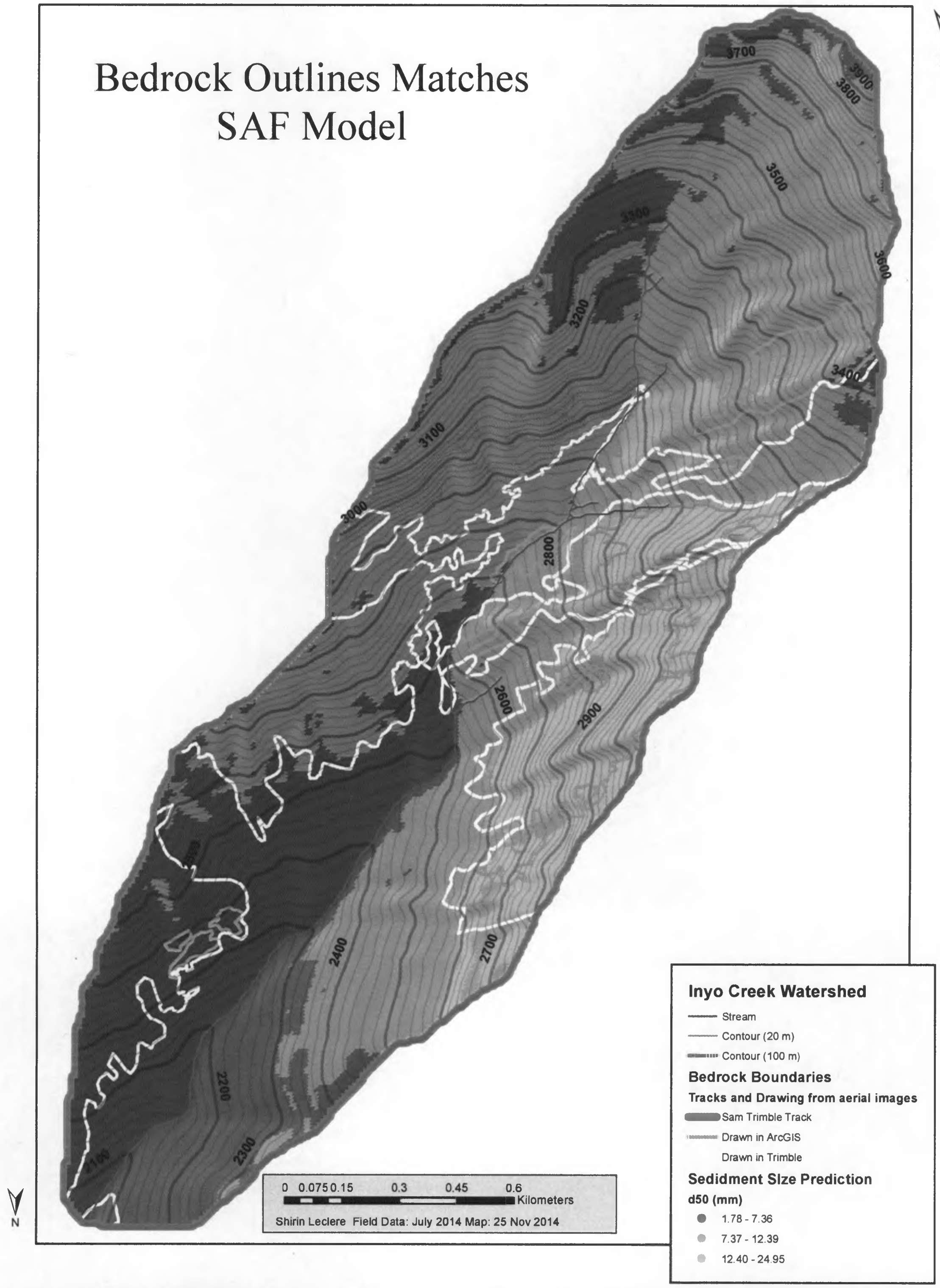

Figure 33. Bedrock Boundaries from field work and satellite imagery analysis overlaying the SAF model binned into three size categories. Note that the boundaries closely match the category boundaries in the middle elevations.

Comparing GLU Map & Regression Analysis

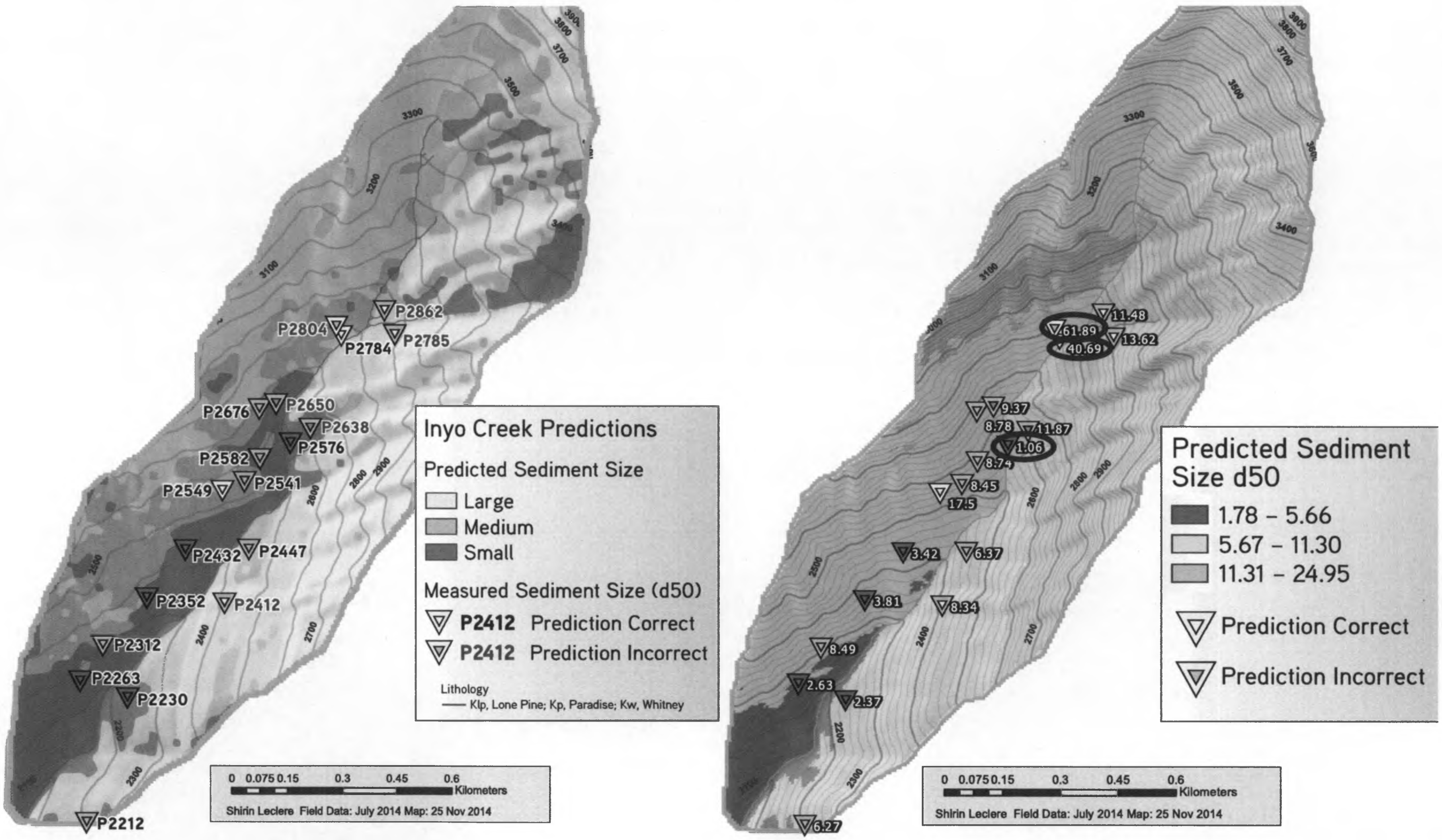

Figure 34. Comparing prediction maps. On the left is the GLU prediction map showing the accuracy of prediction at 19 field sites; the outer triangle color-matches the prediction while the inner triangle matches the measured D50. On the right is a map created from the regression analysis of 16 points measured in the field using the combination of slope, aspect, and frost cracking (SAF). There are three points shown (red circles) that were assessed with the GLU map but were considered outliers by Cook's D analysis.

SAE & E Models - Coarsest Particles Sizes

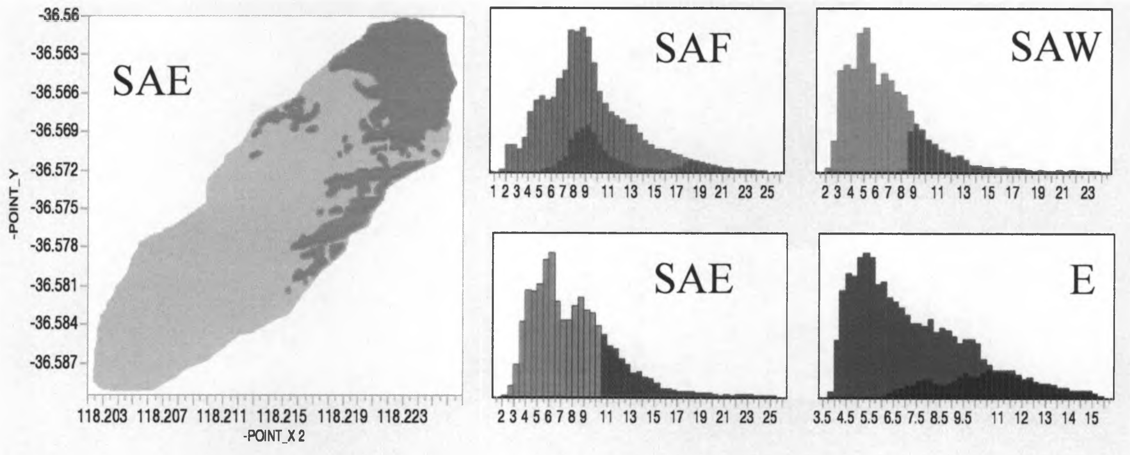

SAE coarsest particles are also SAW coarsest particles

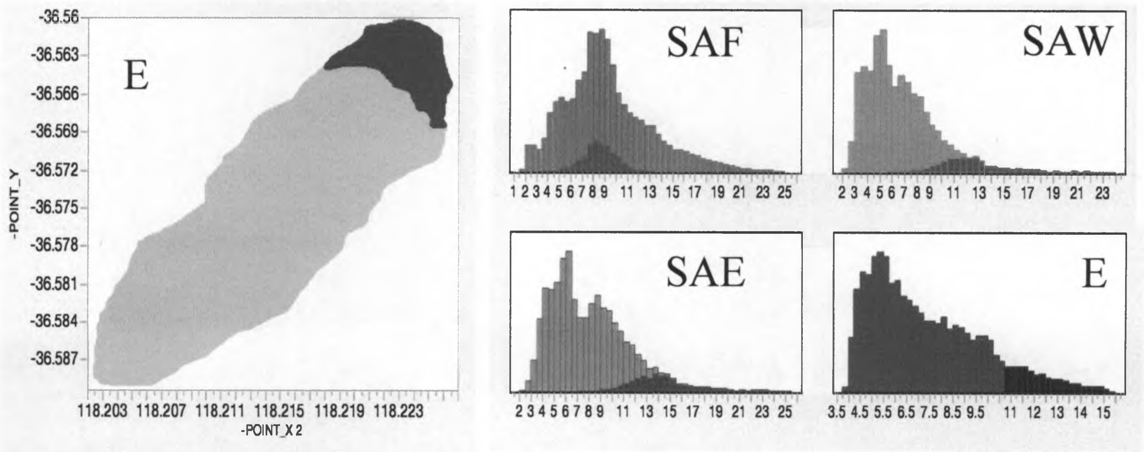

E alone does not predict particles larger than 15mm

Figure 35. Maps and histograms comparing the coarsest particles predicted by slope, aspect, and elevation (SAE) and elevation alone (E). Note that the coarsest particles for SAE match the coarsest particles for slope, aspect, and weathering (SAW) as shown in the upper right green histogram in the top figure. Of all of the predictive models E restricts the coarsest particles to only the highest elevations; this did not match our experience of the watershed. Also E predicts a generally smaller particle size range than the other models.

SAW Model – Location of Coarsest Particle Sizes

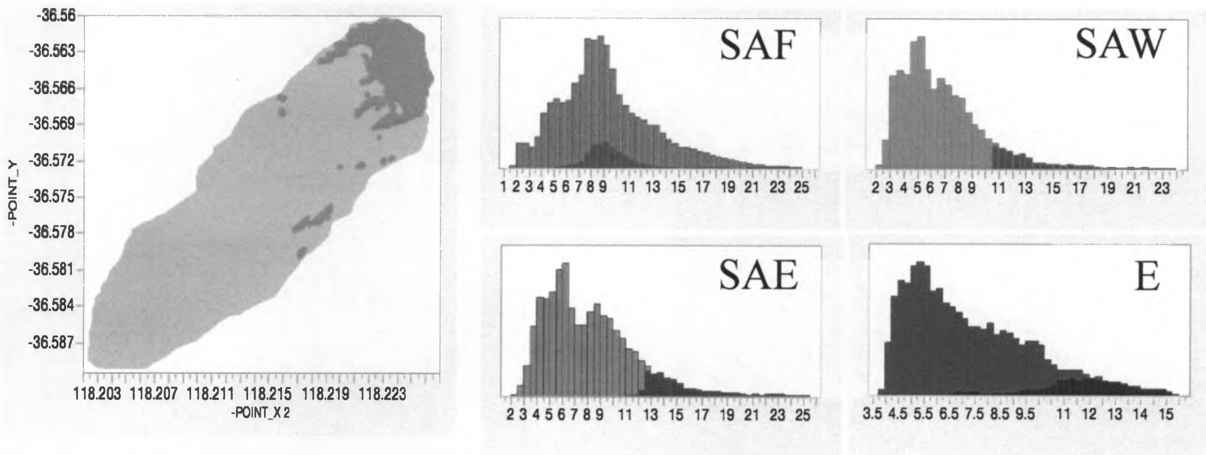

Coarsest particle sizes

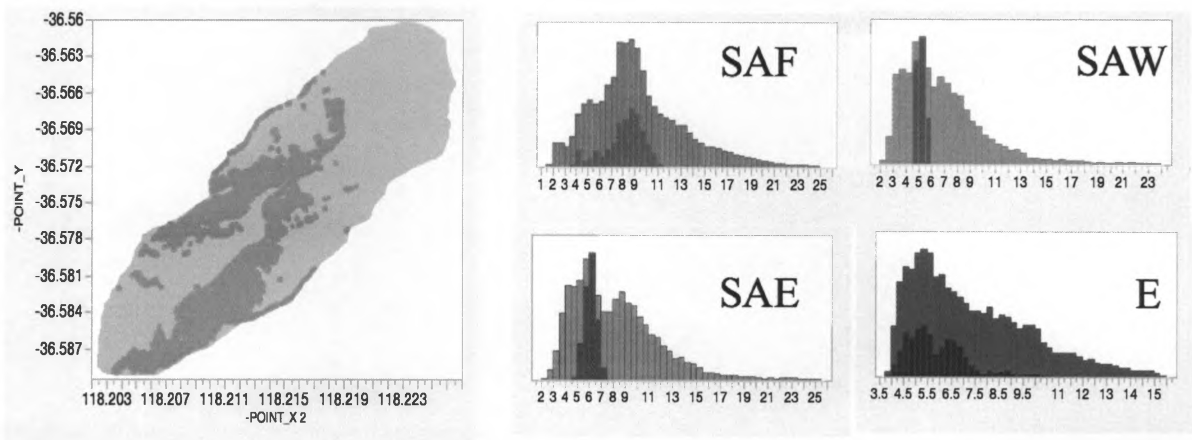

Most common particle sizes

Figure 36. Slope, Aspect, & Weathering (SAW) Model. Green pixels in the map view show the coarsest particle sizes highlighted in the upper right histogram. The lower map view shows the most common particle sizes highlighted in the upper right histogram.

SAF Model – Frequency Peak & Coarsest Particles

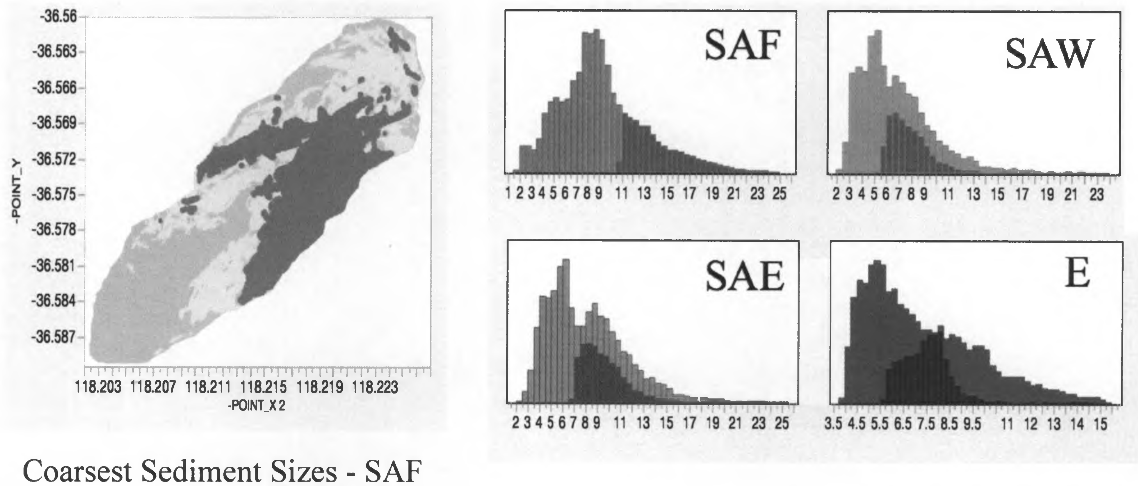

Coarsest Sediment Sizes - SAF

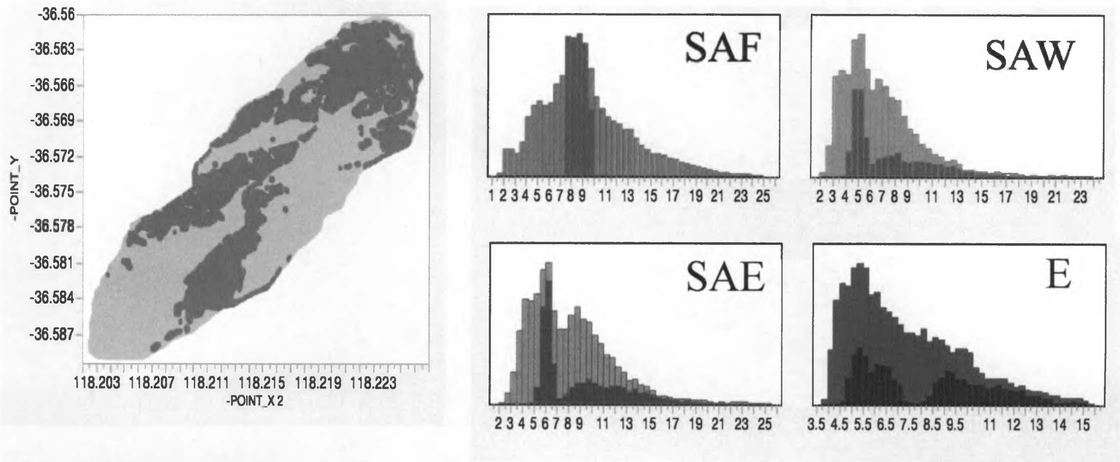

Most Common Sediment Sizes - SAF

Figure 37.Slope, Aspect & Frost (SAF) Model. Bright blue pixels in the upper map view shows the location of coarsest particles in the SAF model. This model suggests the largest sediments might not be at the highest elevations. Note, This model assumes that largest particles are formed where the rock spends the most time within the frost cracking window.

The lower map view shows the location of the most common sediment sizes highlighted in the blue histogram (upper left) This is the peak frequency for sediment sizes predicted by SAF; note the two bands created in the map view because frost cracking is lessened above a certain elevation where it's so cold that ice no longer grows for some portion of the year.

SAE Model – Location of Most Common Particle Sizes

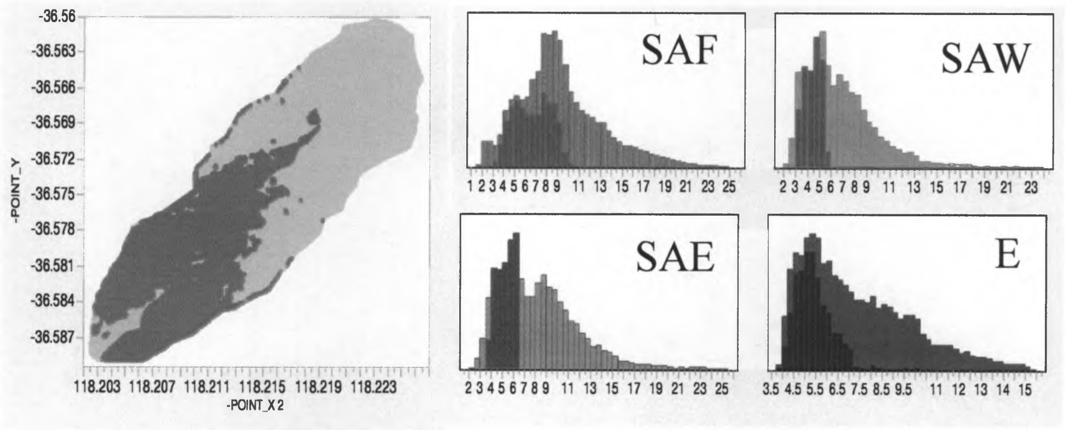

Higher of the two frequency peaks in SAE model.

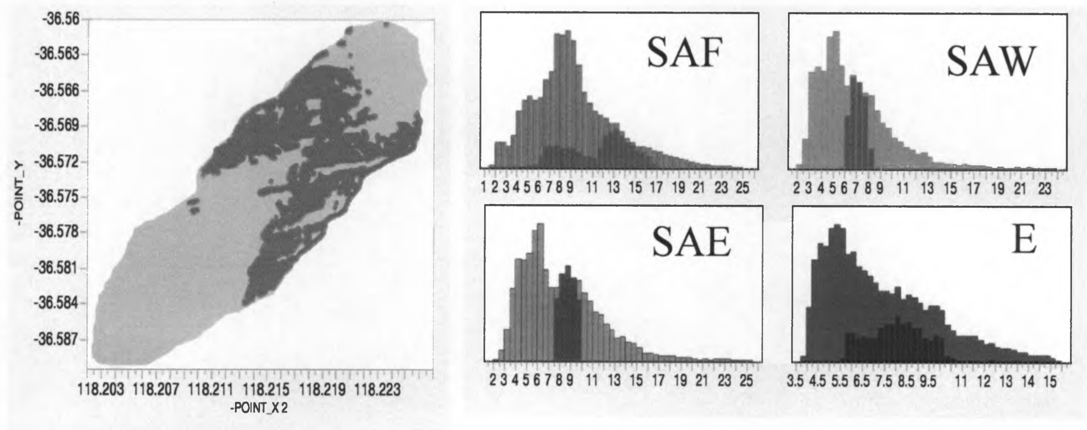

Second frequency peak

Figure 35. Bright blue pixel in the map view show the location of the most common sediment sizes highlighted in the blue histogram (upper left) This is the peak frequency for sediment sizes predicted by Slope, Aspect, and Frost Cracking (SAF); note the two bands created in the map view because frost cracking is lessened above a certain elevation where it's so cold that ice no longer grows for some portion of the year.

SAE has two peaks in the sediment size frequency histogram, the lower images show the location of the second frequency peak.

Comparing the 4 Models – PDF & CDF

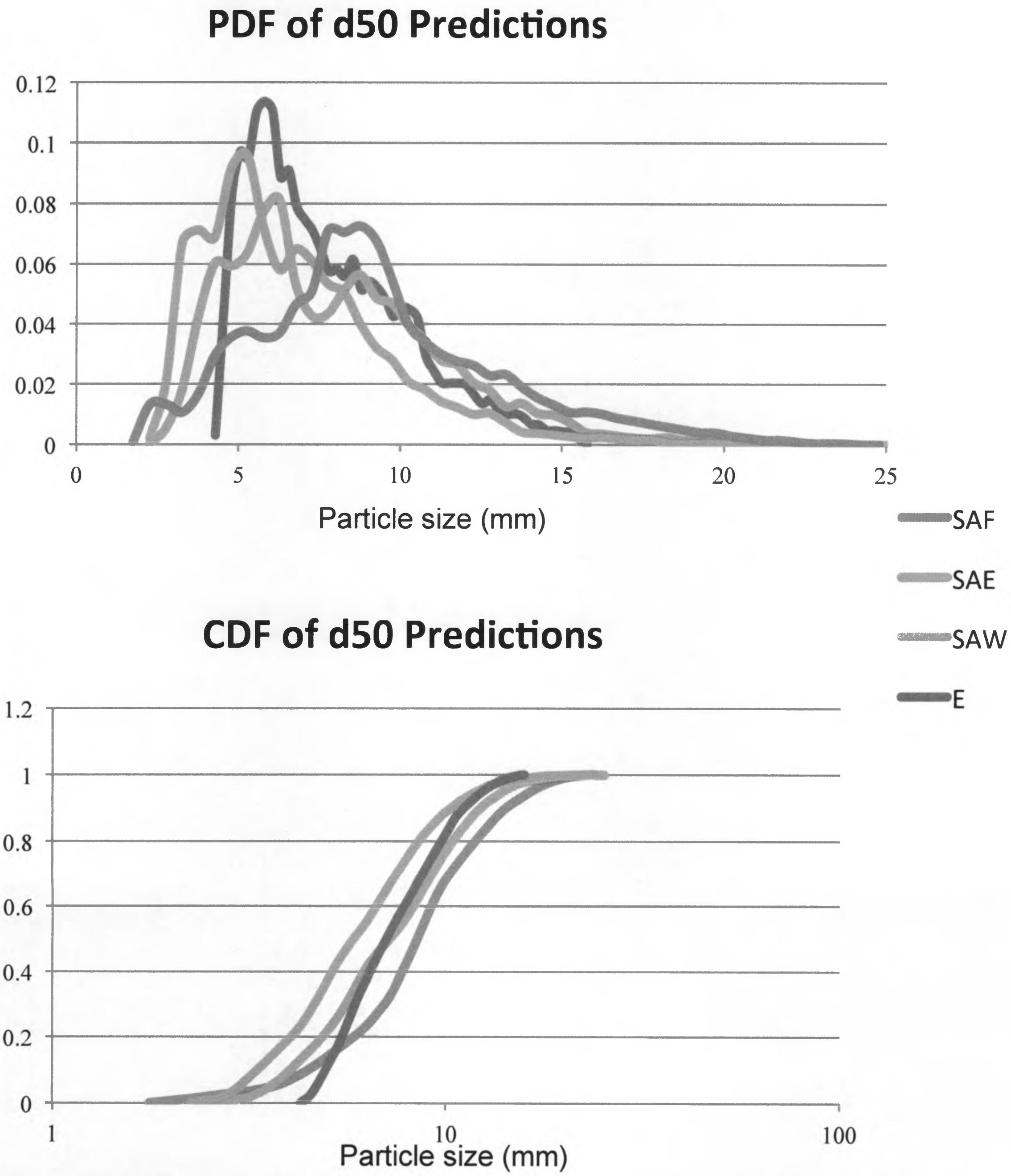

Figure 39. Predicting the d50 value across Inyo Creek using the regression models SAF – Slope Aspect & Frost, SAE – Slope Aspect & Elevation, SAW – Slope Aspect Weathering, and E –Elevation alone. Models built from 16 field site measurements; three sites were excluded as outliers using Cook's D analysis.

The probability density function (PDF) (top) compares the model frequency histograms. The cumulative distribution function (CDF) indicates that the SAF predicts the coarsest particle sizes and SAW predicts a generally finer particle size.

REFERENCES

Adediran, A.O., Parcharidis, I., Poscolieri, M., Pavlopoulos, K., 2004. Computer-assisted discrimination of morphological units on north-central Crete (Greece) by applying multivariate statistics to local relief gradients. Geomorphology 58, 357–370. doi:10.1016/j.geomorph.2003.07.024

Argialas, D.P., Tzotsos, A., 2006. Automatic Extraction Of Physiographic Features And Alluvial Fans In Nevada, USA From Digital Elevation Models And Satellite Imagery Through Multiresolution Segmentation And Object-Oriented Classification. Presented at the ASPRS Annual Conference, American Society of Photogrammetry and Remote Sensing, Reno, NV.

Attal, M., Mudd, S.M., Hurst, M.D., Weinman, B., Yoo, K., Naylor, M., 2015. Impact of change in erosion rate and landscape steepness on hillslope and fluvial sediments grain size in the Feather River basin (Sierra Nevada, California). Earth Surface Dynamics 3, 201–222. doi:10.5194/esurf-3-201-2015

Baatz, M., Schäpe, A., 2000. Multiresolution Segmentation: an optimization approach for high quality multi-scale image segmentation [WWW Document]. URL http://gis.stackexchange.com/questions/165744/fractal-net-evolution-approach-fnea-citation (accessed 5.20.16).

Bartlett, W.H.C., 1832. Experiments on the expansion and contraction of building stones by variations in temperature. American Journal of Science 22, 136–140.

Benz, U.C., Hofmann, P., Willhauck, G., Lingenfelder, I., Heynen, M., 2004. Multi-resolution, object-oriented fuzzy analysis of remote sensing data for GIS-ready information. ISPRS Journal of Photogrammetry and Remote Sensing, Integration of Geodata and Imagery for Automated Refinement and Update of Spatial Databases 58, 239–258. doi:10.1016/j.isprsjprs.2003.10.002

Binnie, S.A., Phillips, W.M., Summerfield, M.A., Fifield, L.K., 2007. Tectonic uplift, threshold hillslopes, and denudation rates in a developing mountain range. Geology 35, 743–746. doi:10.1130/G23641A.1

Blackwelder, E., 1933. The insolation hypothesis of rock weathering. Am J Sci Series 5 Vol. 26, 97–113. doi:10.2475/ajs.s5-26.152.97

Blaschke, T., Strobl, J., 2003. Defining landscape units through integrated morphometric characteristics, in: Buhrman, E., Ervin, S. (Eds.), Landscape Modeling: Digital Techniques for Landscape Architecture. Wichmann-Verlag, Heidelberg, pp. 104–113.

Blumthaler, M., Ambach, W., Ellinger, R., 1997. Increase in solar UV radiation with altitude. Journal of Photochemistry and Photobiology B: Biology 39, 130–134. doi:10.1016/S1011-1344(96)00018-8

Booth, A.M., Roering, J.J., Rempel, A.W., 2013. Topographic signatures and a general transport law for deep-seated landslides in a landscape evolution model. J. Geophys. Res. Earth Surf. 118, 603–624. doi:10.1002/jgrf.20051

Booth, D.B., Leverich, G., Downs, P.W., Dusterhoff, S., Araya, S., 2014. A Method for Spatially Explicit Representation of Sub-watershed Sediment Yield, Southern California, USA. Environmental Management 53, 968–984. doi:10.1007/s00267-014-0251-9

Burkalow, A.V., 1945. Angle of Repose and Angle of Sliding Friction: An Experimental Study. Geological Society of America Bulletin 56, 669–707. doi:10.1130/0016-7606(1945)56[669:AORAAO]2.0.CO;2

Burke, B.C., Heimsath, A.M., White, A.F., 2007. Coupling chemical weathering with soil production across soil-mantled landscapes. Earth Surf. Process. Landforms 32, 853–873. doi:10.1002/esp.1443

Burnett, B.N., Meyer, G.A., McFadden, L.D., 2008. Aspect-related microclimatic influences on slope forms and processes, northeastern Arizona. J. Geophys. Res. 113, F03002. doi:10.1029/2007JF000789

Campbell, D.H., Baron, J.S., Tonnessen, K.A., Brooks, P.D., Schuster, P.F., 2000. Controls on Nitrogen Flux in Alpine/Subalpine Watersheds of Colorado. Water Resources Research 36, 37–47.

Chau, K.T., Tang, Y.F., Wong, R.H.C., 2004. GIS based rockfall hazard map for Hong Kong. International Journal of Rock Mechanics and Mining Sciences, Proceedings of the ISRM SINOROCK 2004 symposium 41, 530. doi:10.1016/j.ijrmms.2003.12.114

Chayka, J., 2011. Quantitative linkages between watershed conditions and mainstem channel characteristics in Lagunitas Creek, northern California (Masters). San Francisco State University, San Francisco, Ca.

Cook, R.D., Weisberg, S., 1982. Residuals and Influence in Regression. Chapman & Hall.

Crouvi, O., Ben-Dor, E., Beyth, M., Avigad, D., Amit, R., 2006. Quantitative mapping of arid alluvial fan surfaces using field spectrometer and hyperspectral remote sensing. Remote Sensing of Environment 104, 103–117. doi:10.1016/j.rse.2006.05.004

Dennis, R.D., 1976. Insect morphogenetic hormones and developmental mechanisms in the nematode, Nematospiroides dubius. Comp Biochem Physiol A Comp Physiol 53, 53–56.

Dietrich, W.E., Bellugi, D.G., Sklar, L.S., Stock, J.D., Heimsath, A.M., Roering, J.J., 2003. Geomorphic transport laws for predicting landscape form and dynamics, in: Wilcock, P.R., Iverson, R.M. (Eds.), Geophysical Monograph Series. American Geophysical Union, Washington, D. C., pp. 103–132.

Dietrich, W.E., Dunne, T., 1978. Sediment budget for a small catchment in mountainous terrain. Zeit. for Geomorph. Suppl. Bd. 29, 191–206.

Dixon, J.L., Heimsath, A.M., Amundson, R., 2009. The critical role of climate and saprolite weathering in landscape evolution. Earth Surf. Process. Landforms 34, 1507–1521. doi:10.1002/esp.1836

Durgin, P.B., 1977. Landslides and the Weathering of Granitic Rocks. GSA III.

Eppes, M.C., McFadden, L.D., Wegmann, K.W., Scuderi, L.A., 2010. Cracks in desert pavement rocks: Further insights into mechanical weathering by directional insolation. Geomorphology 123, 97–108. doi:10.1016/j.geomorph.2010.07.003

Farr, T.G., Chadwick, O.A., 1996. Geomorphic processes and remote sensing signatures of alluvial fans in the Kun Lun Mountains, China. J. Geophys. Res. 101, 23091–23100. doi:10.1029/96JE01603

Ferguson, R., Hoey, T., Wathen, S., Werritty, A., 1996. Field evidence for rapid downstream fining of river gravels through selective transport. Geology 24, 179–182. doi:10.1130/0091-7613(1996)024<0179:FEFRDF>2.3.CO;2

Fu, B., Newham, L.T.H., Ramos-Scharrón, C.E., 2010. A review of surface erosion and sediment delivery models for unsealed roads. Environmental Modelling & Software 25, 1–14. doi:10.1016/j.envsoft.2009.07.013

Gabet, E.J., Mudd, S.M., 2010. Bedrock erosion by root fracture and tree throw: A coupled biogeomorphic model to explore the humped soil production function and the persistence of hillslope soils. J. Geophys. Res. 115, F04005. doi:10.1029/2009JF001526

Gasparini, N.M., Tucker, G.E., Bras, R.L., 1999. Downstream fining through selective particle sorting in an equilibrium drainage network. Geology 27, 1079–1082. doi:10.1130/0091-7613(1999)027<1079:DFTSPS>2.3.CO;2

Hales, T.C., Roering, J.J., 2007. Climatic controls on frost cracking and implications for the evolution of bedrock landscapes. J. Geophys. Res. 112, F02033. doi:10.1029/2006JF000616

Hales, T.C., Roering, J.J., 2005. Climate-controlled variations in scree production, Southern Alps, New Zealand. Geology 33, 701–704. doi:10.1130/G21528.1

Hales, T.C., Scharer, K.M., Wooten, R.M., 2012. Southern Appalachian hillslope erosion rates measured by soil and detrital radiocarbon in hollows. Geomorphology 138, 121–129. doi:10.1016/j.geomorph.2011.08.030

Hall, K., 2004. Evidence for freeze–thaw events and their implications for rock weathering in northern Canada. Earth Surf. Process. Landforms 29, 43–57. doi:10.1002/esp.1012

Hallet, B., Walder, J.S., Stubbs, C.W., 1991. Weathering by segregation ice growth in microcracks at sustained subzero temperatures: Verification from an experimental study using acoustic emissions. Permafrost and Periglacial Processes 2, 283–300. doi:10.1002/ppp.3430020404

Heimsath, A.M., DiBiase, R.A., Whipple, K.X., 2012. Soil production limits and the transition to bedrock-dominated landscapes. Nature Geosci 5, 210–214. doi:10.1038/ngeo1380

Heimsath, A.M., Dietrich, W.E., Nishiizumi, K., Finkel, R.C., 1997. The soil production function and landscape equilibrium. Nature 388, 358–361. doi:10.1038/41056

Heller, P.L., Beland, P.E., Humphrey, N.F., Konrad, S.K., Lynds, R.M., McMillan, M.E., Valentine, K.E., Widman, Y.A., Furbish, D.J., 2001. Paradox of downstream fining and weathering-rind formation in the lower Hoh River, Olympic Peninsula, Washington. Geology 29, 971–974. doi:10.1130/0091-7613(2001)029<0971:PODFAW>2.0.CO;2

Hirt, W.H., 2007. Petrology of the Mount Whitney Intrusive Suite, eastern Sierra Nevada, California: Implications for the emplacement and differentiation of composite felsic intrusions. Geological Society of America Bulletin 119, 1185–1200. doi:10.1130/B26054.1

Hoey, T.B., Ferguson, R.I., 1997. Controls of strength and rate of downstream fining above a river base level. Water Resour. Res. 33, 2601–2608. doi:10.1029/97WR02324

Hupp, C.R., Osterkamp, W.R., 1985. Bottomland Vegetation Distribution along Passage Creek, Virginia, in Relation to Fluvial Landforms. Ecology 66, 670–681. doi:10.2307/1940528

Hurst, M.D., Mudd, S.M., Yoo, K., Attal, M., Walcott, R., 2013. Influence of lithology on hillslope morphology and response to tectonic forcing in the northern Sierra Nevada of California. J. Geophys. Res. Earth Surf. 118, 832–851. doi:10.1002/jgrf.20049

Iqbaluddin, Saifuddin, Javed, A., Moni, M., 1999. Terrain mapping unit-based approach for sustainable agricultural development in India—an example from plains ecosystem at semi-arid interface. Journal of Arid Environments 42, 319–330. doi:10.1006/jare.1999.0519

Jiang, H.-T., Xu, F.-F., Cai, Y., Yang, D.-Y., 2006. Weathering Characteristics of Sloping Fields in the Three Gorges Reservoir Area, China. Pedosphere 16, 50–55. doi:10.1016/S1002-0160(06)60025-8

Jomelli, V., Francou, B., 2000. Comparing the characteristics of rockfall talus and snow avalanche landforms in an Alpine environment using a new methodological approach: Massif des Ecrins, French Alps. Geomorphology 35, 181–192. doi:10.1016/S0169-555X(00)00035-0

Khan, U., Tuteja, N.K., Sharma, A., 2013. Delineating hydrologic response units in large upland catchments and its evaluation using soil moisture simulations. Environmental Modelling & Software 46, 142–154. doi:10.1016/j.envsoft.2013.03.005

Krumbein, W.C., Tisdel, F.W., 1940. Size distribution of source rocks of sediments. Am. J. Sci. 238, 296–305.

Langston, A.L., Tucker, G.E., Anderson, R.S., Anderson, S.P., 2015. Evidence for climatic and hillslope-aspect controls on vadose zone hydrology and implications for saprolite weathering. Earth Surf. Process. Landforms 40, 1254–1269. doi:10.1002/esp.3718

Larsen, I.J., MacDonald, L.H., Brown, E., Rough, D., Welsh, M.J., Pietraszek, J.H., Libohova, Z., de Dios Benavides-Solorio, J., Schaffrath, K., 2009. Causes of Post-Fire Runoff and Erosion: Water Repellency, Cover, or Soil Sealing? Soil Science Society of America Journal 73, 1393. doi:10.2136/sssaj2007.0432

MacDonald, R.C., Simon, S.A., Baer, E., 1976. Ionic influences on the phase transition of dipalmitoylphosphatidylserine. Biochemistry 15, 885–891.

Machala, M., Zejdová, L., 2014. Forest Mapping Through Object-based Image Analysis of Multispectral and LiDAR Aerial Data. European Journal of Remote Sensing 47, 117–131. doi:10.5721/EuJRS20144708

Marchetti, M., Rivas, V., 2001. Geomorphology and Environmental Impact Assessment. CRC Press.

Marshall, J.A., Sklar, L.S., 2012. Mining soil databases for landscape-scale patterns in the abundance and size distribution of hillslope rock fragments. Earth Surf. Process. Landforms 37, 287–300. doi:10.1002/esp.2241

McFadden, L.D., Eppes, M.C., Gillespie, A.R., Hallet, B., 2005. Physical weathering in arid landscapes due to diurnal variation in the direction of solar heating. Geological Society of America Bulletin 117, 161–173. doi:10.1130/B25508.1

McGrath, G.S., Nie, Z., Dyskin, A., Byrd, T., Jenner, R., Holbeche, G., Hinz, C., 2013. In situ fragmentation and rock particle sorting on arid hills. J. Geophys. Res. Earth Surf. 118, 17–28. doi:10.1029/2012JF002402

McGreevy, J.P., 1985. Thermal properties as controls on rock surface temperature maxima, and possible implications for rock weathering. Earth Surf. Process. Landforms 10, 125–136. doi:10.1002/esp.3290100205

Meijerink, A.M.J. (itc, 1988. Data acquisition and data capture through terrain mapping units. ITC-Journal (Netherlands).

Meinel, G., Neubert, M., 2011. A comparison of segmentation programs for high resolution remote sensing data. Presented at the International Society for Photogrammetry and Remote Sensing TC VII Symposium, Vienna, Austria.

Michaelides, K., Singer, M.B., 2014. Impact of coarse sediment supply from hillslopes to the channel in runoff-dominated, dryland fluvial systems. J. Geophys. Res. Earth Surf. 119, 2013JF002959. doi:10.1002/2013JF002959

Miliaresis, G.C., Argialas, D.P., 2000. Extraction and delineation of alluvial fans from digital elevation models and Landsat Thematic Mapper images. PE&RS 66, 1093–1101.

Minár, J., Evans, I.S., 2008. Elementary forms for land surface segmentation: The theoretical basis of terrain analysis and geomorphological mapping. Geomorphology 95, 236–259. doi:10.1016/j.geomorph.2007.06.003

Montgomery, D.R., Brandon, M.T., 2002. Topographic controls on erosion rates in tectonically active mountain ranges. Earth and Planetary Science Letters 201, 481–489. doi:10.1016/S0012-821X(02)00725-2

Nakamura, F., Yajima, T., Kikuchi, S., 1997. Structure and composition of riparian forests with special reference to geomorphic site conditions along the Tokachi River, northern Japan. Plant Ecology 133, 209–219. doi:10.1023/A:1009787614455

Olyphant, J., Pelletier, J.D., Johnson, R., 2016. Topographic correlations with soil and regolith thickness from shallow-seismic refraction constraints across upland hillslopes in the Valles Caldera, New Mexico. Earth Surf. Process. Landforms n/a-n/a. doi:10.1002/esp.3941

Ouimet, W.B., Whipple, K.X., Granger, D.E., 2009. Beyond threshold hillslopes: Channel adjustment to base-level fall in tectonically active mountain ranges. Geology 37, 579–582. doi:10.1130/G30013A.1

Paola, C., Heller, P.L., Angevine, C.L., 1992. The large-scale dynamics of grain-size variation in alluvial basins, 1: Theory. Basin Research 4, 73–90. doi:10.1111/j.1365-2117.1992.tb00145.x

Peltier, L.C., 1973. The Geographic Cycle in Periglacial Regions as it is Related to Climatic Geomorphology, in: Derbyshire, E. (Ed.), Climatic Geomorphology, The Geographical Readings Series. Macmillan Education UK, pp. 131–152.

Phillips, J.D., Marion, D.A., 2006. Biomechanical Effects of Trees on Soil and Regolith: Beyond Treethrow. Annals of the Association of American Geographers 96, 233–247. doi:10.1111/j.1467-8306.2006.00476.x

Phillips, J.D., 2007. The perfect landscape. Geomorphology, Geomorphic Instability and Change - Introduction:Implications of temporal and spatial scalesJoint International Geomorphology Conference (JIGC) 84, 159–169. doi:10.1016/j.geomorph.2006.01.039

Phillips, J.D., Marion, D.A., Turkington, A.V., 2008. Pedologic and geomorphic impacts of a tornado blowdown event in a mixed pine-hardwood forest. CATENA 75, 278–287. doi:10.1016/j.catena.2008.07.004

Potts, A.S., 1970. Frost Action in Rocks: Some Experimental Data. Transactions of the Institute of British Geographers 109–124. doi:10.2307/621644

PRISM Climate Group (2014) Climate Data. Available at: http://www.prismclimate.org., 2014.

Riebe, C.S., Kirchner, J.W., Finkel, R.C., 2004. Erosional and climatic effects on long-term chemical weathering rates in granitic landscapes spanning diverse climate regimes. Earth and Planetary Science Letters 224, 547–562. doi:10.1016/j.epsl.2004.05.019

Riebe, C.S., Kirchner, J.W., Granger, D.E., Finkel, R.C., 2001. Minimal climatic control on erosion rates in the Sierra Nevada, California. Geology 29, 447–450. doi:10.1130/0091-7613(2001)029<0447:MCCOER>2.0.CO;2

Riebe, C.S., Sklar, L.S., Lukens, C.E., Shuster, D.L., 2015. Climate and topography control the size and flux of sediment produced on steep mountain slopes. PNAS 112, 15574–15579. doi:10.1073/pnas.1503567112

Riebe, C.S., Sklar, L.S., Overstreet, B.T., Wooster, J.K., 2014. Optimal reproduction in salmon spawning substrates linked to grain size and fish length. Water Resour. Res. 50, 898–918. doi:10.1002/2013WR014231

Ritchie, 1972. Freeze–thaw action on brick. Journal of the Canadian Ceramic Society.

Roering, J.J., Kirchner, J.W., Sklar, L.S., Dietrich, W.E., 2001. Hillslope evolution by nonlinear creep and landsliding: An experimental study. Geology 29, 143–146.

Roering, J.J., Marshall, J., Booth, A.M., Mort, M., Jin, Q., 2010. Evidence for biotic controls on topography and soil production. Earth and Planetary Science Letters 298, 183–190. doi:10.1016/j.epsl.2010.07.040

Ruxton, B.P., Berry, L., 1957. Weathering of Granite and Associated Erosional Features in Hong Kong. Geological Society of America Bulletin 68, 1263–1292. doi:10.1130/0016-7606(1957)68[1263:WOGAAE]2.0.CO;2

Schlunegger, F., Badoux, A., McArdell, B.W., Gwerder, C., Schnydrig, D., Rieke-Zapp, D., Molnar, P., 2009. Limits of sediment transfer in an alpine debris-flow catchment, Illgraben, Switzerland. Quaternary Science Reviews, Natural Hazards, Extreme Events and Mountain Topography 28, 1097–1105. doi:10.1016/j.quascirev.2008.10.025

Schmidt, K.-H., 2009. Hillslopes as Evidence of Climatic Change, in: Parsons, D.A.J., Abrahams, A.D. (Eds.), Geomorphology of Desert Environments. Springer Netherlands, pp. 675–694.

Schmoldt, A., Benthe, H.F., Haberland, G., 1975. Digitoxin metabolism by rat liver microsomes. Biochem. Pharmacol. 24, 1639–1641.

Shirzadi, A., Saro, L., Joo, O.H., Chapi, K., 2012. A GIS-based logistic regression model in rock-fall susceptibility mapping along a mountainous road: Salavat Abad case study, Kurdistan, Iran. Nat Hazards 64, 1639–1656. doi:10.1007/s11069-012-0321-3

Sklar, L.S., Dietrich, W.E., 2006. The role of sediment in controlling steady-state bedrock channel slope: Implications of the saltation–abrasion incision model. Geomorphology, The Hydrology and Geomorphology of Bedrock Rivers 82, 58–83. doi:10.1016/j.geomorph.2005.08.019

Sklar, L.S., Riebe, C.S., Marshall, J.A., Genetti, J., Leclere, S., Lukens, C.L., Merces, V., 2016. The problem of predicting the size distribution of sediment supplied by hillslopes to rivers. Geomorphology 5/6/2016. doi:10.1016/j.geomorph.2016.05.005

Stock, G.M., Ehlers, T.A., Farley, K.A., 2006. Where does sediment come from? Quantifying catchment erosion with detrital apatite (U-Th)/He thermochronometry. Geology 34, 725–728. doi:10.1130/G22592.1

Taramelli, A., Melelli, L., 2008. Detecting Alluvial Fans Using Quantitative Roughness Characterization and Fuzzy Logic Analysis, in: Gervasi, O., Murgante, B., Laganà, A., Taniar, D., Mun, Y., Gavrilova, M.L. (Eds.), Computational Science and Its Applications – ICCSA 2008, Lecture Notes in Computer Science. Springer Berlin Heidelberg, pp. 1–15.

Terra, H. de, 1933. E. Blackwelder's challenge of the insolation hypothesis of rock weathering; discussion. Am J Sci Series 5 Vol. 26, 523–524. doi:10.2475/ajs.s5-26.155.523

Turowski, J.M., Wyss, C.R., Beer, A.R., 2015. Grain size effects on energy delivery to the streambed and links to bedrock erosion. Geophys. Res. Lett. 42, 2015GL063159. doi:10.1002/2015GL063159

Wagner, D.L., Lancaster, J.T., DeRose, M.B., 2012. The Oak Creek Post Fire Debris and Hyperconcentrated Flows of July 12, 2008 Inyo County, California: A Geologic Investigation (CGS Special Report No. 225). California Geological Survey, Sacramento, California.

Walder, J., Hallet, B., 1985. A theoretical model of the fracture of rock during freezing. Geological Society of America Bulletin 96, 336–346. doi:10.1130/0016-7606(1985)96<336:ATMOTF>2.0.CO;2

West, A.J., Galy, A., Bickle, M., 2005. Tectonic and climatic controls on silicate weathering. Earth and Planetary Science Letters 235, 211–228. doi:10.1016/j.epsl.2005.03.020

Wilkinson, M.T., Humphreys, G.S., 2006. Slope aspect, slope length and slope inclination controls of shallow soils vegetated by sclerophyllous heath—links to long-term landscape evolution. Geomorphology 76, 347–362. doi:10.1016/j.geomorph.2005.11.011

Willett, S.D., 2006. Tectonics, Climate, and Landscape Evolution. Geological Society of America.

Wright, J.S., 2007. An overview of the role of weathering in the production of quartz silt. Sedimentary Geology, From Particle Size to Sediment Dynamics 202, 337–351. doi:10.1016/j.sedgeo.2007.03.024

Zhang, Y., Maxwell, T., Tong, H., Dey, V., 2010. Development Of A Supervised Software Tool For Automated Determination Of Optimal Segmentation Parameters For eCognition. Presented at the ISPRS TC VII Symposium – 100 Years ISPRS, Vienna, Austria.

Zinck, J.A., Metternicht, G., Bocco, G., Valle, H.F.D., 2015. Geopedology: An Integration of Geomorphology and Pedology for Soil and Landscape Studies. Springer.

Zonneveld, I., 1989. The land unit - A fundamental concept in landscape ecology, and its applications. Landscape Ecology 3, 67–86.